Chapter 6

Post-Translational Modification Profiling of Burn-Induced — Insulin Resistance and Muscle Wasting

Xiao-Ming Lu, Ronald G. Tompkins and
Alan J. Fischman

Additional information is available at the end of the chapter

http://dx.doi.org/10.5772/54849

1. Introduction

The maintenance of glucose levels represents one of the most tightly regulated systems in the body. All cells require glucose, however, it is only available from exogenous sources or hepatic production. Since glucose cannot be stored in significant amounts except as glycogen in the liver and muscle, glucose transport into the cell by specific transport proteins is critical for cell function. Insulin plays a major role in the maintenance of normal glucose levels. When blood glucose levels rise, insulin secretion is stimulated, resulting in increase in uptake of glucose by skeletal muscle via glucose transporter protein 4 (GLUT4), and decreased production by the liver. Binding of insulin to its receptor leads to activation of insulin receptor tyrosine kinase, which phosphorylates IRS proteins that function as docking platforms for the two main signalingpathways are responsible downstream regulation [1]; the phosphatidyl inositol 3-kinase (PI3K)-Akt/protein kinase B (PKB) pathway and the Ras-mitogen-activated protein kinase (MAPK) pathway. There appear to be several key proteins in the insulin/glucose and protein turnover regulatory cascade, including IRS-1 the predominent form of IRS in muscle. When levels of insulin and glucose are abnormally high in the fasting state, a condition called insulin resistance exists. Insulin resistance and muscle wasting during the persistent high grade inflammation induced by severe burn injury increases the patients risk for infection, sepsis, and death. Clinical data indicate that a resting metabolic rate switch occurs after burn injuries that involve ~40-60% total body surface area (TBSA). Based on studies of 189 pediatric burn patients [2,3,4], it was determined that burn size determines the inflammatory and hypermetabolic response to injury; serum glucose and insulin levels increased to 144 mg/dl and 32 ng/ml on day 8 after injury. Metabolic alterations such as abnormal cytokine release [5, 6], altered gene expression [7,8] and increased protein catabolism are common in patients with

burn injuries [9,10,11]. Glucose intolerance and elevated insulin levels may contribute to hyperglycemia, even in non-diabetic patients [12,13,14,15,16,17]. Hyperglycemia and glucose intolerance are frequently associated with the metabolic response to major trauma. Following injury [18], burn shock [19,20] or systemic infection [21,22], oral and intravenous glucose tolerance tests have demonstrated delayed disposal of glucose from plasma into tissues. This "diabetes of injury" could be explained if there was an insulin deficiency, and several studies [23] have shown that early after trauma ("ebb phase") insulin concentrations are reduced even in the face of hyperglycemia. After resuscitation of trauma patients ("flow phase"), beta cell responsiveness to glucose administration and plasma insulin levels are appropriate or even higher than expected. However, despite this appropriate acute insulin response to glucose administration, glucose intolerance and hyperglycemia continue. This finding suggests that some of the tissues in trauma patients are relatively insensitive to the effects of insulin.

There are numerous reports that describe insulin resistance in burn patients and animal models [24,25,26,27,28,29,30,31,32,33,34,35,36,37,38,39]. Direct measurements show that liver and skeletal muscle are resistant tissues. In addition, lipolysis is not attenuated in trauma patients after glucose administration. The precise mechanism for insulin resistance after burns or other stressors is unknown. It is likely, however, that insulin binding to its membrane receptors is normal, and that there is a post receptor mechanism for the insulin resistance. Alterations in levels of cytokines, such as TNF, IL-1, and IL-6, have been reported in burn patients and animal models of burn injury by our laboratory and other investigators [38]. Infusion of endotoxin, TNF, and IL-1 can produce alterations in glucose metabolism and insulin resistance *in vivo* [40, 41]. In addition, it has also been shown that endotoxin [42] and IL-6 [43] can produce insulin resistance in isolated hepatocyte cultures and that IL-6 inhibits insulin mediated stimulation of glucokinase in isolated hepatocytes. Cortisol, glucagon and epinephrine, can produce insulin resistance [44]. These molecules oppose the actions of insulin and are termed counter-regulatory hormones. Since these counter-regulatory hormones are elevated, at least initially, after burn injury, it has been proposed that counter-regulatory hormones may play a role in burn induced insulin resistance. The levels of cytokines and counter-regulatory hormones are dramatically altered in burn patients and animal models [45,46]. It has been demonstrated that TNF suppresses insulin-induced tyrosine phosphorylation of insulin receptor, and inhibits downstream signaling from the insulin receptor [47,48]. Furthermore, the insulin resistance produced in spontaneously obese rats can be overcome by pretreatment of the animals with antibodies to TNF [49].

Although the number of investigations that address the mechanism(s) of insulin resistance in trauma patients has been limited, one important study [50] using the euglycemic insulin clamp technique demonstrated: (i) the maximal rate of glucose disposal is reduced in trauma patients; (ii) the metabolic clearance rate of insulin is almost twice normal in these patients; and (iii) post-trauma insulin resistance appears to occur in peripheral tissues, probably skeletal muscle, and is consistent with a post-receptor effect. Unfortunately, the procedures used in this study were not capable of independently accessing the contributions of glucose transport, phosphorylation, and subsequent intracellular metabolism of glucose. Ikezy*et al* [51] demonstrated that burn injury to rats resulted in impaired insulin-stimulated transport of [^{3}H]-2-deoxyglu-

http://dx.doi.org/10.5772/54849

cose into soleus muscle strips *in vitro*. These investigators also demonstrated that insulin stimulated phosphoinositide 3-kinase (PI3K) activity, that is pivotal for glucose transport in muscle by GLUT 4, was decreased by burn injury to rats as measured by its IRS-1 associated activity. These data are consistent with alterations in post-receptor signaling following burn injury, which results in burn induced insulin resistance and muscle wasting.

Dynamic and stress dependent multi-site phosphorylations of IRS-1 tyrosine, serine and threonine residues have been described to have both positive and negative insulin effects. IRS proteins contain a conversed pleckstrin homology (PH) domain located at their N termini and that anchors them to membrane phosphoinositides in close proximity to the insulin receptor. The PH domain is flanked by a phosphotyrosine-binding (PTB) domain. PhosporylatedSer/The residues in the PTB proximity are likely to dissociate IRS-IR binding and weaken insulin signaling. Tyrosine phosphorylations, in the N- or C-terminal regions of IRS-1 are generally considered to be positive PTM in the insulin signaling pathways. In other words, IRS-1 binds several Src homology 2 domain (SH2) proteins through its multiple tyrosine phosphorylation sites with YMXM or YXXM motifs to propagate the signal. In contrast, phosphorylations of serine and threonine residues at the C-terminal region are usually considered to be negative PTMs, however, some positive effects of serine phosphorylations have been reported. A number of phosphorylation sites have been identified with different approaches such as: radiolabeling with [γ-^{32}p] ATP [52,53,54,55,56], immunoblotting with anti-phosphopeptide antibodies [57,58,59,60,61,62,63,64,65,66], studies with mutated IRS-1 [67,68,69] and HPLC online or offline interfaced with MALDI-TOF or ESI-TOF [70,71,72,73,74]. The large variation and poor reproducibility in the reported phosphorylation sites are explained by: method sensitivities, enzymatic and chemical stabilities of the phosphorylated sites and stimulus intensity /timing. Proposed mechanisms for impairment of the insulin signaling system by phosphorylations of serine and threonine residues include: feedback inhibition, cooperative interactions, uncoupling of the protein signaling network [75,76,77,78, 79] and ubiquitin-proteasome degradation [80,81,82,83,84,85,86]. It is fair to state that, to date, burn-induced phosphorylations patterns of IRS-1 are poorly understood. However, since these negative biological effects may provide some clues for exploring the mechanism of insulin resistance [87,88,89], after burn injury [90,91], evaluation of this issue has become a major focus of our laboratory.

Determination of the phosphorylation pattern of IRS-1 is essential for understanding the metabolic basis for many disease processes [92]. However, neither the causative factors nor the cellular mechanisms of the muscle wasting and insulin resistance associated with the massive acute inflammation induced by burn injury have been elucidated. Recent publications suggest that insulin resistance may be in part due to phosphorylation based negative-feedback in two different pathways: 1) Phosphorylated Ser/Thr residues in the IRS-1 phosphorylated tyrosine binding (PTB) domain may simply uncouple downstream processes from the insulin receptor β - subunit, terminating downstream signal transduction without changing IRS-1 protein integrity. 2) Phosphorylated Ser/Thr sites may become proteolytic targets for CUL7 E3 ubiquitin ligase in a manner that depends on the mammalian target of rapamycin (mTOR) and p70 S6 kinase activities. These Ser/Thr sites located in the proximal C-terminal region of IRS-1

may provide multiple cleavage sites. Other studies have shown a role for SOCS-1 and SOCS-3 with the elongin BC ubiquitin ligase complex in IRS protein degradation.

There are 50 to 70 potential phosphorylation sites in IRS-1, and some of these sites up- and/or down-regulate insulin signaling [93,94]. Sequencing of the human genome has allowed the identification of more than 500 kinases and 60 phosphatases which may be involved in the regulation of IRS-1 binding under physiological conditions [95]. To date, approximately 29 Ser/Thr phosphorylation sites in IRS1 have been reported from various *in vivo* and *in vitro* experiments [96,97,98]. Unfortunately, no systematic IRS-1 phosphorylation data associated with burn injury is currently available. Mapping of all the phosphorylation sites of IRS-1 remains a challenge issue. One of the major reasons for this is that intact IRS-1 is present at very low concentrations (~ 51.9 ng/gram muscle tissues as described below); even in tissues in which it is most abundant such as soleus muscle. However, it is possible to analyze these phosphor-Ser/Thr residues in response to burn injury with tandem mass spectrometry.

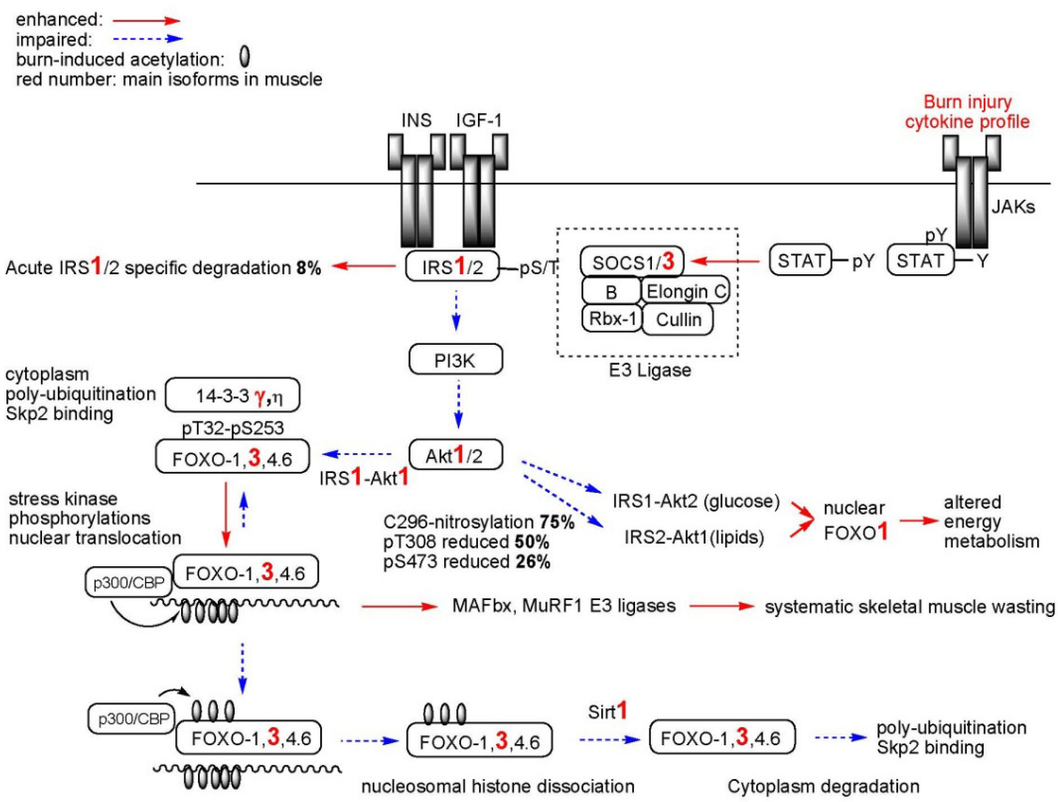

Figure 1. Insulin resistance and muscle wasting: unsymmetrical two tales in murine burn model. Insulin resistance and muscle wasting occurred at 10% and 70% likelihoods, respectively. IRS-1 integrity is reduced by 10% and thus is not a major caustic factor in downstream signaling. However, impaired Akt1/PKBα activity by 70% due to enhanced *S*-nitrosylation of Cys^{296} and reduction of phosphor-Thr^{308} and Ser^{473} has major impact on FOXO3 sub-cellular distribution and activities. Muscle wasting is significant in burned vs sham treated animals after day 3 post-burn injuries, but insulin resistance not significant under the same conditions.

http://dx.doi.org/10.5772/54849

We hypothesis that burn-induced PTMs that alter insulin sensitivity and muscle wasting occur not only at the IRS-1 level, but also at two critical downstream nodes: *S*-nitrosylated Cys^{296} in the Akt1 kinase loop and acetylated Lys residues in FOXO3. Specifically, (1) the docking platform integrity of IRS-1 may be partially disabled due to stress kinase mediated Ser/Thrphosphorylations which become E3 ligase targets. In other words, the reduction in glucose transport in skeletal muscle following burn injury may secondarily affect abundance and/or phosphorylation of IRS-1. (2) *S*-nitrosylated Cys^{296} interacts with phosphor-Thr^{308} in regulation of Akt1/PKBα kinase loop conformational changes which consequently inhibit kinase activity. (3) In addition of FOXO3 phosphorylation and reversible acetylation play major roles in transcriptional activities which trigger apoptosis and muscle wasting under the conditions of impaired Akt1/PKBα and IGF1 signaling as in the above two hypothesis. In contract to other biochemical approaches that are currently in use, all these PTM effects, such as E3 ligases cleaved IRS-1 fragments as well as site specific PTMs, can only be unambiguously analyzed with sensitive NanoLC-Q-TOF tandem mass spectrometry techniques. However, a major limitation of this approach is the low abundance of the signaling proteins for *in vivo* studies. Figure 1 illustrates the genesis of insulin resistance and muscle wasting at several crucial nodes: insulin resistance has been observed at 10% likelihood, while muscle wasting occurs at 70% likelihood in our murine models described below.

2. Materials

Methanol, acetonitrile (LC-MS Chromasolv, ACN), formic acid (FA), glacial acetic acid, LC-MS grade water, dithiotheretol (DTT) and iodoacetic acid, iodoacetamide, [Glu^1]-Fibrinopeptide B, methyl methanethiolsulfonate (MMTS), *S*-nitrosoglutathione (GSNO), sodium L-ascorbate, neocuproine, *N,N*-dimethylformamide (DMF), dithiothreitol (DTT), dimethyl sulfoxide (DMSO), Trypsin digestion kits (#PP0100), Phenylmethanesulfonyl fluoride (PMSF, cat# P-7626) and goat IgG were obtained from Sigma Chemical Co. (St. Louis, MO). SDS-PAGE ready gels (7.5%, #161-1100), SDS-PAGE ready gels (12 % Tris-HCl, #161-1102),SDS-PAGE ready gels (4-15% Tris-HCl, #161-1122), Laemmli sample buffer (#161-0737) and Coomassie brilliant blue R250 (#161-0436) were obtained from BIO-RAD (Hercules, CA, USA). Streptavidin agarose CL-4B was a product of Fluka (Cat#: 85881, Milwakee, WI). HPDP-Biotin (Cat#: 21341) and iodoacetyl-LC-Biotin (Cat#: 21333), immobilized monomeric avidin beads (Cat#: 20228), Iodoacetyl-LC-Biotin (Cat#: 21333) were purchased from Pierce (Rockford, IL).

Recombinant rat IRS-1 (#12-335, lot# 23015A purchased in 2005), assay buffer 5X (#20-145) and Mg^{++}/ATP 5X (#20-113), Anti-Akt1/PKBα monoclonal antibody (Cat# 05-798, Lot: 26860) and inactive Akt1/PKBα (Cat#: 14-279) were obtained from Upstate Technology (Lake Placid, NY, USA). Anti-ubiquitin (rabbit polyclonal, Ab19247) and anti-C-terminal IRS-1 (rabbit polyclonal, Ab653) antibodies were purchased from Abcam (Cambridge, MA, USA). Anti-N-terminal IRS-1 (rabbit polyclonal, SC560) was obtained from Santa Cruz Biotechnology (Santa Cruz, CA, USA). Protein G agarose (cat# 16-266) was obtained from Millipore (Billerica, MA, USA). Cell lysis buffer (cat# 9803), anti-FOXO3 rabbit antibodies (Cat#2497) were purchased from

Cell Signaling (Beverly, MA, USA). IRS-1 (total) ELISA kit (KHO0511), Akt pThr308 ElISA kit (KHO0201) and pSer473 kit (KHO0111) were purchased from Invitrogen (Carlsbad, CA, USA).

TRI reagent solution (cat# AM9738) was a product of Applied Biosystem (Framingham, MA, USA). 1-bromo-3-chloropropane (cat# BP 151) was purchased from Molecular Research Center, Inc. (Cincinnati, OH, USA). Qproteome cell compartment kit (Cat#: 37502) was obtained from Qiagen(Valencia, CA, USA).

The diet with depletion of L-Leu was obtained from Dyets, Inc., Bethlehem, Pennsylvania, DYET #510133, meets 1995 NRC nutrient requirements. [isopropyl-$^{2}H_{7}$]-L-Leu was product of Cambridge Isotope Lab (Andover, MA, USA).

Protein molecular weight markers (Cat#928-40000), secondary antibody (Cat# 926-3221, anti-Rabbit IgG) were purchased from LI-COR Biosciences (Lincoln, NE, USA). All PCR primers were obtained from the Massachusetts General Hospital primer bank.

3. Methods

3.1. Degradation of recombinant human IRS-1 stimulated with high insulin dose

Mammalian 293 cells were transfected with a recombinant IRS-1 FLAG tagged plasmid using a liposome reagent and Opti-MEM medium to deliver the plasmid DNA into the cells. Transfected cells were grown to confluence and placed in serum-free Dulbecco's modified Eagle's medium. The cells were then treated with insulin (1 μM) for 10 min. The medium was aspirated, and the cells were lysed in Reporter lysis buffer with phosphatase cocktail inhibitors containing 50 nM Potassium Bisperoxo(bipyridine)oxovanadate and 5 nMCalyculin A (Discodermia calyx) at 4°C. Fragments of Flag-IRS-1 C-terminal were immunoprecipitated with mAb to the first C-terminal 14 amino acid residues of IRS-1. The reaction mixtures were gently stirring in PBS (200 ml) at 4°C for 1 hr and excess mAb was removed with PBS (1 ml x 3). Flag-IRS-1 was released and cysteine residues were alkylated with Laemmli sample buffer (with 3% 2-mercaptoethanol, 100 mM DTT, 50 ml) for 5 min at 95°C and then 1 hr at room temperature under stirring. The reaction mixtures were separated by SDS-PAGE (7.5% Tris-HCl); IRS-1 bands stained with Coomassie brilliant blue R-250 were excised. In-gel trypsin digestion was performed (0.4 μg trypsin in 70 ml reaction buffer, 37°C, and overnight).

3.2. Mouse burn model

The protocol for the studies was approved by the Massachusetts General Hospital and Shriners Hospital for Children Animal Care Committees. Our animal care facility is accredited by the Association for Assessment and Accreditation of Laboratory Animal Care. Male CD-1 mice (Charles River Breeding Laboratories, Wilmington, MA, USA) weighing about 22-25 g were used. Sixteen animals were used for full thickness third degree burn injury produced under anesthesia (ketamine xylazine). After clipping of back hair, animals were placed in a template designed to expose 25% of their dorsum, and immersed into a water bath at 90?C for 9 second. After burn, the animals were immediately resuscitated with saline (2ml / mouse) by intraper-

http://dx.doi.org/10.5772/54849

itoneal injection. Buprenorphin (0.1 mg/kg, I.P.) was administered every 6-12 hours after injury. The sham group (n=5, matched for weight) was treated in the same manner as the burn group (n=14) with the exception that they were exposed to warm water (~36^{o}C). The mice were sacrificed by cervical dislocation and skeletal and liver were dissected and quickly placed in liquid nitrogen. All biological studies were performed with skeletal muscle excised from the animals at day 7 after burn injury or sham treatment.

3.3. Skeletal muscle preparation

Due to sequence analysis using NanoLC-Q-TOF tandem mass spectrometry for very low abundant IRS-1 in muscle, total whole body skeletal muscle (~2.5-3.0 g/animal) was evaluated; fast and slow twitch muscles could not be studied independently. The muscle groups studied included: trapezius, gluteus superficialis, rectus femorus, latissimusdorsi, shoulder deltoid, serratus anterior, vastusmedialis, semitendinosus, biceps femoris, adductor longus, gracilis, triceptsbrachi, soleus and rectus abdominus. The muscle was harvested by careful dissection which excluded skin, bone and other non muscular tissues. Immediately after dissection, tissue samples were immersed in liquid nitrogen. Frozen tissue samples were cut into pieces smaller than ~50 mg, and homogenized by 5 strokes over 30 seconds (full speed, model CTH-115, Cole Parmer). For tandem mass spectrometry, muscle tissue samples were processed in freshly prepared Cell Signaling lysate buffer (5 ml per gram tissue) containing fresh PMSF (1mM) on ice. Homogenates were sonicated briefly in ice cold water, and centrifuged at 14,000 g for 10 minutes at 4^{o}C. Supernatants were collected and stored at -80^{o}C for further studies.

3.4. IRS-1 in-gel digestion

skeletal muscle were processed in freshly prepared Cell Signaling lysate buffer (5 ml per 1 gram tissues) containing fresh PMSF (1 mM) on ice. The homogenates were sonicated briefly in ice-cold water, and centrifuged at 14,000 g for 10 minutes. The supernatants were collected and mixed with protein G agarose beads (100 ml, 50% slurry) for 2 hours to remove IgG and non-specific proteins. The protein G beads were removed by centrifugation at 14,000 g for 30 seconds. Anti-C-terminal IRS-1 antibody (Ab653, 2 ml) was added to the supernatants to immunoprecipite IRS-1 (overnight at 4^{o}C). The immune complexes were recovered by adding protein G agarose slurry (50%, 100 ml) with rotating for two hours at room temperature. The recovered beads (~ 50 ml) were washed (six times) with PBS (1 ml) and treated with Laemmli sample buffer (2X, 50 ml) containing 2-mercaptoethanol (3%, v/v, 100 mM DTT) at 95^{o}C for 5 min. SDS-PAGE separation and in-gel trypsin digestion were described as above.

3.5. Skeletal muscle IRS-1 ELISA

Mouse skeletal muscle tissue (20 mg) was homogenized with a TissueRuptor using a Qproteome cell compartment kit according to the manufacture's protocol. IRS-1 C-terminal fragments in cytosolic, membrane, nuclear and cytoskeletal fractions were measured using IRS-1 (total) ELISA kit. Homogenate aliquots (100 μl) from muscle tissue harvested from 16 burned and 8 sham treated muscle tissues were diluted with Standard Diluent Buffer (400 μl) provided from the ELISA kits. IRS-1 standard calibration curves were prepared according to

the manufacturer's protocol. Diluted tissue lysates (100 μl) were pipetted into the 96-well plates. The ELISA plates were gently shaken to capture IRS-1 at 4ºC overnight. Rabbit anti-ubiquitin antibody, rabbit anti-N-terminal IRS-1 antibody and rabbit anti-C-terminal IRS-1 antibody were diluted by 500 fold using horseradish peroxidase (HR) diluents at room temperature. After six washings (0.4 ml Wash Buffer, gentle shaking for 30 seconds) at room temperature, rabbit anti-IRS-1 antibody provided with the IRS-1 ELISA kit together with the three detection antibodies (100 μl) were pipetted into each well. Detection was performed by gentle shaking with the detection antibodies at room temperature for 1 hour. After removal of excess detection antibodies, anti-rabbit IgG-HRP antibody was added and analyzed according to the manufacturer's directions.

3.6. RT-PCR analysis of degradation pathways

To understand the roles of FOXO3 in skeletal muscle wasting as well as to evaluate FOXO3 degradation, we need to first distinguish FOXO3 and 14-3-3γ mediated proteasomal proteolysis (MuRF1, MAFbx/atrogin1) and lysosomal autophagy (Bnip3, Atg4a, Atg12, Gabarapl1) degradation pathways at the mRNA level. These studies will be performed in both thermally injured (n=16) and sham treated animals (n=6). Skeletal muscle excised from the animals on day 3,7 and 14 after burn injury or sham treatment is frozen, tissue samples (~50 mg) are cut into small pieces in RNase-free tubes, and homogenized with 5 strokes (5 seconds each) of an Omni TH-tissue homogenizer in sterilized Eppendorf tubes (2 ml) containing TRI reagent solution. RNA extraction is performed according to the TRI standard protocol. With this procedure the average 260nm/280nm ratio is ~ 1.95, and the RNA yield is ~1.2 μg/mg skeletal muscle. The quality of the isolated RNA is assessed with agarose gel electrophoresis. Samples are analyzed in triplicate using the comparative threshold cycle SYBR green method. Expression levels of target genes are corrected by normalization to the expression level of GAPDH, and relative expression levels are calculated: $\Delta C_t = C_t$(target gene)- C_t(GAPDH), $\Delta\Delta C_t = \Delta C_t$(burn) - ΔC_t(sham), targeted gene normalized to the endogenous reference is given by: $2^{-\Delta\Delta Ct}$. The primers that will be used for RT-PCR are tabulated below (F= forward, R=reverse):

FOXO3	F: CCTACTTCAAGGATAAGGGCGAC,	R: GCCTTCATTCTGAACGCGCATG
14-3-3γ	F: GGACTATTACCGTTACCTGGCAG,	R: CTGCATGTGCTCCTTGCTGATC
MuRF1	F: TACCAAGCCTGTGGTCATCCTG,	R: TCTTTTGGGCGATGCCACTCAG
Bnip3	F: GCTCCAAGAGTTCTCACTGTGAC,	R: GTTTTTCTCGCCAAAGCTGTGGC
Atg4a	F: CAGTCTCCACAGCGGATGAGTA,	R: GTGTGATGGGTGCTTCTGAACC
Atg12	F: GAAGGCTGTAGGAGACACTCCT,	R: GGAAGGGGCAAAGGACTGATTC
Gabarapl1	F: GTGGAGAAGGCTCCTAAAGCCA,	R: AGGTCTCAGGTGGATCCTCTTC
GAPDH	F: GTCTCCTCTGACTTCAACAGCG,	R: ACCACCCTGTTGCTGTAGCCAA

Table 1. PCR primers for proteasomal proteolysis and lysosomal autophagy analysis

http://dx.doi.org/10.5772/54849

Using these primers, GAPDH mRNA levels were not significantly different between burned and sham treated mice 16.12 ±0.93 vs 15.62±2.98 (p=0.162, unpaired t-test).

3.7. Mapping of Akt1/PKB*α* cysteine residues

Inactive Akt1/PKB*α* (10 μg, 0.18 nmol, in 10 μl stock solution) was transferred into a siliconizedEppendorf tube (0.6 ml) containing Laemmli sample buffer (2X,10 μl, pH adjusted to 8.0) and DDT (2 μl, 20 nmol, PBS, pH = 8.0) and the solution was kept at 95°C for 5 min. Freshly prepared iodoacetyl-LC-Biotin (15 μl, 55 nmol, in DMF) was added to the denatured protein solution followed by stirring for additional 15 min at room temperature. The resulting biotinylated Akt1/PKB*α*was purified by SDS-PAGE (4-15% Tris-HCl) and stained with Coomassie brilliant blue R-250. The protein bands were excised (~ 1 mm size) and digested (Akt1/PKB*α*: trypsin = 25, over night at 37°C) with a trypsin profile IGD kit. The biotinylated peptide mixture was captured by gentle stirring with streptavidin agarose CL-4B (30 μl packed) at room temperature for 1 hr (final vol. 100 μl). The streptavidin beads were washed with PBS (0.5 ml x 3), followed by water/acetonitrile (ACN 10%, 0.5 ml x 3). Biotinylated peptides were released from the streptavidin beads with formic acid (FA, 70%, 100 μl) at room temperature for 15 min with brief vortexing. The supernatant containing biotinylated peptides was transferred into a new vial and the formic acid was evaporated with a SpeedVac. The biotinylated peptide mixture was resuspended in water/acetonitrile (ACN, 2%, with 0.1% FA, 70 μl) and aliquots (10 μl) were analyzed.

3.8. Identification of disulfide bonds in inactive Akt1/PKB*α*

Inactive Akt1/PKB*α* (10 μg, 0.18 nmol, in 10 μl stock solution) was transferred into a siliconizedEppendorf tube (0.6 ml) containing Laemmli sample buffer (2X, 10 μl, pH = 8.0) and iodoacetamide (2 μl, 20 nmol, PBS, pH = 8.0). The mixture solution was kept at 95^{0}C for 5 min and stirred at room temperature for additional15 minutes. The Akt1/PKB*α*derivative was purified by SDS-PAGE (4-15% Tris-HCl) and stained with Coomassie brilliant blue R-250. The protein bands were excised (~ 1 mm size) and digested (Akt1/PKB*α*: trypsin = 25, overnight) with a trypsin profile IGD kit. Supernatant (~ 70 μl) was neutralized with formic acid (5 μl) and aliquots of the final solution (10 μl) were analyzed.

3.9. Analysis of NO acceptor sites in inactive Akt1/PKB*α*

Three samples of inactive Akt1/PKB*α* (10 μg, 0.18 nmol, in 10 μl stock solution) were treated with GSNO (250 nmol, 50 μl PBS, pH = 8.0) for 5 min at room temperature in the dark in siliconizedEppendorf tubes (0.6 ml). Separation of Akt1/PKB*α* and GSNO was achieved by two successive acetone/water precipitations (0.3 ml, 70% ACN) at – 40°C for 10 min. The supernatants (containing GSNO) were removed by centrifugation at 14,000 X g for 2 minutes. The kinase pellets were resuspended in blocking buffer (100 μl, 20 mMTris-HCl, pH 7.7, 2.5% SDS, 20 mM MMTS, 1 mM EDTA, 0.1 mMneocuproine) at room temperature for 1 hr with gently stirring (I mm ID X 5 mm bar). Excess MMTS was removed by acetone (100%, 0.3 ml) precipitation (as above) and the protein pellets were resuspended in PBS (50 μl, pH = 8.0). Freshly prepared iodoacetic acid (5 μl, 2 mM in PBS, pH = 8.0), Biotin-HPDH (5 μl, 2 mM in

DMSO), iodoacetyl-LC-Biotin (5 μl, 2 mM in DMF) and sodium ascorbate (20 μl, 5 mM, PBS) were added to the three vials containing nitrosylated Akt1/PKBα. The reaction mixtures were stirred at room temperature for 5 min (iodoacetic acid and iodoacetyl-LC-Biotin) or 1 hr for the thiol-disulfide exchange reaction. Aliquots of SDS sample buffer (2x, with 3% 2-mercaptoethanol, 100 mM DTT, 50 μl) were added to the protein solutions and the mixtures were incubated at 95°C for 5 min. The derivatized proteins were separated with SDS-PAGE Ready gels. The gels were stained with Coomassie brilliant blue R-250 and the Akt1/PKBα bands were excised as 1 X 1 mm pierces. The proteins were digested with the trypsin profile IGD kit. Carboxylmethylcysteine (CMC) containing peptides were neutralized with FA (5 μl) and sequenced via parent ion discovery trigged by the CMC immonium ion (134.02 ± 0.05 mDa). Biotinylated peptides were sequenced with data dependent acquisition after capture with streptavidin agarose beads. Ten μl aliquots of each final solution were analyzed.

3.10. Analysis of the Cys^{296}-Cys^{310} disulfide bond formation in Akt1/PKBα after treatment with *S*-nitrosoglutathione

Inactive Akt1/PKBα (10 μg, 10 μl, 0.18 nmol) and freshly prepared GSNO (5 μl, 250 nmol, PBS, pH = 8.0) were stirred in an Eppendorf tube (0.6 ml) in the dark at room temperature for 1 hr. Separation of Akt1/PKBα and GSNO was performed with acetone/water (70%) as above. The kinase pellet was resuspended in PBS (10 μl) and SDS sample buffer (with 100 mM of iodoacetamide, 10 μl, 1 mmol) was added. The cysteine alkylation was performed at room temperature for 15 min. The protein samples were separated with SDS-PAGE Ready gels and digested as above. Aliquots of the final solution (10 μl) were analyzed.

3.11. Measurement of the free and disulfide bonded Cys^{296} in Akt1/PKBα from soleus muscle of burned rats

The lysates (~10 mg/ml total soleus proteins) were diluted to about 3-5 mg protein / ml protein with PBS, and filtered through 0.22 μm membranes. Immunoprecipitation was performed as following: anti-Akt1/PKBαmAb (Upstate, clone AW24, 5 μg) and prewashed protein G agarose beads (50 μl, packed) were kept at 4°C for 1 hrs under gently stirring, without washing the beads, the soleus lysates (5 ml) were added and maintained under stirring for another 90 minutes. The non-specific proteins were washed with PBS three times, then treated with Laemmli sample buffer (pH adjusted to 8) containing acetyl-LC-Biotin (400 μM) at 95°C for 5 min. The procedures for SDS-PAGE separation and in-gel trypsin digestion were the same as described above.

3.12. Metabolic labeling with [isopropyl-$^2H_7$]-L-Leu and natural L-Leu Diets

The diet with depletion of L-Leu was obtained as L-amino acids defined diet for rats and mice. For producing the light diet, natural L-Leu was added to the diet powder (1% by weight) and producing the heavy diet, the same amount of [isopropyl-$^2H_7$]-L-Leu was added to the diet powder. For both diets, a minimal amount of water was added to make biscuits of adequate size. The biscuits were dried at room temperature for 1 week as suggested by Dyets in order to maintain the original nutrients. Burned and sham treated mice were caged separately and

http://dx.doi.org/10.5772/54849

maintained in a temperature controlled facility with a 12-h light/dark cycle. Burned mice were fed with the diet containing [isopropyl-$^2H_7$]-L-Leu and sham treated mice fed with the diet containing natural L-Leu. Five grams of light and heavy diets were provided daily to each mouse for 7 days. The animals had ad libitum access to water.

3.13. Biotinylation of Cys^{296} in Akt1/PKBα kinase loop

Following immunoprecipitation of metabolically labeled Akt1/PKBα, Laemmil sample buffer (50 μl, X2) was added to the washed immunocomplex beads (packed 50 μl, washed with PBS, 1 ml X three 5 min cycles). This was followed by addition of freshly prepared Iodoacetyl-LC-Biotin solution (10 μl, stock solution: 2 mg in 1ml of DMF). Cysteine acylation was performed at room temperature for 15 min with stirring. The reaction was quenched by addition of 2-mercaptoethanol (5 μl). The beads were then heated at 95^{o}C for 5 min and kept at room temperature for 30 min prior to loading on SDS-PAGE gels.

3.14. Avidin purification

Immobilized monomeric avidin beads (30 μl, 50 % aqueous slurry) were placed in siliconized polypropylene Eppendorf tubes (0.6 ml), and washed with PBS. The digested peptides (70 μl) were added to the packed avidin beads (15 μl) and the mixture was placed on a rocking platform for 30 min to capture the biotinylated peptides. Supernatant was collected, dried via Speed-Vac, and resuspended in mobile phase A (as described below, 15 μl) for control peptide ^{252}FYGAEIVSALDYLHSEK^{268} analysis. The beads were then washed with PBS (200 μl X 3), followed by ACN/water (10/90 = v/v, 200 μl X 3). The biotinylated peptides were recovered by addition of formic acid (30 μl, 70%) and gently rocking for 5 min at room temperature. This recovery step was repeated three time and the supernatants were combined, dried via Speed-Vac, and resuspended in mobile phase A (15 μl) for biotinylated loop peptide ^{290}ITDFGLCK^{297} analysis.

3.15. Measurements of skeletal muscle Akt1 pThr^{308} and pSer^{473}

According to the manufacture's protocols of the pThr^{308} and pSer^{473} ELISA kits, one unit of phosphorylation standard is defined as the amount of Akt pThr^{308} or pSer^{473} derived from 500 pg or 100 pg of Akt protein, which is phosphorylated by MAPKAP 2 and PDK 1. Muscle tissues lysates obtained with the Cell Signaling buffer described as above were used for measurement of Akt pThr^{308} and pSer^{473}. The phosphorylation levels were normalized to tissue weight.

3.16. Western blot and acetylation characterization of muscle FOXO3 post burn injury

Immunoprecipitations of muscle lysates from burned and sham treated mice were performed using anti-C-terminal antibody (sc-34895, 2 μg). SDS-PAGE was performed with 12% Ready Gels and protein molecular weight markers. Western blot analysis was performed with primary rabbit antibodies (Cell Signaling, Cat#2497, 20 μl + Tween-20, 20 μl + Odyssey blocking buffer, 20 ml) at 4^{o}C overnight, and secondary antibody (Odyssey, Cat# 926-3221, anti-Rabbit IgG 2 μl + Tween-20 20 μl + Odyssey blocking buffer, 20 ml) at room temperature for 1 hour.

The membrane was scanned over near-infrared range. Recombinant human FOXO3 was loaded onto the 12% Ready Gels with intact and reduced goat IgG. Two FOXO3 bands were also found with molecular weights of above 87 and 80 kDa as compared with intact IgG (150 kDa) and reduced IgG heavy chains (50 kDa). The FOXO3 bands were digested and analyzed for acetylation using DDA approach.

3.17. NanoLC-Q-TOF^{micro}

All experiments were performed using a Waters CapLC-Q-TOF^{micro} system (Waters Corporation, Milford, MA, USA). An analytical column (75 μm I.D. X 150 mm, Vydac C18, 5 μm, 300 A, LC Packings, Dionex Company, San Francisco, CA) was used to connect the stream select module of the CapLC and the voltage supply adapter for ESI. After washing with mobile phase C (auxiliary pump, 0.1% formic acid in water/acetonitrile, 2% acetonitrile) for 2 minutes, the trapped peptides were back washed from the precolumn onto the analytical column using the 10-position stream switching valve. A linear gradient was used to elute the peptide mixture from mobile phase A (0.1% FA in water/ACN, 2% ACN) to mobile phase B (0.1% FA in ACN). The gradient was segmented as follow: isocratic elution with 2% solvent B for 3 min, 2-80 % solvent B from 3 to 45 min and 80 to 2% B from 45-50 min. The gradient flow rate was adjusted to ~70 nl/min. The electrospray voltage was set to ~ 3000 V to obtain an even ESI plume. Sample cone and extraction cone voltages were set at 45 and 3 V, respectively. The instrument was operated in positive ion mode with the electrospray source maintained at 90^{o}C. The instrument was calibrated with synthetic human [Glu^{1}]-Fibrinopeptide B (100 fmol/μl in acetonitrile/water = 10:90, 0.1% formic acid, v/v) at an infusion rate of 1 μl/min in TOF MS/MS mode. The collision energy was set at 35 V. Instrument resolution for the [Glu^{1}]-Fibrinopeptide B parent ion, m/z = 785.84, was found to be ~5000 FWHM. Neutral loss for p-Ser and p-Thr parent ion discovery was set at 97.977 ± 0.03 Da with CE 35 and 5 V, respectively. All data were acquired and processed using MassLynx 4.1 software.

4. Results and discussion

4.1. Phosphorylated Ser/Thr triggers skeletal muscle IRS-1 C-terminal degradation

A total of 260 tryptic IRS-1 peptides, both doubly and triply charged under ESI, were located within the Q-TOF mass survey window setting (from m/z 400 to 1200). The chromatographic elution time window was ~30 min under our NanoLC gradient conditions and it was impossible to chromatographically separate the digested IRS-1 peptide mixture at the single peptide level; since many of the tryptic peptides overlapped. To overcome this problem, up to eight precursor ions were set for MS survey which provided secondary mass resolution in addition to the chromatographic separation. False positive precursor ions attributable to contaminations were eliminated by IRS-1 MS/MS sequence analysis. The NanoLC interfaced with Q-TOF settings that we used also had some false negative discoveries. These missed precursor ions may be due to their week hydrophobic properties (escaping from the trapping C18 column for desalting), week ionization, miss-digestion of large peptides and chemical alternations in

http://dx.doi.org/10.5772/54849

predictable peptide structures. However, the confidently identified precursor ions represent desirable candidate peptides for *in vivo* phosphorylation studies. Thus, unambiguously discovered peptides were selected as relative MS fingerprints for IRS-1 protein expression as well as PTM analysis in insulin treatment studies. Confirmation of the phosphorylation of Ser/Thr sites was performed by the following three step procedure: (1) Phosphorylated parent ion discoveries by MS survey via neutral loss (H_3PO_4) or phosphor-Tyr immonium ion approaches; the peptide mass tolerance was set at 0.2 Da; (2) Analysis of candidate parent ions with PepSeq of MassLynx V4.1 software to verify IRS-1 tryptic peptide sequences. Mercaptocysteine was searched as a fixed modification, whereas oxidation of methionine and phosphorylations were searched as variable modifications. (3) Confirmations of phosphorylated Ser/Thr sites with the diagnostic mass difference of 80.00 ± 0.15 Da (HPO_3 moiety) between phosphorylated and non-phosphorylated y or b ions, as well as phosphor-Tyr containing ions with S/N > 2. Figure 2, 3, 4 demonstrate the neutral approach to identify phosphor-Ser/Thr sites, while tryptic peptides containing phosphor-Tyr sites are as shown in Figure 5, 6, 7.

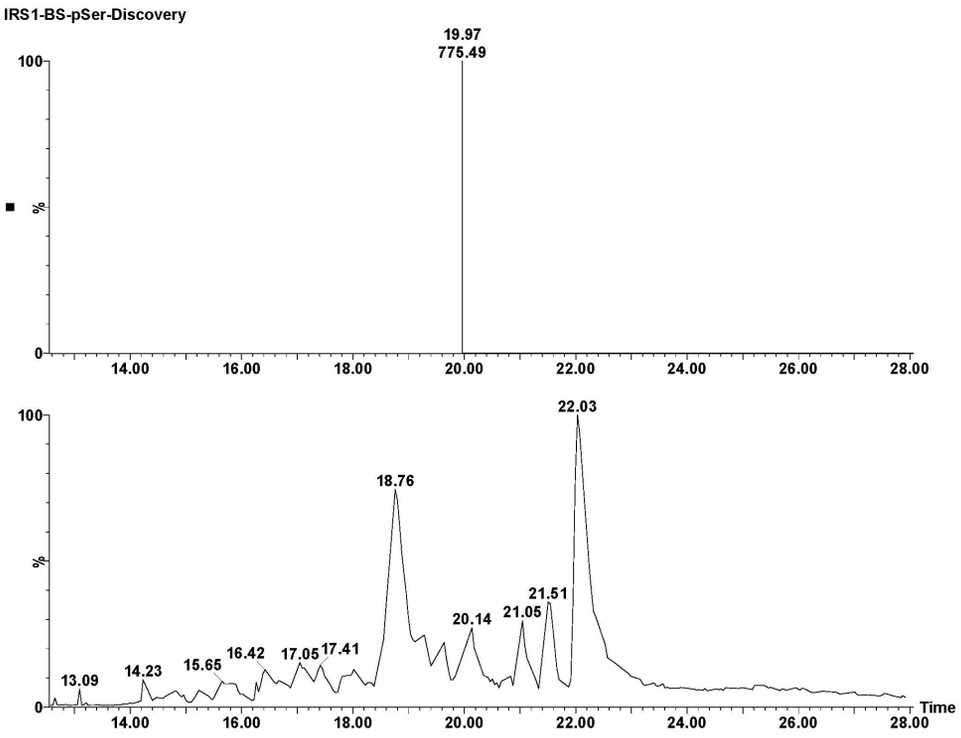

Figure 2. NanoLC base peak ion chromatogram of tryptic IRS-1 parent ion discovery with the neutral loss approach. Top panel: TOF MS/MS BPI chromatogram of IRS-1 doubly charged tryptic peptide ^{298}SRTESITATSPASMVGGKPGSFR^{320} (m/z 776.43), eluted at retention time 19.97 min, discovered with neutral loss of H_3PO_4. Bottom panel: TOF MS BPI neutral loss survey chromatogram obtained with collision energy 5 V.

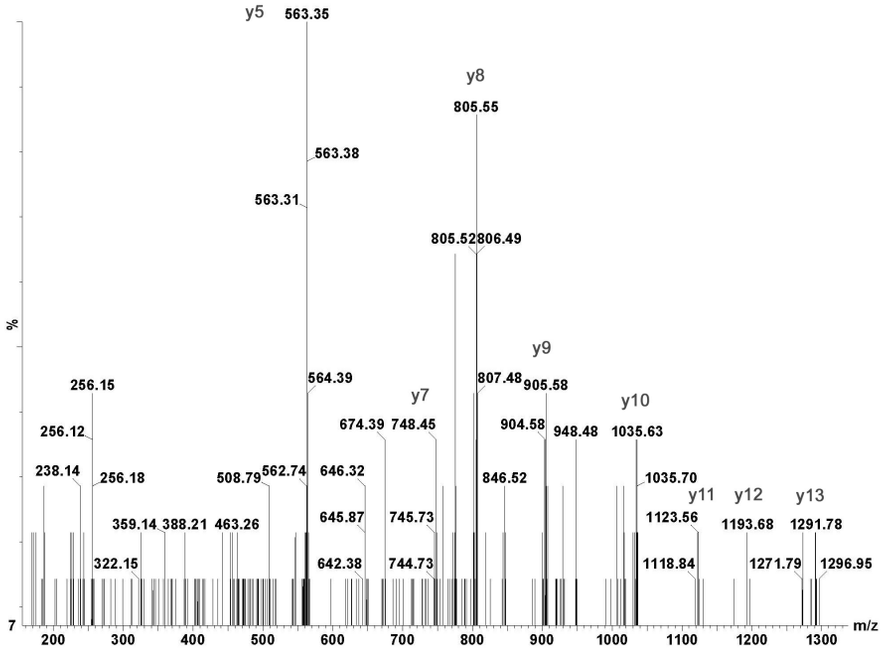

Figure 3. Sequence profile of IRS-1 phospho-Ser/Thr peptide acquisition triggered with the neutral loss approach. Doubly charged tryptic[298]SRTESITATSPASMVGGKPGSFR[320] (m/z 776.43) parent ion eluted at 19.97 min as shown in the top panel Figure 2. The y ion series ranging from y5 to y13 confirm the correct sequence.

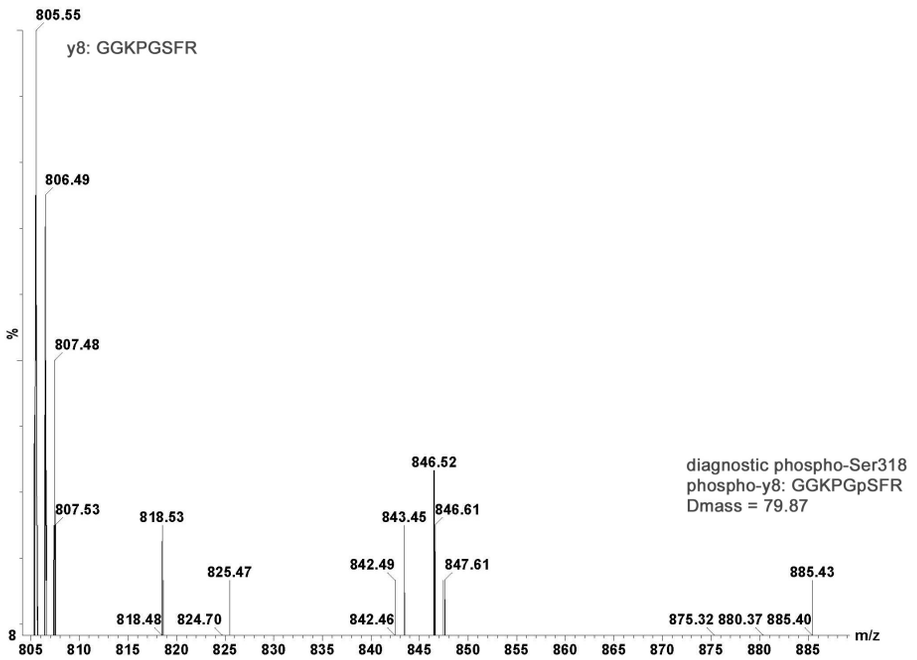

Figure 4. The zoom spectrum of Figure 3 shows diagnostic phosphor-Ser[318] in the [298]SRTESITATSPASMVGGKPGpSFR[320] peptide. Non-phospho-y8 ion (GGKPGSFR, m/z 805.56) and phosho-y8 ion (GGKPGpSFR, m/z = 885.43) indicates Δmass shift of 79.87 Da for HPO_3 modification.

http://dx.doi.org/10.5772/54849

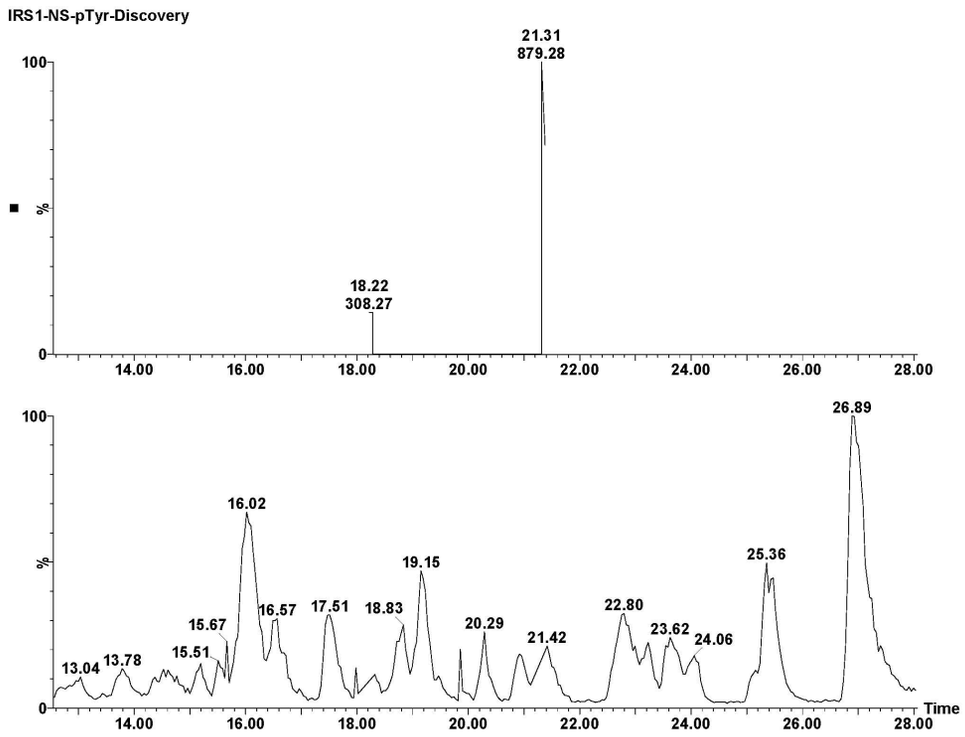

Figure 5. NanoLC base peak ion chromatogram of tryptic IRS-1 parent ion discovery with phospho-Tyr immonium ion approach. Top panel: phospho-Tyr parent ion eluted at retention time 21.31 min with triply charged m/z 879.28. Singly charged contaminant eluted at retention time 18.22 min with m/z 308.27. Immonium ion survey collision energy was kept between 5 and 100 V. Bottom panel: TOF MS BPI p-Tyr immonium ion survey chromatogram obtained with collision energy 5 V.

Having validated the site specific phosphorylation methods as described above, an *invitro* transfected IRS-1 model system was developed in order to analyze those stress induced phosphorylation sites and its degradation Typical MS/MS sequence data of insulin dependent phosphorylation sites pSer^{641} are shown in Figure 8.

The striking insulin dependent phosphorylation pattern indicates that pThr^{475}, pThr^{477} and pSer^{641} were induced by high dose insulin stress. These phosphorylated sites at high dose insulin stimulation provided the first clue for understanding possible mechanism(s) for insulin resistance up stream of the insulin/IRS-PI3K-Akt-FOXO and growth factors-PI3K-Akt-FOXO pathways. In order to evaluate IRS-1 degradation at these phosphorylation sites, SILAC was used for relative quantification of IRS-1 at the insulin dosage. Tryptic peptide T23 (^{162}EVWQVILKPK^{171}) labeled with heavy isotope (under insulin stress) and light isotopes (without insulin) was used as a mass marker to evaluate IRS-1 protein level. Relative peak areas of precursor peptides indicated that at least 50% of IRS-1 was degraded rapidly. The critical question is whether IRS-1 degradation is trigged at the three phosphorylated sites? The predicated C-terminal fragment cleaved at sites pThr^{475} /pThr^{477} is expected at 80,673 Da and the second fragment cleaved at site pSer^{641} expected at 64,441 Da. When C-terminal specific

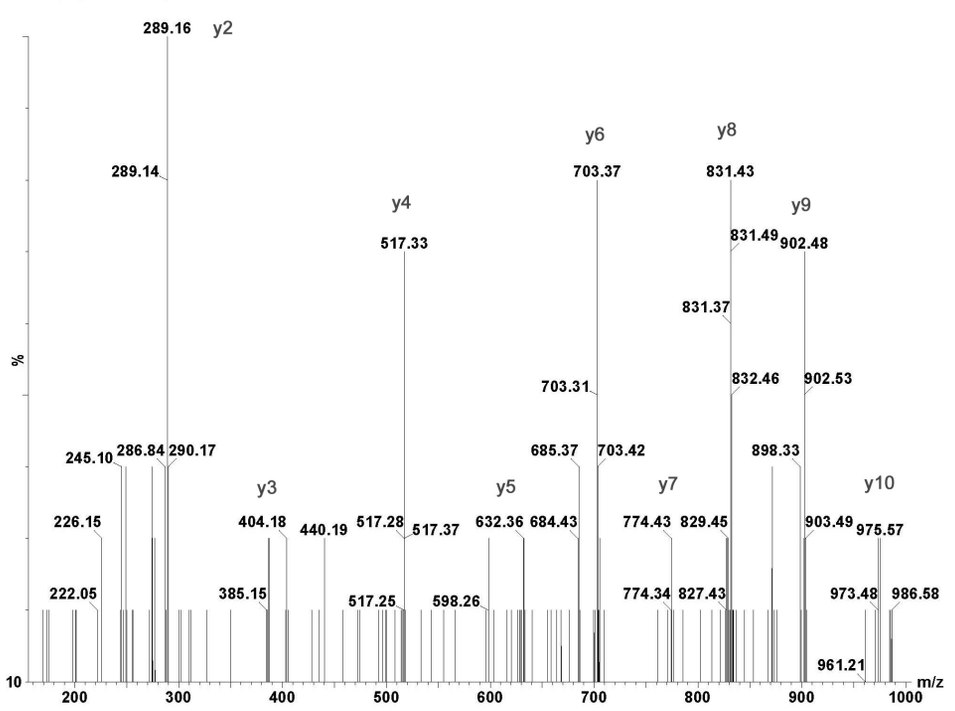

Figure 6. Sequence profile of phopspho-Tyr[489] peptide acquisition triggered with the immonium ion approach. Triply charged Parent ion [489]YIPGATMGTSPALTGDEAAGAADLDNR[515] (m/z 879.28)elutedat 23.31 min as shown in the top panel of Figure 5, MS/MS acquisition was obtained with collision energy of 35 V. The y ion series ranging from y5 to y13 confirmed the correct sequence.

mAb was used to repeat the insulin stimulation studies, SDS-PAGE showed that the IRS-1 band was reduced by ~50% with insulin stress as compared with the control; which is in agreement with the SILAC result. The multiple bands located between 50 kDa (IgG heavy chain) and 100 kDa (dimmer of heavy chain, 2-mercaptoethanol and DTT are not sufficient to achieve complete reduction of all disulfide bonds) were excised, digested and subjected to NanoLC-Q-TOF sequence analysis. The 65% sequence coverage confirmed that the FLAG tagged human IRS-1 bands were slightly lower in MW than the standard rat IRS-1 band. One fragment band (~ 80 kDa estimated from SDS-PAGE) was confirmed with two human IRS-1 sequences: [639]SVSAPQQIINPIR[651] and [1017]TGIAAEEVSLPR[1028]. At the same time the cleavage site precursor ion ([472]GPS$_P$TL$_P$TAPNGHYILSR[487]) was no longer detected. Another fragment band (~ 65 kDa from SDS-PAGE) was confirmed with [1017]TGIAAEEVSLPR[1028] only. For the same reason, the precursor ion ([639]SV$_p$SAPQQIINPIR[651]) corresponding to this cleavage was missed from our MS survey list. These three facts confirm a negative regulated mechanism: stressed cells at the high insulin dose activate unknown kinases to phosphorylate threonine and serine residues located in the middle of the C-terminus of IRS-1 (for human IRS-1, C-terminus refers from the PTB domain residue aspartic acid 262 to the last glutamine 1242) and the multiple phosphorylated sites may trigger the ubiquitin-proteosome pathway to yield these major fragments. The C-terminus of IRS-1 cleaved around pThr[475] /pThr[477] afforded the fragment with MW ~ 80 kDa, while the fragment with MW ~65 kDa was related to pSer[641]. The

http://dx.doi.org/10.5772/54849

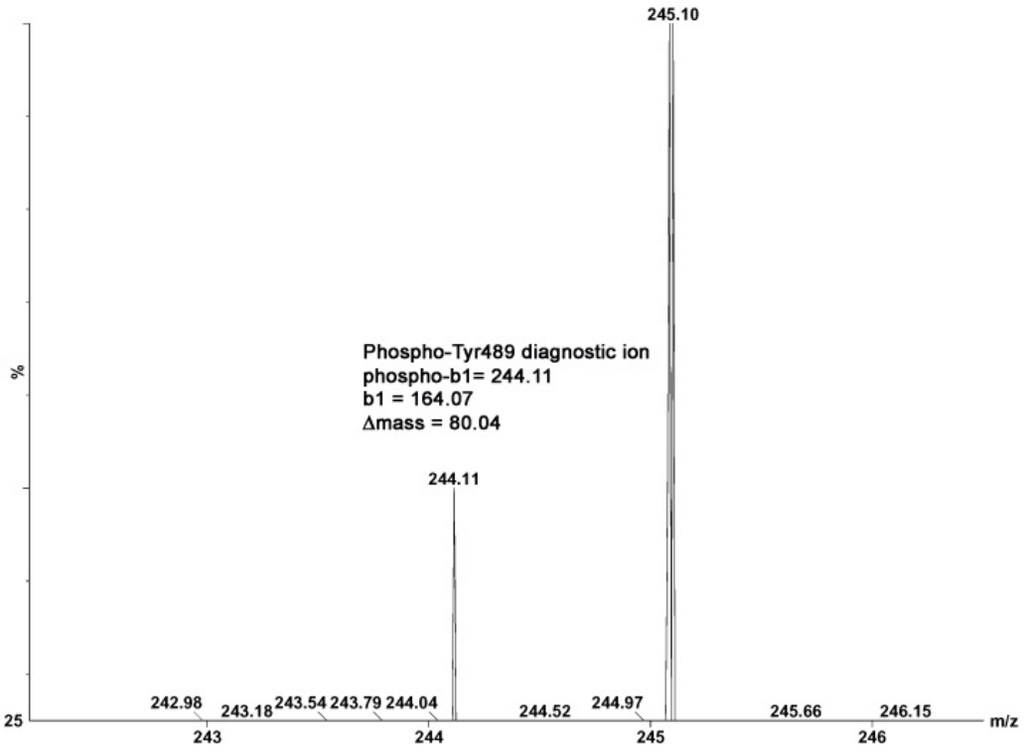

Figure 7. The zoom spectrum of Figure 6 shows Diagnostic phospho-Tyr[489] in the IRS1 triply charged parent ion [489]YIPGATMGTSPALTGDEAAGAADLDNR[515]. Non-phospho-b1 ion (Tyr, m/z 164.07) and phosho-b1 ion (pTyr, m/z = 244.11) indicates Δmass shift 80.04 for the HPO_3 modification.

observation that serine phosphorylation decreases insulin-stimulated tyrosine phosphorylation of IRS-1 and the observation of proteolytic turnover of the protein suggest the IRS-1 functions in both positive (N-terminal) and negative (C-terminal) feedback loops, The negative feedback is related to serine phosphorylation at the N-terminal half of the protein, with the C-terminal boundary at approximately amino acid residue 574 [99]. Positive signaling effects at low insulin dosages were associated with pSer[308], pThr[305] and pTyr[1012]. Phosphorylated Tyr[1012] may be the one of the downstream SH2 domain binding sites since it possesses the characteristic sequence YADM. Thus the sequence specific Ser/Thr kinase list might present pharmaceutical targets for modulating insulin resistance.

In vitro phosphorylation sites of rat IRS-1 C-terminal region provided "similarity" degradation references for further *in vivo* studies. The IRS-1 fragment sizes estimated from SDS-PAGE and their sequences are listed in Table 2.

For quantitative measurement of IRS-1 degradation in muscle of burned mice, additional studies were performed to explore sub-cellular distributions, C-terminal fragments and ubiquitinated IRS-1. An antibody specific to the 14 C-terminal amino acid residues of IRS-1 was used to capture IRS-1 irrespective of its post-translational modifications and integrity. Subsequently anti-ubiquitin, anti-C-terminal and anti-N-terminal polyclonal antibodies were used as the primary antibodies for ELISA analysis. The sub-cellular distribution of skeletal

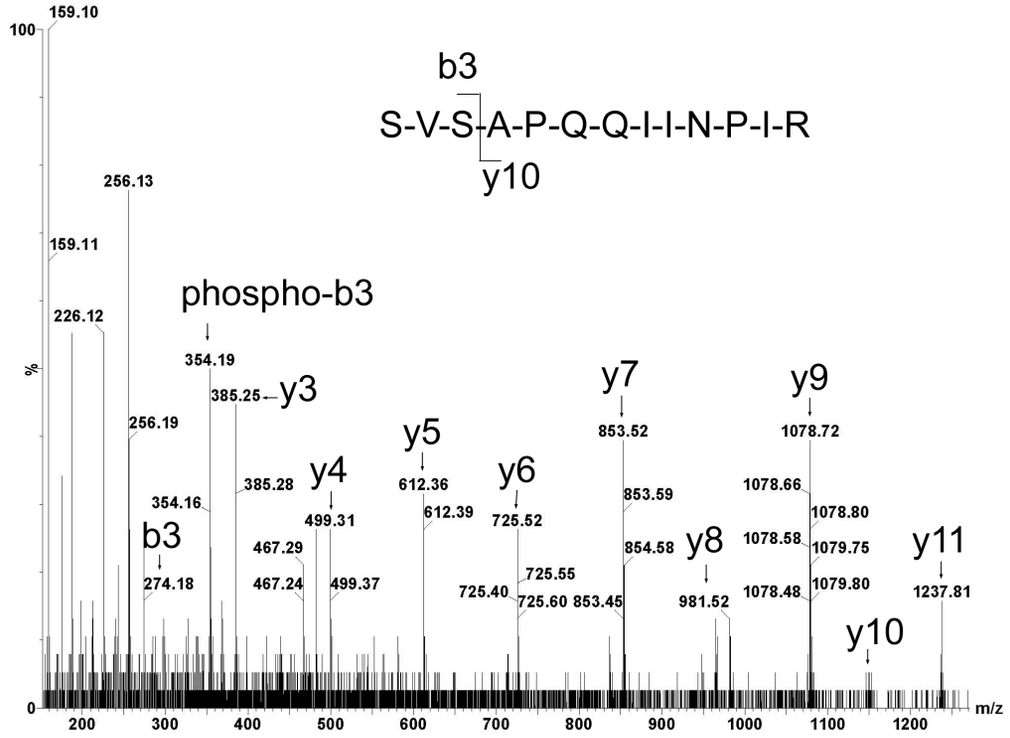

Figure 8. Analysis of pSer[641] peptide of recombinant human IRS-1 stimulated with high insulin dose. Doubly charged parent ion was discovered with the neutral loss approach: $[M+2H]^{2+}$ = 711.91, [639]SVpSAPQQIINPIR[651]. [639]Ser-Val, b2 ion = 187.12. No corresponding phosphorylated [639]Ser b2 ion was observed, however, [639]Ser-Val-Ser[641], b3 ion at m/z = 274.14 and phosphorylated b3 ion at m/z = 354.17 (Δmass = 80.03 Da), indicated phosphorylation of Ser[641] rather than Ser[639].

position	$M+H^+$	Sequence	Sequenced in SDS-PAGE bands (kDa)
1170-1180	1263.67	SLNYIDLDLAK	95, 44, 42
1156-1169	1363.61	ESAPVCGAAGGLEK	95, 44, 42
993-1010	1984.92	QSYVDTSPVAPVSYADMR	44
1135-1155	2242.11	HSSASFNVWLRPGDLGGVSK	95

Table 2. Tandem mass spectrometry (MS/MS) characterization of mouse skeletal muscle IRS-1 C-terminal fragments after burn injury

muscle IRS-1 post-burn injury is illustrated in Figure 9. The physiological distribution pattern in sham treated mice demonstrates nearly equal amounts of membrane bound IRS-1 (102.7 ng/g) and the IRS-1 in the cytosolic and nuclear compartments (49.1 and 44.9 ng/g). No detectable IRS-1 was observed in the cytoskeletal compartment.

The total cellular IRS-1 from the three compartments was found to be 196.7 ng/g. Results with the anti-N-terminal antibody data indicated that about 26.3% of the IRS-1 pool remained as intact protein. Thus, the majority of IRS-1 was present as C-terminal fragments. Ubiquitinated

http://dx.doi.org/10.5772/54849

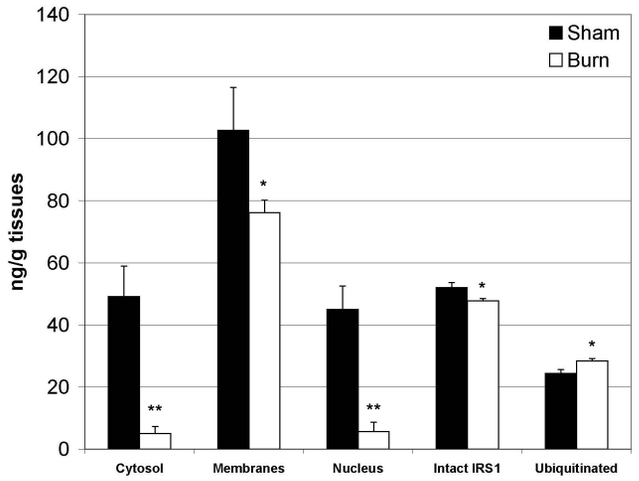

Figure 9. Quantitative measurement of IRS-1 integrity and sub-cellular distribution. IRS-1 was captured with anti-C-terminal mAb, and detected with anti-ubiquitin, anti-N-terminal, and anti-C-terminal rabbit polyclonal antibodies. For total intact and ubiquitinated IRS-1, sub-cellular components were isolated using a Qproteome cell compartment kit according to the Qiagen protocol. Values represent mean ± sem for 14 burned and 5 sham treated mice. *: $p<0.05$, **: $p<0.005$.

IRS-1 was found to represent 12.4% of total IRS-1. Burn-induced changes in the sub-cellular distribution of IRS-1 were clearly driven by the 15.9 % increase in ubiquitination. Consequently, total IRS-1 in the three sub-cellular compartments was reduced by 55.8%, while intact cellular IRS-1 was decreased by 7.7%. A striking feature revealed from the sub-cellular distribution pattern of IRS-1 is that equilibrium between the cytosolic and nuclear compartments occurs by day 7 after burn injury.

The level of intact IRS-1 protein was found to be only ~51.9 ng/g in the skeletal muscle, which is too low to map phosphorylation sites with tandem mass spectrometry. However, those burn-induced phosphor-Ser/Thr sites provide one to get into the insight of the mechanism of insulin resistance and muscle wasting at the initial Ins/Ir/IRS-1 signaling transduction level. On the other hand, with the mixed-muscle preparations that were evaluated, it was not possible to determine the percentage of slow and fast twitch fibers. These issues in conjunction with the small amount of skeletal muscle harvestable from mice, the low level of IRS-1 in muscle and the low sensitivity of the site specific MS/MS sequencing for low abundant phosphorylated residues are an unavoidable limitation of current studies. The *in vitro* and *in vivo* IRS-1 data suggest that in 8-10 week old mice with burn injury insulin resistance occurs in only ~10% of the animals. The observations that significant muscle wasting occurs both clinically and in animal models (~70% of animals) suggest a pivotal role for downstreamAkt1/PKBα.

4.2. *S*-nitrosylated Cys^{296} catalyzes disulfide bond formation with Cys^{310} in Akt1/PKBα | | active loop

Akt1/PKBα is a central mediator of the IR/IRS/ PI3K/FOXO pathway. In addition, to the role of reversible phosphorylation/ dephosphorylation at Thr^{473} and Ser^{308} in its regulation, reversible inactivation can also be mediated by *S*-nitrosylation at cysteine residues. We performed *in vitro* and *in vivo* studies to verify this hypothesis. Here, for the first time, tandem mass spectrometry data revealed that *S*-nitrosylated Cys^{296} mediates kinase loop conformational changes mediated via *S*-nitrosylation and phosphorylation.

For the *in vitro* studies, Akt1/PKBα was *S*-nitrosylated with the NO donor *S*-nitrosoglutathione (GSNO) and derivatized by 3 methods. The derivatives were isolated by SDS-PAGE, trypsinized and analyzed by tandem MS. For the *in vivo* studies, Akt1/PKBα in muscle lysates from burned rats was immunoprecipitated, derivatized with HPDP-Biotin and analyzed. The *in vitro* studies provided unambiguous MS fingerprints for the *in vivo* studies. The *invivo* studies demonstrated that NO free radical reacts with the free thiol of Cys^{296} to produce a Cys^{296}-SNO intermediate which accelerates interaction with vicinal Cys^{310} to form a Cys^{296}-Cys^{310} disulfide linkage, at the same time, dephosphorylation at Thr^{308} was observed. The disulfide bond between Cys^{296} and Cys^{310} was not detected in lysates from sham animals. As a result of this dual effect produced by burn injury, the loose conformation that is slightly stabilized by the kinase loop Lys^{297}-Thr^{308} salt-bridge may be replaced by a more rigid structure which may block substrate access and down-regulate activity. *S*-nitrosylated C^{296}, located inside the Akt1 activity loop, was observed in tryptic peptide ITDFGLCK. Also, significant reductions in phosphorylation of Ser^{473} and Thr^{308} of Akt1 were measured as 26.2% ($p<0.05$) and 49.8% ($p<0.005$), respectively.

Akt1/PKBα consists of three structural features: the N-terminal pleckstrin homology (PH) domain, a large central kinase domain and a short C-terminal hydrophobic motif. High specific binding of the PH domain with membrane lipid products of PI3-kinase recruits Akt1/PKBα to the plasma membrane where phosphorylations of Thr^{308} in the kinase domain and Ser^{473} located in the C-terminal hydrophobic motif occur. Phosphorylation of Thr^{308} partially stimulates kinase activity; however, additional phosphorylation of Ser^{473} is required for full activity. Activation is associated with a disordered to ordered transition of a specific αC helix of Akt1/PKBα via an allosteric mechanism. A salt bridge between the side-chain of Lys^{297} and the phosphate group of $pThr^{308}$ in this αC helix contributes to an ordered activation segment from ^{292}DFG to APE^{319} [99,100,101,102]. Reversible dephosphorylations of Thr^{308} and Ser^{473} by protein phosphatase 2A (PP2A) and PH domain leucine-rich repeat protein phosphatase (PHLPPα) also occur in the Akt1/PKBα activation/deactivation cycle [103,104,105,106]. In addition to the role of reversible phosphorylation/dephosphorylation in the regulation of Akt1/PKBα activity, this kinase is also reversibly inactivated by *S*-nitrosylation under conditions that result in persistently increased production of nitric oxide; such as after burn injury [107,108,109,110]. Thiol titration and NMR data indicate that a disulfide bond (Cys^{60}-Cys^{77}) exists in the kinase PH domain [111]. A second disulfide bond in the critical kinase activation loop (Cys^{297}-Cys^{311}) has been reported to be associated with dephosphorylation under oxidative stress *in vitro*[112]. In addition, it has been shown that when Cys^{224} of Akt1/PKBα is mutated to a Ser residue, the

http://dx.doi.org/10.5772/54849

kinase becomes resistant to NO donor-induced *S*-nitrosylation and inactivation; suggesting that this residue is a major *S*-nitrosylation acceptor site [109]. *In vivo*S-nitrosylations of the insulin receptor (β) and Akt1/PKBα result in reductions in their kinase activities [108]. These data suggest that the redox status of Akt1/PKBα, regulated by NO, is a second factor in the post translational modifications that modulate kinase activity (via dynamic conformational changes) and thus GLUT-4 trafficking and cellular FOXO translocation. Nevertheless, up to now, published data on the reversible phosphorylation(s) and *S*-nitrosylation(s) relevant to Akt1/PKBα activation, conformation and regulation have not provided conclusive information about their interrelationships nor critical *S*-nitrosylation sites involved in the kinase activation/deactivation cycle.

Recent technical developments have made it feasible to study the molecular details of these important processes. These techniques include: 1. sensitive and site-specific procedures for the detection of *S*-nitrosylation based upon NanoLC interfaced with tandem MS/MS; 2. the Biotin-Switch method for qualitative discrimination of thiol state between free, disulfide bonded and *S*-nitroylated cysteine residues under carefully defined conditions [113,114,115,116,117,118]; and 3. highly specific anti-Akt1/PKBαmAb's that can be used to immunoprecipitate quantities of the protein that are sufficient to yield SDS-PAGE bands with Coomassie brilliant blue R-250 staining which are compatable with tandem MS analysis.

The following issues need to be taken in considerations: 1. the ability of Cys^{296} to chemically quench elevated levels of free radicals, specifically nitric oxide; 2. loop conformational changes associated with two types of PTM; 3. quantitative proteomics of Akt1/PKBα by stable isotope labeling in mice. We obtained MS/MS sequence data to characterize the thiol states of Cys^{296} in the kinase activity loop of Akt1/PKB. These measurements were possible despite the extremely low level of nitrosylated protein (at the 10^{-15}pmol level, the chance of positive hits is ~25% with lysates prepared from 25 mg of soleus muscle). The biochemical role of *S*-nitrosylation at Cys^{296} was characterized as an intermediate state which reduces the kinetic barrier to form the disulfide bond with Cys^{310} within the activity loop. This occurs simultaneously with dephosphorylation of $pThr^{308}$ after burn injury. The facts that no other disulfide bonds associated with Cys^{296} were detected suggest that they may be thermodynamically forbidden; due to geometry and/or dihedral angle strain. The data obtained with soleus muscle from burned and sham treated rats indicates that NO mediated formation of the Cys^{296}-Cys^{310} disulfide bond (which likely down-regulates kinase activity) plays a reciprocal role with formation of a Lys^{297}-$pThr^{308}$ salt bridge (which up-regulates kinase activity) during disease associated reversible activation/deactivation processes.

To further the proof-of-concept about formation of a Cys^{296}-Cys^{310} disulfide bridge after burn injury, metabolically labeled Akt1/PKBα was characterized with NanoLC-Q-TOF tandem mass spectrometry based on the classic isotope dilution principle. Akt1/PKBα in liver extracts from mice with burn injury that were fed with [$^2H_7$]-L-Leu was immunoprecipitated and isolated with SDS-PAGE. Two tryptic peptides, one in the kinase loop and a control peptide just outside of the loop were sequenced. Their relative isotopologue abundances were determined by stable isotope labeling by amino acids in mammalians (SILAM)[119]. Relative quantifications based on paired heavy/light peptides were obtained in 3 steps. 1. Homogeni-

zation of mixtures of equal amounts of tissue from burned and sham treated animals (i.e., isotope dilution) and acquisition of uncorrected data based on parent monoisotopic MS ion ratios; 2. Determination of isotopic enrichment of the kinase from burned mice on Day 7; and 3. Enrichment correction of partially labeled heavy and light monoisotopic MS ion ratios for relative quantification of bioactivity (loop peptide) and expression level (control peptide). Our data demonstrate that protein synthesis and enrichment after injury were dependent on tissue and turnover of individual proteins. Three heavy and light monoisotopic ion ratios for albumin peptides from burned mice indicated ~55% enrichment and ~16.7 fold down regulation. In contract, serum amyloid P had ~66% enrichment and was significantly up regulated. Akt1/PKBα had ~56% enrichment and the kinase level in response to burn injury was up regulated compared with the control peptide. However, kinase bioactivity, represented by the Cys^{296} peptide, was significantly reduced. Overall, we demonstrate that 1. Quantitative proteomics can be performed without completely labeled mice; 2. Measurement of enrichment of acyl-tRNAs is unnecessary and 3. Cys^{296} plays an important role in kinase activity after burn injury.

Stable isotope labeling by amino acids in cell culture (SILAC) provides relative quantification of *in vitro* protein synthesis and functional proteomics under conditions that mimic disease states [120,121,122,123,124]. Typically, two cell populations are cultured for six doublings times; control cell medium contains the natural amino acid (e.g., $^{12}C_6$-Lys and/or $^{12}C_6$-Arg, 99% natural abundance), and the second medium contains the same levels of amino acids with heavy isotopes (e.g., $^{13}C_6$-Lys and/or $^{13}C_6$-Arg, 98% abundance) and disease related stimuli. The two cell populations are mixed with equal amounts of total proteinand digested peptides are accurately measured by mass spectrometry with a mass difference of 6 Da for singly charged parent ions. Six doubling times allows isotopic enrichment of the precursor acyl-tRNA pool to reach ~98% in cancer cell lines. Labeling above 95% is generally required for comparative and quantitative proteomics by MS. Thus, the relative abundance of any paired peptide's monoisotopic MS ion chromatogram with SILAC can be used to measure protein synthesis in comparison with the controls under *in vitro* conditions. The SILAC approach has been used with *C. elegans*fed with >98% ^{15}N labeled *E. coli* [125], skeletal muscle from chickens fed with a synthetic diet containing 50% of [$^2H_8$]-Val [126,127], partially labeled rat diet with >99% ape ^{15}N algal cells for 44 days [128] and F1-F4 offspring of mice fed with lysine-free diet containing 1% of L-$^{13}C_6$-Lys [129]. Complete labeling has been reported to be achieved by the F2 generation. Metabolic labeling with ^{15}N can be performed efficiently and economically, however, data interpretation can be challenging since the monoisotopic peak can shift, due to the distribution of positional isotopomers as a function of labeling time [130,131]. Global labeling with ^{15}N has been used as a tool for characterization of enrichment under partially labeling conditions [132,133,134]. Stable isotope labeled amino acids, such as L-$^{13}C_6$-Lys and L-$^{13}C_6$-Arg, provide ideal residues at C-terminal labeling positions for trypsin digestion. Protein synthesis depends on 2 factors: acyl-tRNA levels and protein turnover rate. These factors are tissue, cell type, time and treatment dependent. To minimize individual variability, full incorporation of L-$^{13}C_6$-Lys can be achieved in mice; however, it is very costly.

Analysis of the hypermetabolic/inflammatory response under acute phase conditions is very challenging for several reasons: 1. Significant changes in protein expression are associated with

http://dx.doi.org/10.5772/54849

high levels of reactive oxygen species (ROS) and post translational protein modifications; i.e. not only protein levels but also biological activities have to be quantified; 2. Individual protein enrichments and incorporated isotope distributions may vary with the partially isotope enriched precursor t-RNA pool (>50%) and corresponding protein turnover rates during the acute phase response.

To address these considerations and explore the feasibility of the basic SILAC approach in animals under acute phase and partial isotope labeling conditions, a mouse model with full-thickness 40% TBSA burn was used to proteomically characterize liver Akt1/PKBα|| from the perspectives of both protein expression and biological activity. [Isopropyl-$^2H_7$]-L-Leu was selected for labeling based on 4 considerations: 1. L-Leu is an essential amino acid with high abundance in proteins. 2. Compared with other amino acids, [isopropyl-$^2H_7$]-L-Leu is relatively inexpensive; 3. None of the 7 deuterium atoms of [isopropyl-$^2H_7$]-L-Leu are attached at the α-carbon which may be exchangeable with hydrogen atoms; thus in contrast to studies with [$^2H_{10}$]-Leu, MS offset can be eliminated as a confounding variable; 4. The hydrophobicity of L-Leu reduces false negative discovery during C18 reversed phase trapping and desalting.

It has been reported that NO production is elevated by stressors such as burn injury and in patients with type 2 diabetes [110,135,136]. It has also been shown that the Cys^{297}–Cys^{311} disulfide bond in the critical kinase activation loop of Akt1/PKBα may be formed in association with dephosphorylation under oxidative stress *in vitro* [112]. Thus, we hypothesized that reversible *S*-nitrosylation at either Cys^{296} or Cys^{310} in the kinase active loop may be a PTM factor which complements reversible phosphorylation at Thr^{308} in the regulation of kinase activity and sought to determine how *S*-nitrosylation interacts with phosphorylation during the Akt1/PKBα activation cycle [103]. To address these issues, GSNO was used as the only NO donor in a model *S*-nitrosylation system to randomly target the seven cysteine residues of the kinase at pH = 8. The nucleophilic role of sulfhydryl groups is well documented and it is clear that cysteine residues located in the enzyme hydrophobic loop are important catalytic entities in both transfer and addition reactions. Vicinal Cys^{296} and Cys^{310} take advantage of the pK_a for dissociation of the thiol to thiolate and these electron-rich thiolate groups can lead to formation of an intradomain disulfide bond [137].Therefore, Cys^{296} and Cys^{310} are potential *S*-nitrosylation sites as predicted from the 3D structure of the kinase. NO donors, such as thioredoxin and thiol/disulfide oxidoreductases were excluded from the system to prevent possible interferences [138,139], however, a small amount of 2-mercaptoethanol (~0.05% v/v) was necessary to prevent oxygen effects.

The simple, but well-defined, *S*-nitrosylation reaction model was used to probe for particular NO acceptor sites in human Akt1/PKBα (inactive, 89% pure containing 2-mercaptoethanol and EGTA, Upstate) in three steps: A. Mapping of all cysteine residues with DTT reduction, iodoacetyl-LC-Biotin alkylation and affinity capture provided relative MS ionization efficacies and charge states; B. Detection of disulfide bonds with and without GSNO, provided an understanding of NO-mediated disulfide bond formation. C. MS/MS pinpointed the *S*-nitrosylated sites with three different thiol-specific derivatives. False negatives may occur with the Biotin-Switch method, whereas false positives are more common with the other methods, however, thiolether derivatives can be identified with MS/MS data. The findings of these

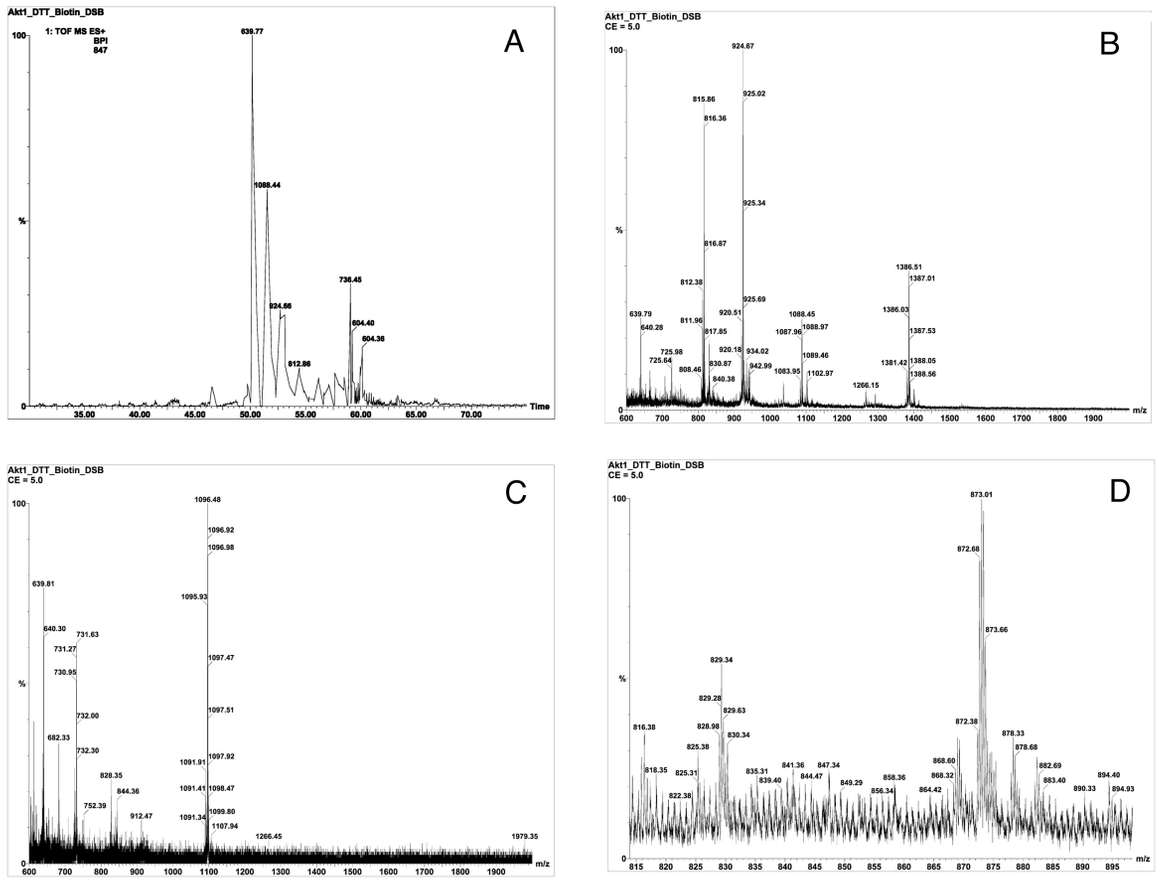

Figure 10. Mapping of cysteine residues in inactive Akt1/PKBα (a) Base peak intensity (BPI) NanoLC chromatogram of affinity capture of all seven cysteine residues that were biotinylated with iodoacetyl-LC-Biotin (b) TOF MS analysis of parent ions co-eluted at retention time of ~53 min. Parent ions m/z 924.67 and m/z 1386.51 are triply and doubly charged ions from the same tryptic peptide ^{308}TFCGTPEYLAPEVLEDNDYGR^{328} which contains Cys^{310}. Parent ion m/z 1266.09 is a triply charged ion from the tryptic peptide, ^{437}YFDEEFTAQMTITPPDQDDSMECVDSER^{465}, which contains Cys^{460}. Parent ion m/z 815.87 is a doubly charged ion derived from the tryptic peptide, ^{77}CLQWTTVIER^{86}, which contains Cys^{77}. The parent ion at m/z 1088.49 results from CH_4 neutral loss from m/z 1096.46 as shown in Figure 10C. (c) TOF MS analysis of parent ions co-elutting at retention time of ~50.8 min. Parent ions m/z 731.33 and m/z 1096.46 are triply and doubly charged ions from the same tryptic peptide, ^{49}ESPLNNFSVAQCQLMK^{64}, which contains Cys^{60}. Parent ion m/z 639.79 is doubly charged and is derived from tryptic peptide, ^{290}ITDFGLCK^{297}, which contains Cys^{296}. (d) TOF MS analysis of parent ions co-eluting at retention time of ~53.5 min. Parent ion m/z 829.00 is triply charged and derived from tryptic peptide, ^{329}AVDWWGLGVVMYEMMCGR^{346}, which contains Cys^{344}. Parent ion m/z 872.70 is triply charged and derived from tryptic peptide, ^{223}LCFVMEYANGGELFFHLSR^{241}, which contains Cys^{224}.

studies were used to study the biological consequences of *S*-nitrosylation of Akt1/PKBα in soleus muscle from burned rats. This *in vivo* system was used because soleus muscle is an insulin sensitive tissue with relatively high levels of IRS-1.

A base peak intensity (BPI) Nano-LC chromatogram of all seven affinity captured cysteine residues that were biotinylated with iodoacetyl-LC-Biotin is shown in Figure 10A. Cysteine residue monoisotopic mass of C_3H_5NOS = 103.01 Da was replaced with derivatizedCys residue monoisotopic mass of $C_{21}H_{35}N_5O_4S_2$ = 485.21 Da. The relative simplicity of the NanoLC

http://dx.doi.org/10.5772/54849

chromatogram indicates the high purification efficacy for removing non-biotinylatedtryptic peptides from streptavidin agarose beads. Three predominate TOF MS tryptic parent ions were identified; m/z 639.81 (T41, $M+2H^+ = 639.83$) eluting at 50.5 min, m/z 1088.49 (T9, $M-CH_4+2H^+ = 1088.03$) at eluting at 51.5 min and m/z 924.67 (T44, $M+3H^+ = 924.43$) eluting at 53 min are doubly and triply charged tryptic peptides containing Cys^{296}, Cys^{310} and Cys^{60}, respectively. Figure 10B shows the parent ions co-eluting at ~ 53 min as well as the charge state assignments. Parent ions m/z 924.67 (T44, $M+3H^+ = 924.43$) and m/z 1386.51 (T44, $M+2H^+ = 1386.14$) are triply and doubly charged ions from the same tryptic peptide, ^{308}TFCGTPEYLAPEVLEDNDYGR^{328}, which contains Cys^{310}. Parent ion m/z 1266.09 (T58, $M+3H^+ =1266.41$) is triply charged and derived from the peptide, ^{437}YFDEEFTAQMTITPPDQDDSMECVDSER^{465}, which contains Cys^{460}. Parent ion m/z 815.87 (T11, $M+2H^+ = 815.93$) is doubly charged from the peptide, ^{77}CLQWTTVIER^{86}, which contains Cys^{77}. Parent ion m/z 1088.49 resulted from CH_4 neutral loss from m/z 1096.48. Figure 10C shows TOF MS parent ions that co-eluted at ~50.8 min; chromatographic peak tailing the most intense peak at 50.5 min. Parent ions m/z 731.33 (T9, $M+3H^+ = 731.03$) and m/z 1096.46 (T9, $M+2H^+ = 1096.04$) are triply and doubly charged ions from the same tryptic peptide, ^{49}ESPLNNFSVAQCQLMK^{64}, which contains Cys^{60}. Parent ion m/z 639.81 (T41, $M+2H^+ =639.83$) is a doubly charged ion from the tryptic peptide, ^{290}ITDFGLCK^{297}, which contains Cys^{296}. Figure 10D shows the TOF MS parent ions that co-eluted at ~53.5 min. Parent ion m/z 829.00 (T45, $M+3H^+ = 829.05$) is triply charged and derived from the tryptic peptide, ^{329}AVDWWGLGVVMYEMMCGR^{346}, which contains Cys^{344}. Parent ion m/z 872.70 (T32, $M+3H^+ = 872.43$) is triply charged and derived from the tryptic peptide, ^{223}LCFVMEYANGGELFFHLSR^{241}, which contains Cys^{224}. No doubly charged T58, T45 or T32 ions were observed. It is clear that the ionization efficacies for the peptides containing Cys^{296} ($M+2H^+$), Cys^{310} ($M+2H^+$ and $M+3H^+$), Cys^{60} ($M+2H^+$ and $M+3H^+$) and Cys^{77} ($M+2H^+$) are much higher than for the triply charged peptides containing Cys^{460} ($M+3H^+$), Cys^{334} ($M+3H^+$) and Cys^{224} ($M+3H^+$) under the same conditions.

When Akt1/PKBα was treated with GSNO without cleavage of disulfide bonds and the free cysteine residues were alkylated with iodoacetamide, two intradomain disulfide bonds were identified: Cys^{60}-Cys^{77} in the PH domain and Cys^{296}-Cys^{310} in the kinase active loop.

The monoisotopic parent ion with m/z = 821.35, shown in Figure 11A, represents two tryptic peptides containing the Cys^{296}-Cys^{310} disulfide bond in the kinase loop. The isotopic peaks at m/z 821.61 and m/z 821.35 are attributed to the M + 1 and M + 0 ions. A mass difference of 0.26 Da (expected 0.25 Da) indicated 4 positive charges: two at n-terminals and two at side chains of the c-terminals of the dipeptides. The expected quadruply charged disulfide bond linked Cys^{296} and Cys^{310} containing peptides (T41-SS-T44, $M + 4H^+$) were calculated to be m/z 821.38 [(894.45 + 2387.06 + 4)/4]. The monoisotopic parent ion with m/z = 764.41, shown in Figure 11B, represents the two tryptic peptides containing the Cys^{60}-Cys^{77} disulfide bond in the PH domain. The quadruply charged state is calculated as m/z 764.66 (M + 1) – 764.41 (M + 0) = 0.25 which indicates 4 positive proton charges. The quadruply charged disulfide bond linked Cys^{60} and Cys^{77} containing peptides (T9-SS-T11, $M + 4H^+$) are calculated as m/z 764.37 [(1806.86 + 1246.63 + 4)/4]. Without GSNO treatment, only the Cys^{60}-Cys^{77} disulfide bond was detected. The mass accuracies for the two measurements were found to be 36 ppm (Cys^{296}-Cys^{310}

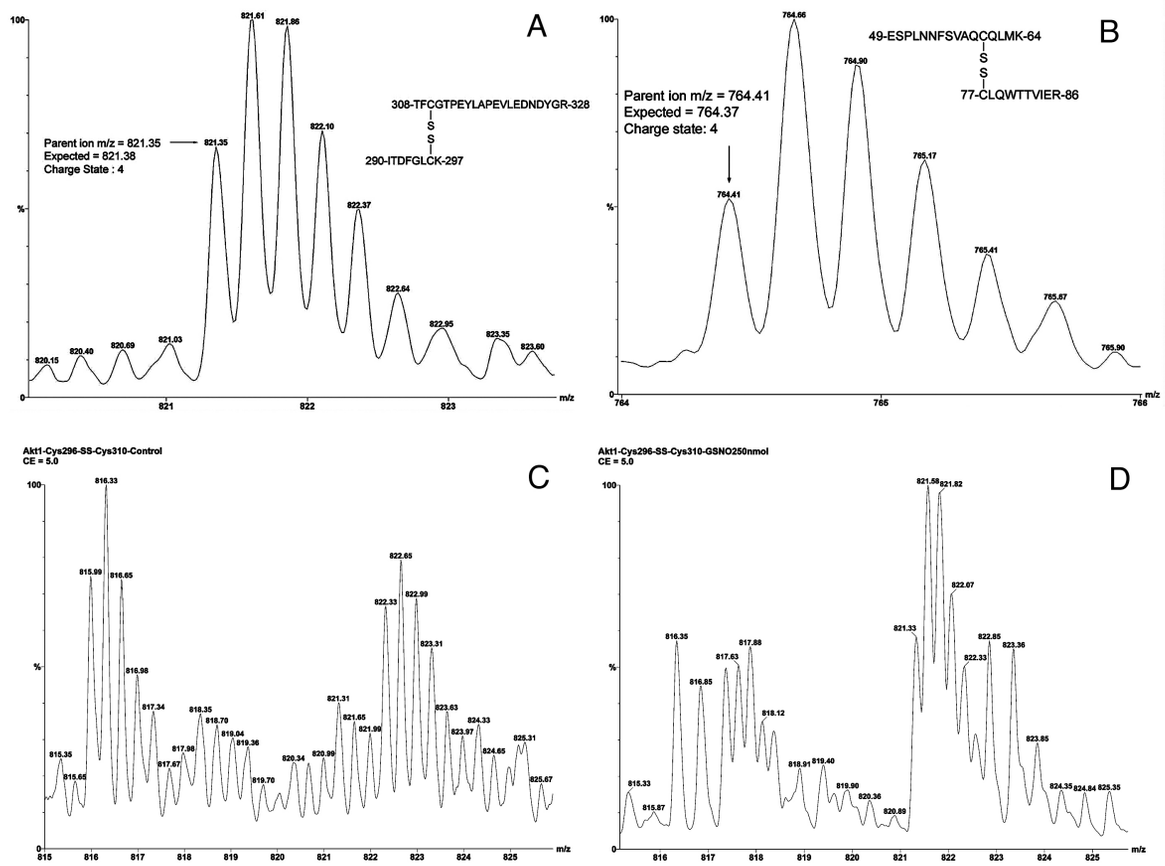

Figure 11. Detections of two intradomain disulfide bonds in Akt1/PKBα (a) Detection of intradomain Cys^{296}-Cys^{310} disulfide bond in the kinase loop. Inactive Akt1/PKBα (10 μg) was treated with GSNO and iodoacetamide (50 μM) in Laemmli sample buffer. In-gel trypsin digestion was performed after SDS-PAGE separation (BIO-RAD, 4-15% Tris-HCl). Monoisotopic parent ion at m/z 821.35, charge state: 4. Expected quadruply charged disulfide linked Cys^{296} and Cys^{310} containing the peptide at m/z 821.38. (b) Detection of the intradomain Cys^{60}-Cys^{77} disulfide bond in the PH domain. Monoisotopic parent ion at m/z 764.41, charge state: 4. Expected quadruply charged disulfide bond linked Cys^{60} and Cys^{77} containing peptide at m/z 764.37. (c) Free thiol state of Cys^{310} in the kinase loop without NO donor. The triply charged parent ion m/z 815.99: ^{308}TFCGTPEYLAPEVLEDNDYGR^{328} (expected: m/z 816.03, carboxyamidomethylcysteine, CAM derivative) represents the completely free thiol state of Cys^{310}, while the triply charged m/z 821.31 is not from disulfide linked Cys^{296}-Cys^{310} dipeptides (expected charge state: 4). The Cys^{296}-Cys^{310} disulfide bond was not detected in the absence of NO donor. (d) Nitric oxide promotes the formation of the Cys^{296}-Cys^{310} disulfide bond in the kinase loop. Inactive Akt1/PKBα (10 μg) was treated with GSNO (250 nmol, 50 μl PBS, pH = 8.0, 1 hr at room temperature in the dark) prior to alkylation with iodoacetamide and SDS-PAGE. The doubly charged m/z 816.35 ion is not from a Cys^{310} containing tryptic peptide (expected charge state: 3), and quadruply charged m/z 821.33 occurs at the expense of diminished triply charged Cys^{310} peptide. The free thiol of Cys^{310} is completely converted into the disulfide bond with Cys^{296}.

disulfide bond linked dipeptides) and 78 ppm (Cys^{60}-Cys^{77} disulfide bond linked dipeptides). The impact of GSNO on Cys^{296}-Cys^{310} disulfide bond formation is demonstrated in Figure 11C and D. The *S*-nitrosylation reaction without GSNO (Figure 11C) shows the triply charged tryptic peptide, ^{308}TFCGTPEYLAPEVLEDNDYGR^{328}, (CAM derivative) containing Cys^{310} at m/z 815.99 (expected monoisotopic parent ion: 816.03). The observed M+1 isotopic peak was at m/z 816.33. The difference between the isotopic M+1 and M+0 peak of 0.34 Da indicates 3

http://dx.doi.org/10.5772/54849

proton charges. In contrast, the triply charged ions at m/z 821.31 and m/z 821.65 (difference = 0.31 Da) do not represent the quadruply charged Cys^{296}-Cys^{310} dipeptides in Figure 11C. The triply charged Cys^{310} containing peptide was found to be totally absentwith GSNO treatment as shown in Figure 11D. The doubly charged ions at m/z 816.35 and m/z 816.85 (difference = 0.50 Da) are not related to the triply charged tryptic peptide ^{308}TFCGTPEYLAPEVLEDN-DYGR^{328} (CAM derivative) containing Cys^{310} at m/z 815.99 as shown in Figure 11C. In contrast, the ions at m/z 821.33 and m/z 821.58 (difference = 0.25 Da) are indeed from quadruply charged Cys^{296}-Cys^{310} linked dipeptides. Since quadruply charged Cys^{296}-Cys^{310} linked dipeptides are formed at the expense of triply charged Cys^{310} containing peptide after GSNO treatment, it is obvious that *S*-nitrosylation and disulfide bond formation occur simultaneously in the kinase loop.

We next sought to determine which cysteine residue is the NO acceptor that initializes Cys^{296}-Cys^{310} disulfide bond formation. There are three possibilities for the two cysteine residue thiol states: single *S*-nitrosothiol, double *S*-nitrosothiols and nitroxyl disulfide. The last case (nitroxyl disulfide) can be ruled out from the list, since expected net mass increases of 28 Da (NO - 2H = 30 - 2 Da) were not observed for the corresponding dipeptides. The second case, double *S*-nitrosothiols of Cys^{296} and Cys^{310}, may occur if both pKa's are acidic inside the kinase loop. The Biotin-Switch method was used to identify the *S*-nitrosothiol within the loop under gentle reaction conditions (GSNO 250 nmol, 1 hour). In addition, two other thiol-specific reagents, iodoacetic acid and iodoacetyl-LC-Biotin (leaving molecule: HI, fast and quantitative), were evaluated.

Chem derivatives	Parent calc.	Parent found	y2 ion calc.	y2 ion found
CMC	953.45	953.42	308.13	308.17
HPDP-Biotin	1323.64	1323.68	678.32	678.29
Acetyl-LC-Biotin	1277.65	1277.58	632.33	632.38

Table 3. Characterization of the thiol-specifically modified Akt1/PKBαpeptide ^{290}ITDFGLCK^{297}

Confirmations of the *S*-nitrosylation sites were performed by the following 3 step procedure: A. Parent ion discoveries with automated data dependent acquisition (DDA); the peptide mass tolerance was 0.2 Da for the carboxymethyl cysteine (CMC) immonium ion. Under these conditions, only a few false positive ions were observed and these were eliminated manually from the expected CMC parent ion list. B. Confidently discovered parent ions were analyzed with PepSeq of MassLynx V4.1 software; oxidation of methionine was searched as a variable modification. C. For peptides, with MS/MS scores < 35, manual interpretations of candidate parent ions were performed with the following procedure: continuum MS/MS spectra were smoothed, the upper 80% was centroided and cysteine residues were confirmed with three different thiol-specifically derivatized y ions. Cysteine residue monoisotopic mass C_3H_5NOS = 103.01 Da was replaced with CMC residue monoisotopic mass $C_5H_7NO_3S$ = 161.01 Da, HPDP-Biotin derivatized adduct residue monoisotopic mass $C_{22}H_{37}N_5O_4S_3$ = 531.20 Da and iodoacetyl-

LC-Biotin derivatized adduct residue monoisotopic mass $C_{21}H_{35}N_5O_4S_2$ = 485.21 Da, respectively.

Table 3 shows the expected results of Cys^{296}*S*-nitrosylation in the kinase loop with the three different chemical modifications. The resulting *S*-nitrosylatedCys was reduced with ascorbate and then derivatized with iodoacetic acid to afford the CMC derivative (the Cys residue with a monoisotopic mass C_3H_5NOS = 103.01 Da was replaced by the CMC residue with a monoisotopic mass $C_5H_7NO_3S$ = 161.01 Da) for sequence analysis. The CMC derivative of the y2 ion of the doubly charged tryptic peptide, ^{290}ITDFGLCK^{297}, was confirmed at m/z 308.17 (expected 308.13 = 161.01 + 145.10 +2.02). The Cys HPDP-Biotin adduct (Cys residue monoisotopic mass C_3H_5NOS = 103.01 Da was replaced with the adduct residue monoisotopic mass $C_{22}H_{37}N_5O_4S_3$ = 531.20 Da) was used for sequence analysis. The corresponding y2 ion of the Biotin-HPDP derivatized, ^{290}ITDFGLCK^{297}, was confirmed at m/z 678.29 (expected 678.32 = 531.20 + 145.10 +2.02). The CysIodoacetyl-LC-Biotin adduct (Cys residue monoisotopic mass C_3H_5NOS = 103.01 Da was replaced with adduct residue monoisotopic mass $C_{21}H_{35}N_5O_4S_2$ = 485.21 Da) was used for peptide sequence analysis. The corresponding y2 ion of iodoacetyl-LC-Biotin derivatized, ^{290}ITDFGLCK^{297} was confirmed at m/z 632.38 (expected 632.33 = 485.21 + 145.10 +2.02). Since the y2 ions of ^{296}Cys-Lys^{297} produced with the three different derivatization procedures were unambiguously observed it is likely that Cys^{296} is a favorable *S*-nitrosylation site under the conditions used. Although studies with mutated Akt1/PKBα|| (C^{224}S) indicated that Cys^{224} is a major S-nitrosylation acceptor site *in vitro*, the biological role of *S*-nitrosylated Cys^{224} in kinase regulation needs to be further explored. In the current study it was determined that significant *S*-nitrosylation of Cys^{224} is improbable, since using the three alkylation approaches and trypsin digestion, the levels of positive ionization of Cys^{224} containing peptides were below the level of detection. This failure in detection of *S*-nitrosylated Cys^{224} might be a false negative under our experimental conditions and clearly warrants further investigation. Nevertheless, our findings clearly demonstrate that *S*-nitrosylated Cys^{296} is directly relevant to the kinase activation regulation cycle.

One possible explanation for the kinetics of Cys^{296}-Cys^{310} disulfide bond formation in the kinase loop may be that there is a high kinetic barrier without GSNO. Due to its highly labile nature [140], *S*-nitrosylated Cys^{296}, which forms rapidly in the presence GSNO, may function as an intermediate state. Since this intermediate is likely to have a lower kinetic barrier for Cys^{296}-Cys^{310} disulfide bond formation, the overall speed of the reaction should increase greatly. It has been reported that trans-nitrosylation reactions between vicinal thiols can occur and accelerate disulfide bond formation [141]. The well characterized Cys^{296}-Cys^{310} disulfide bond can be used as a signature peptide for detection of *S*-nitrosylation of Cys^{296} after immunoprecipitation. The separation of tryptic peptide mixtures with our NanoLC interfaced Q-TOF is demonstrated in Figure 12 (bottom panel). The extracted mass ion peak m/z 821.62, as shown in Figure 12 (top panel), is the M+1 isotopic peak of the quadruply charged dipeptides (the most intense isotopic peak due to high number of carbon atoms).

The *in vitro* system allowed us to determine conditions that are favorable for evaluation of *S*-nitrosylation of Cys^{296} by MS/MS and was useful for studying the mechanism of intradomain disulfide bond formation. The reason for using inactive Akt1/PKBα (unphosphorylated) in these studies was to find possible *S*-nitrosylation sites in relationship with the following

http://dx.doi.org/10.5772/54849

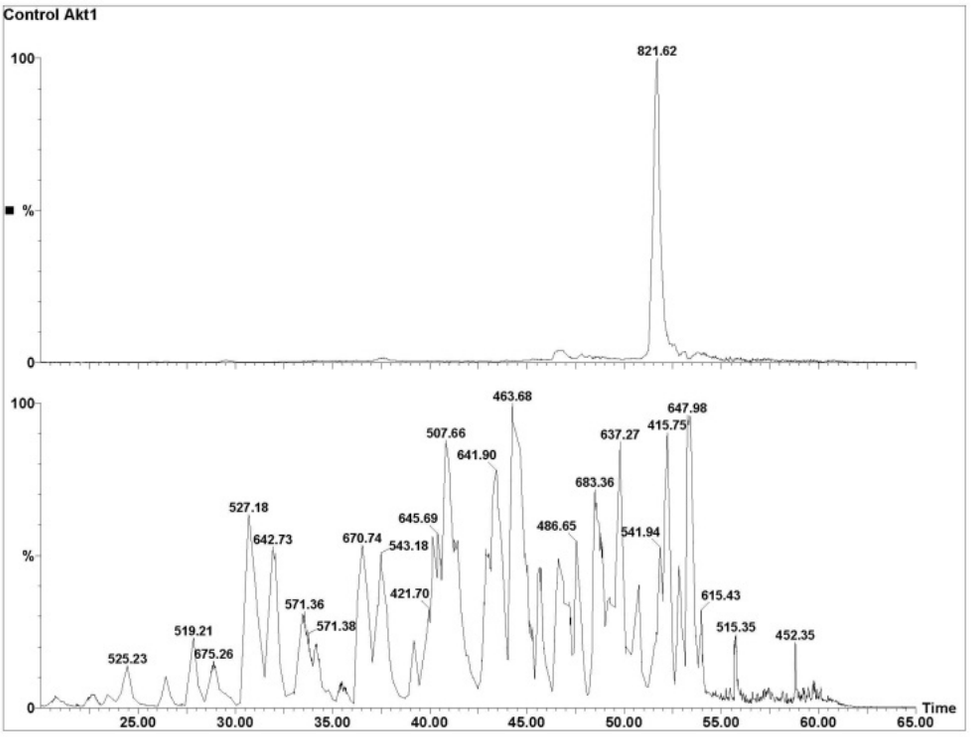

Figure 12. NanoLC chromatogram of tryptic peptides of Akt1/PKBα in soleus muscle Top panel: Mass ion chromatogram of the dipeptides m/z 821.62: M+1 isotopic peak of the quadruply charged dipeptides (intensity of M+0 monoisotopic peak is lower than M+1 due to isotope abundant as shown in Figure 11A). Bottom panel: BPI chromatogram of the Akt1/PKBαtryptic peptides after immunoprecipitations and in-gel digestion from NanoLC interfaced with Q-TOF tandem mass spectrometry.

published data: 1. Akt1/PKB*α* undergoes transient phosphorylation/ dephosphorylation which regulates the kinase activity conformation cycle; 2. Kinase disulfide bond formation, Cys^{297}-Cys^{311}, and dephosphorylation at $pThr^{308}$ are induced simultaneously by H_2O_2 oxidative stress *in vitro*; 3. High levels of nitric oxide production occur both after burn injury and in diabetic patients. Previous results from our laboratory have indicated that there is *S*-nitrosylation at Cys^{296} in rat soleus muscle. A parention at m/z 690.83 containing Cys^{296} (T41-T42: ^{290}ITCFGLCKEGIK^{301}) was observed with CAM immonium trigged parent ion discovery, however, MS/MS sequencing data was not obtained. As a continuation of these studies to explore *S*-nitrosylation in the kinase active loop, large amounts of rat soleus muscle lysate (~ 3-5 mg/ml total proteins, 3 ml for each experiment, day 4 after 40% TBSA, 3rd degree burn) were used. In the present study, detailed MS/MS analysis of HPDP-biotinated free Cys^{296} peptide and Cys^{296}-Cys^{310} disulfide bound dipeptides of Akt1/PKB*α* were performed with lysates of rat soleus muscle after burn injury. The tryptic parent ion derivatized from free Cys^{296} after burn injury was observed at m/z 662.84 ($M+2H^+$, expected 662.82) and the MS/MS sequence data is shown in Figure 13. A low sequence score of 18 was obtained from the parent ion with S/N = 3. However, the critical diagnostic y2, y4 and y5 ions at m/z 678.29, m/z 849.34 and m/z 995.51 confirmed that trace amounts of free Cys^{296} are indeed present after intrado-

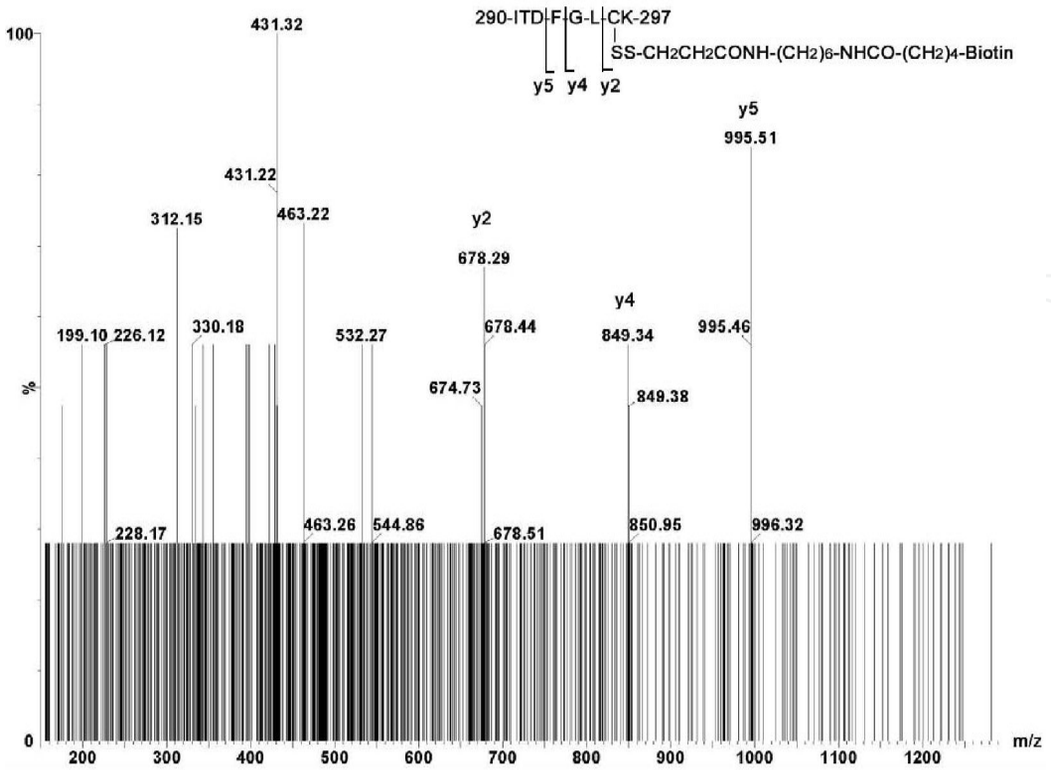

Figure 13. Sequence analysis of biotinated free Cys[296] peptide of Akt1/PKBα after burn injury Rat soleus muscle lysates (30 mg total protein) were treated with anti-Akt1/PKBαmAb and in-gel biotination was performed with HPDP-Biotin. Parent ion m/z 662.84 ($M+2H^+$, expected 662.82) was sequenced. Cys residue monoisotopic mass C_3H_5NOS = 103.01 Da is replaced with the adduct residue monoisotopic mass $C_{22}H_{37}N_5O_4S_3$ = 531.20 Da. A low sequence score of 18 was obtained from the parent ion with S/N = 3, however the critical diagnostic y2, y4 and y5 ions at m/z 678.29, 849.34 and 995.51 confirmed that trace amounts of free Cys[296] are presentafterburn injury.

main disulfide bond formation induced by burn injury. In addition, partial sequencing data for Cys[296]-Cys[310] disulfide linked dipeptides is shown in Figure 14.

The phosphorylation status of Akt1 Thr[308] and Ser[473] were evaluated by ELISA and the results were expressed as units per gram tissues. Figure 15 shows that phosphorylations of Akt1 at Thr[308] and Ser[473] in skeletal muscle of burned mice were reduced by 49.8% ($p<0.005$) and 26.2% ($p<0.05$) compared with sham treated control animals.

The C-terminal y ion series of Cys[310] containing peptide, [308]TFCGTPEYLAPEVLEDNDYGR[328], was observed for the quadruply charged parent ion (T41-SS-T44, $M + 4H^+$). Cys[296]-Cys[310] disulfide linked dipeptides were not observed in muscle lysates from sham treated animals. The chance of obtaining the MS/MS sequence using our *in vivo* experimental conditions is only about 20-25%. This indicates that one interpretable MS/MS outcome (score > 25) is expected in 4 or 5 independent experiments in which 3 successive injections are performed. Nevertheless, these MS/MS data for peptides containing free Cys[296] and Cys[296]-Cys[310] linked dipeptides are sufficient to verify our hypothesis that *S*-nitrosylation promotes intradomain disulfide bond formation and dephosphorylation at pThr[308] after burn injury as illustrated in Figure 16. Due to the high lability of Cys[296]-SNO,direct identification of this species *in vivo* was not possible.

http://dx.doi.org/10.5772/54849

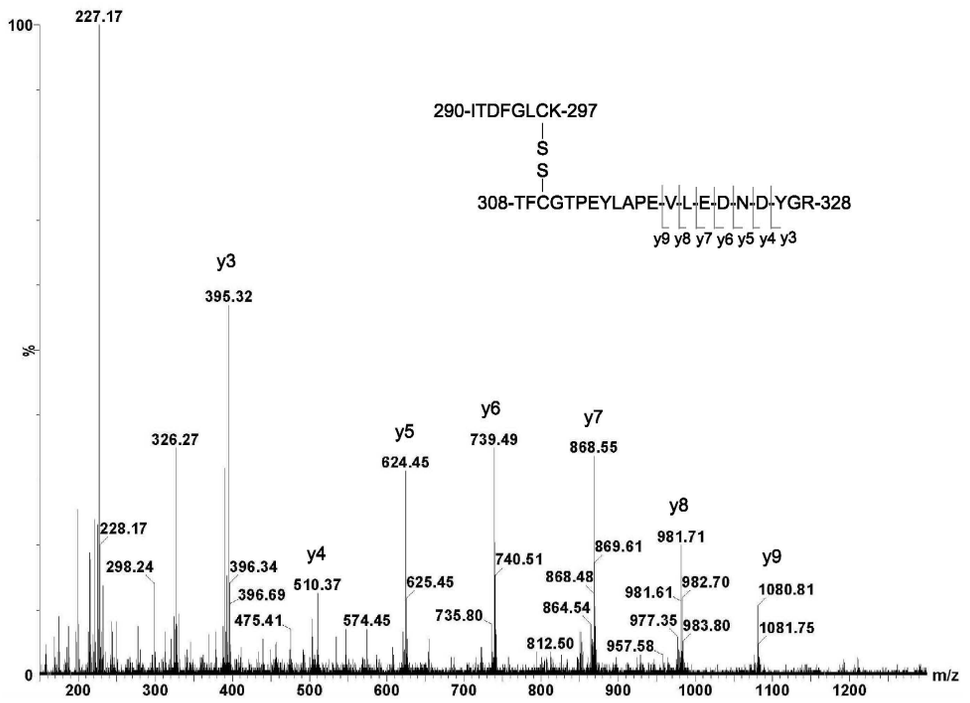

Figure 14. Identification of the Cys^{296}-Cys^{310} disulfide linked peptide with dephosphoryated Thr^{308} in soleus muscle from burned rats MS/MS sequence of Cys^{296}-Cys^{310} disulfide linked dipeptides: C-terminal y ion series (y3 to y9) of Cys^{310} containing peptide, ^{308}TFCGTPEYLAPEVLEDNDYGR^{328}, were observed from the quadruply charged parent ion (T41-SS-T44, $M + 4H^+$).

Proposed mechanism for burn-induced Akt1/PKB*α* kinase loop conformational changes via phosphorylation and *S*-nitrosylation cross-taking in skeletal muscle. Phosphorylation of Thr^{308} stabilizes the disordered loop structure between ^{292}DFG and APE^{319} via a salt bridge with Lys^{297} as illustrated in the loop peptide 1, which up-regulates Akt1/PKB*α* kinase activity. NO free radical production is increased after burn injury, consequently, a large portion of Cys^{296} undergoes *S*-nitrosylation at Cys^{296} (peptide 2), however, some free Cys^{296} remains, which can be biotinylated for MS/MS confirmation (peptide 3). *S*-nitrosylation activates Cys^{296}-Cys^{310}intradomain disulfide bond formation (peptide 4). *S*-nitrosylation at Cys^{296} is associated with dephosphorylation of Thr^{308} and inaccessibility to the kinase site as shown in Akt1 crystal structure [142]; which down-regulates kinase activity.

S-nitrosylation of Akt1/PKB*α* is a key factor for understanding the regulation of glucose transport and downstream protein synthesis. A recent report demonstrated that blockade of iNOS prevents the *S*-nitrosylations of Akt and IRS-1 and results in insulin resistance *in vivo* [143]. Although it is clear that two PTMs of Akt1/PKB*α*, phosphorylation at Thr^{308} and *S*-nitrosylation at Cys^{296}, are critical for the regulation of Akt1/PKB*α* activity under stress conditions, there are still many unanswered questions concerning how reversible phosphorylation/ dephosphorylation and *S*-nitrosylation/denitrosylation modulate Akt1/PKB*α* activity.

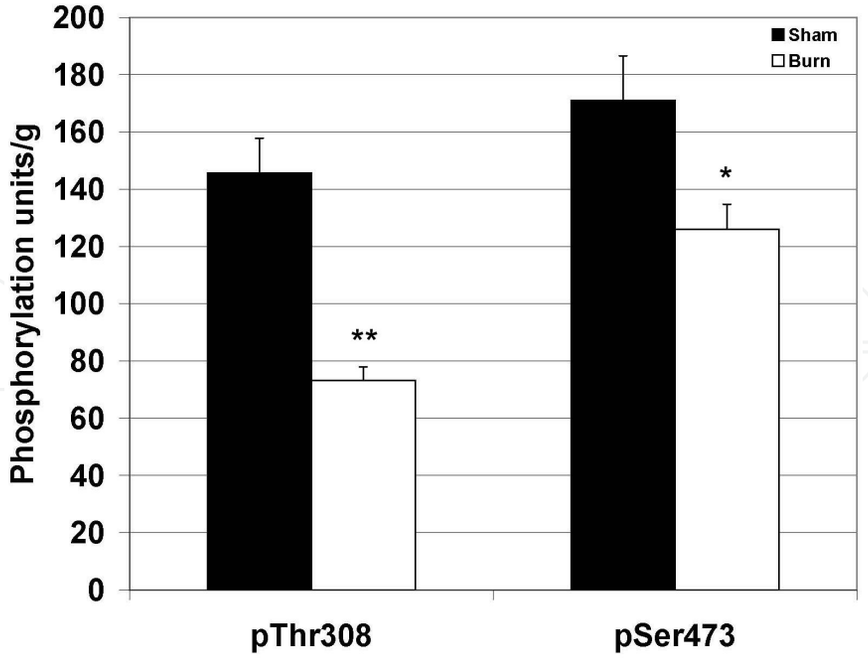

Figure 15. Impaired phosphorylation of Thr^{308} and Ser^{473} of Akt1 in skeletal muscle of burned mice. Skeletal muscle tissues from burned mice were homogenized with Cell Signaling buffer and phosphorylation levels of Thr^{308} and Ser^{473} in Akt1 were measured by ELISA. Akt pThr^{308} ELISA kit (KHO0201) and pSer^{473} kit (KHO0111) were purchased from Invitrogen. The phosphorylation units were normalized to tissue weight. Values represent mean ± sem for 15 burned and 8 sham treated mice. *: p<0.05, **: p<0.005.

For example, it has been reported that the Cys^{296}-Cys^{310} disulfide bond is present only when there is binding of substrate to the active kinase loop and phosphorylation at Thr^{308}; indicating that both disulfide bond formation as well as phosphorylation of Thr^{308} are important for kinase activity. In contrast, this disulfide bond was not observed under similar conditions in two studies of the ternary structure of the kinase; even though, oxidative stress was shown to induce dephosphorylation of pThr^{308} and disulfide bond formation in the kinase loop in an *in vitro* study [112].

In summary, our data establishes that Cys^{296} is an important *S*-nitrosylation site in the kinase loop of Akt1/PKBα under gentle reaction conditions: (a) iodoacetic acid as previously described; (b) the HPDP-Biotin switch method and (c) the iodoacetyl-LC-Biotin method to ensure indirect capture of Cys^{296}-SNO which may be undetectable with HPDP-Biotin. The corresponding derivatized y2 ions (^{296}Cys-Lys^{297}) in the tryptic peptide (Ile-Thr-Asp-Phe-Gly-Leu-Cys-Lys) were obtained with mass sequences to eliminate false positive discovery. Although no other *S*-nitrosylated cysteine residues were detected, it is possible that *S*-nitrosylations at Cys^{224}, Cys^{344} and Cys^{460} were missed due to very low ionizations (i.e., false negative discoveries). As a consequence of *S*-nitrosylation at Cys^{296}, there is rapid disulfide bond formation with vicinal Cys^{310} in the kinase loop. This affords a stable disulfide bond linked quadruply charged parent ion at m/z 821.35 (M + 4H$^+$). Partial sequencing data for Cys^{296}-Cys^{310} linked dipeptides from soleus muscle lysates indicated that burn injury is associated with bothde-phorsphorylation of pThr^{308} and disulfidebond formation. Current qualitative results have

http://dx.doi.org/10.5772/54849

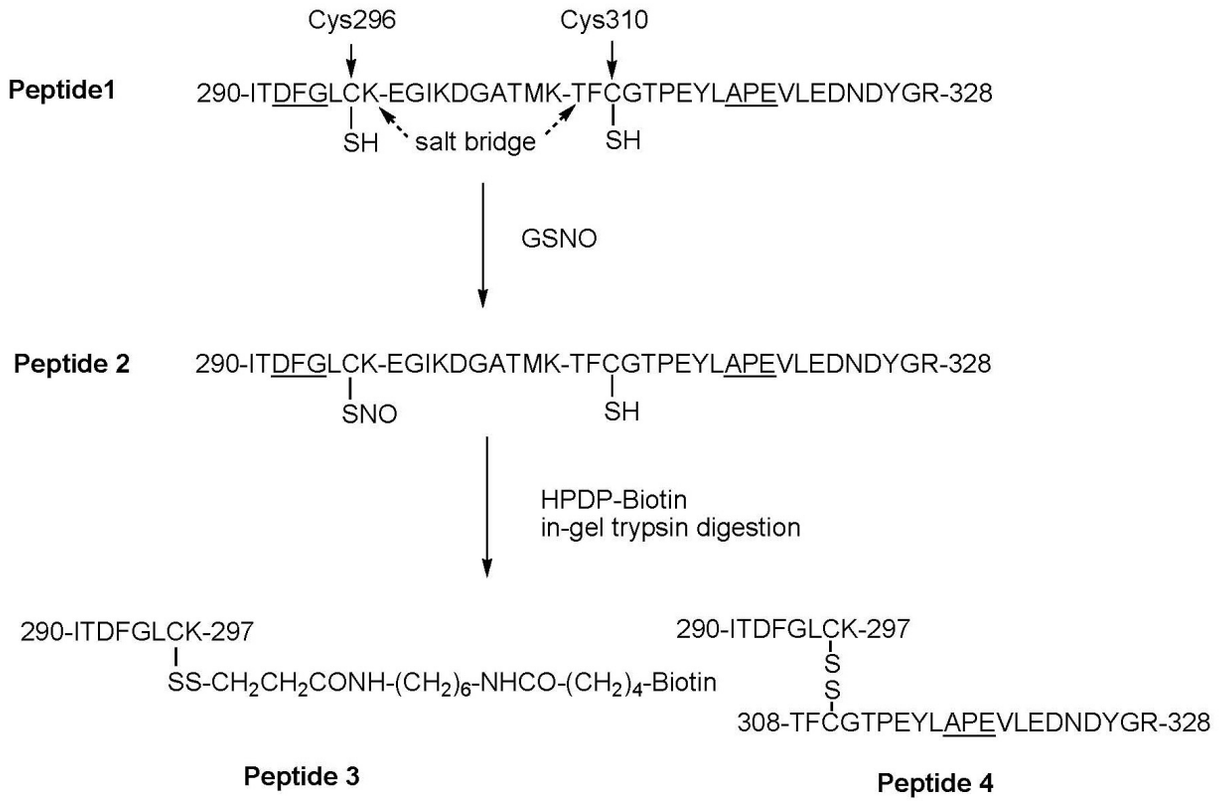

Figure 16.

provided important mechanistic information; however, quantitative measurements of Cys^{296}thiol states post-burn injury remain very challenging.

The essential issue for any isotope dilution method is to precisely characterize the heavy isotope labeled internal standard in terms of atomic and chemical purities. To determine the relative quantification of liver Akt1/PKBα after burn injury, two typical serum acute phase proteins, negative regulated albumin and positive regulated amyloid P component, as well as liver Akt1/PKBα were characterized in a preliminary study with tissue and blood samples from 3 mice with burn injury (40% TBSA). To eliminate possible mathematical and biological complexities associated with of multiple isotopomer population distributions for individual tryptic peptides produced with partial labeling conditions, peptides with only one instance of [isopropyl-$^2H_7$]-L-Leu were selected for measurement of relative labeling efficiencies. A tryptic peptide may be positively charged at its N-terminal α-amine group and the side-chain amine group of a Lys residue or the guanido group of an Arg residue; thus, a doubly charged parent ion, $[M + 2H^+]$, may be observed with ESI mass spectrometry. In addition, triply charged tryptic parent ions, $[M+3H^+]$, may be obtained for peptides containing proline or histidine residues or with larger size peptides. Peptides with one instance of [isopropyl-$^2H_7$]-L-Leuincorporation yield paired light and heavy parent ions with monoisotopic mass ion differences of 3.5 Da (doubly charged) or 2.3 Da (triply charged) under ESI conditions. Charge state dependent DDA

allows these multiply charged peptides to be focused in the CID chamber with charged argon cleavages. The singly charged and predominated light and heavy MS/MS y ion series from the light and heavy parent ions are produced with mass difference of 7 Da. This allows unambiguous relative quantification of parent ion enrichments from possible false positive discoveries. Characteristics of three proteins with enrichments of greater than 50% are shown in Table 4.

	Sequence, (charge state observed)	Enrichments %, (SD)
albumin	^{243}**L**SQTFPNADFAEITK^{257}, (2)	53 (3.2)
	^{559}HKPKATAEQ**L**K^{669}, (2)	57 (3.8)
	^{439}APQVSTPT**L**VEAAR^{452}, (2)	54 (4.1)
amyloid P component	^{66}SQS**L**FSYSVK^{75}, (2)	66 (4.9)
	^{88}VGEYS**L**YIGQSK^{99}, (2)	65 (4.6)
	^{147}APPSIV**L**GQEQDNYGGGFQR^{166}, (3)	69 (5.2)
liver Akt1/PKBα	^{9}EGW**L**HKR^{15}, (2)	59 (4.0)
	^{184}EVIVAKDEVAHT**L**TENR^{200}, (3)	56 (2.7)
	^{290}ITDFG**L**B*KEGIKDGATMK^{307}, (3)	55 (3.3)

Table 4. Protein enrichment levels on day 7 after 3rd degree burn of 40% TBSA

The negative acute phase protein albumin and the positive acute phase protein amyloid P component had enrichments of ~55% and ~66%, respectively. The enrichment level (56%) of liver Akt1/PKB*α* was found to very similar to that of albumin. These enrichment values represent ultimate [isopropyl-$^{2}H_{7}$]-L-Leuincorporation in each individual protein which can be used as the isotopic correction factor for the light and heavy parent ion MS ratio obtained by mixing exact the same weight of labeled and non-labeled liver tissues.

Akt1/PKB*α* was immunoprecipitated from the mixture of [isopropyl-$^{2}H_{7}$]-L-leucine labeled liver from burned mice an equal amount tissue from sham treated animals and processed further by the methods described above. The relative expression of Akt1/PKB*α* at the protein level from livers of burned and sham treated mice is shown in Figure 17.

The triply charged monoisotopic parent ion at m/z 647.99 was detected for the control peptide ^{252}FYGAEIVSALDYLHSEK^{268}; calculated [M+3H^{+}] = 647.99. Two heavy monoisotopic parent ions at m/z 650.34 and m/z 652.36 indicates one and two instances of [isopropyl-$^{2}H_{7}$]-L-Leu incorporation into the control peptide. Triply charged MS differences were found to be 2.3 Da (calculated MS difference for one heavy Leu incorporation: 7/3 = 2.3 Da) and 4.3 Da (calculated MS difference for two heavy Leu incorporation: 14/3 = 4.6 Da), respectively. MS/MS y ion series from y3 to y12 of the m/z 647.98 confirms the control peptide for studying protein expression. The intensities of the m/z 650.34 and m/z 652.36 ions represent the heavy Akt1/PKB*α* populations from burn injured mice, whereas the m/z 647.99 ion is derived from the sham treated animals. Estimated total ion intensity was ~9.5 after burn injury and ~6.5 after sham treatment. Due to the low S/N of ~2 for the heavy ions and the enrichment of 56% in Table 1, Akt1/PKB*α* protein expression, was observed to be up-regulated in response to burn injury the

http://dx.doi.org/10.5772/54849

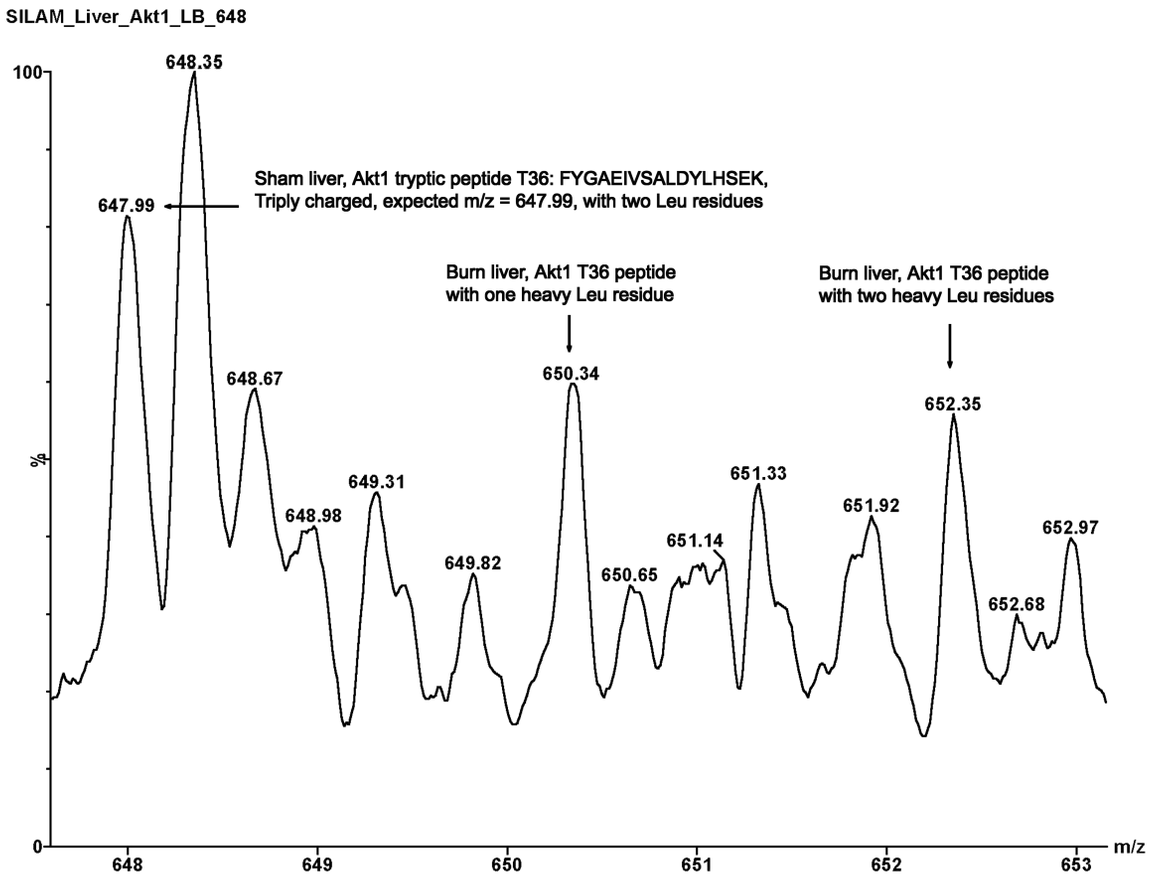

Figure 17. Changes in liver Akt1/PKBα expression at protein level after burn injury A triply charged monoisotopic parent ion at m/z 647.99 was found for the control peptide ^{252}FYGAEIVSALDYLHSEK^{268}; calculated [M+3H^{+}] = 647.99. Two heavy monoisotopic parent ions at m/z 650.34 and m/z 652.36 indicate one and two instances of [isopropyl-2H7]-L-Leu incorporation into the control peptide. Akt1/PKBα protein expression, estimated from both heavy ions, was found to be up regulated after correction for both enrichment and background.

mice.However, the heavy ion for the biotinylated peptide, ^{290}ITDFGLCK^{297}, which was used as a marker for kinase activity, was significantly reduced (almost to background) after injury as illustrated in Figure 18.

Biotinylated light peptides ^{290}ITDFGLCK^{297} of Akt1/PKB*α* from sham treated mice was detected at m/z 639.88 and was doubly charged as indicated by the natural abundance carbon isotope peak at m/z 640.33. Three biotinylated y2, y4 and y6 ions at m/z 632.44, 802.51 and 1064.59 confirmed the loop peptide sequence with biotin modification as shown in Figure 19. The corresponding y2 ion of iodoacetyl-LC-Biotin derivatized, ^{296}CK^{297}, was confirmed at m/z 632.44 (expected 632.33 = 485.21 + 145.10 +2.02). DDA with low S/N occurred *in vivo* studies was performed with continuum mode to enhance the parent ion discovery. On the other hand, centroided spectra are found to be necessary to obtain accurately the diagnostic modifications in the y ions. Biotinylated heavy peptide ^{290}ITDFGLCK^{297} in Akt1/PKB*α* from burn injured mice (n = 3) was identified at m/z 643.38 with its natural carbon isotopic peak at m/z 643.88. A MS

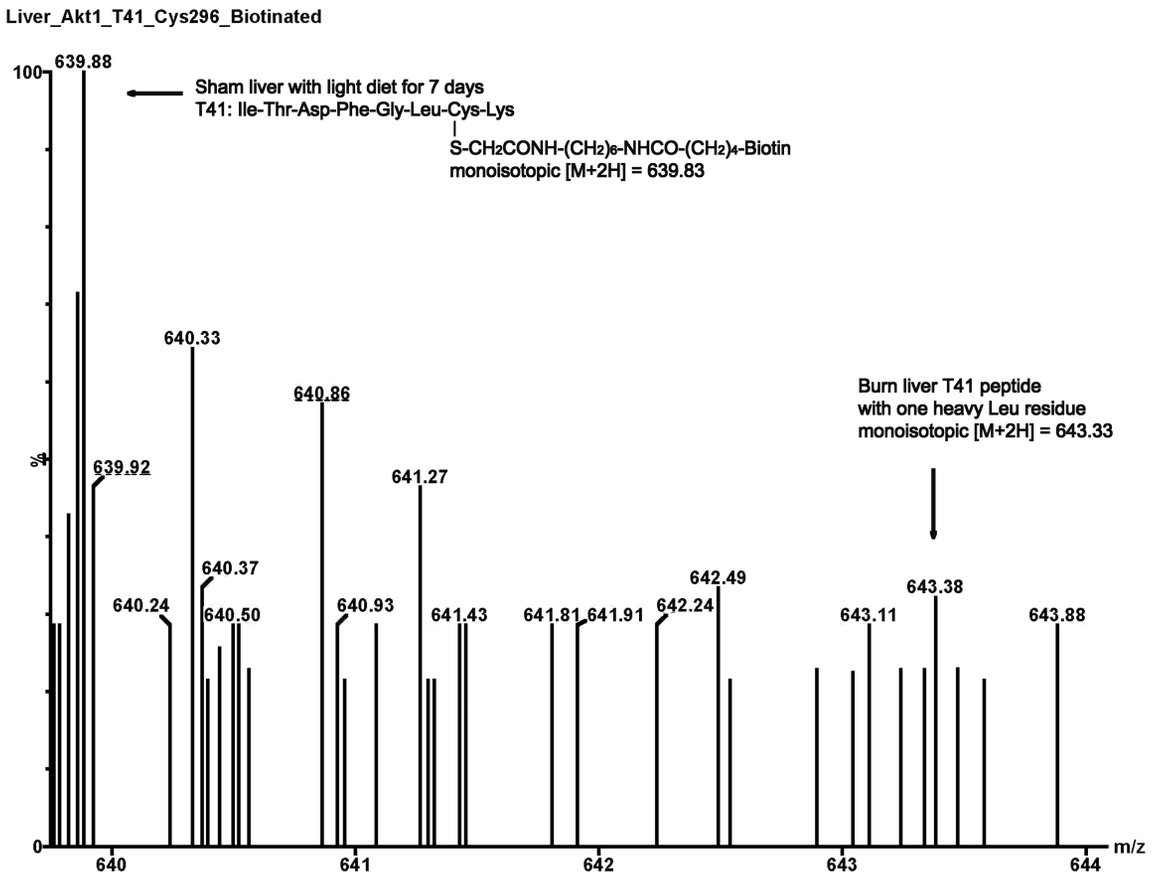

Figure 18. Liver Akt1/PKBα activity measurement via the loop peptide Light peptide, ^{290}ITDFGLCK^{297}, of Akt1/PKBα from sham treated mice was detected at m/z 639.88; doubly charged as indicated by the natural abundance carbon isotope peak at m/z 640.33. Biotinylated heavy peptides ^{290}ITDFGLCK^{297} of Akt1/PKBα from the burn injured mice were detected at m/z 643.38; doubly charged as indicated by the natural abundance carbon isotope peak at m/z 643.88. The MS difference of 3.5 Da between the paired light and heavy parent ions indicates one instance of [isopropyl-$^{2}H_{7}$]-L-Leu incorporation into the heavy ion at m/z 643.38 after burn injury. The intensity of the m/z 643.38 ion indicates that the loop peptide containing Cys^{296} was markedly reduced (almost to baseline) in response to burn injury (n = 3).

difference of 3.5 Da between the paired light and heavy parent ions clearly indicated that one instance of [isopropyl-$^{2}H_{7}$]-L-Leu was incorporation into the doubly charged parent ion at m/z 643.38 with doubly charged state (n = 3). MS ion intensity at m/z 643.38 indicated that loop peptide containing Cys^{296} was almost undetectable after burn injury. These observations were evaluated with MS/MS sequencing; peptide charge status and MS shift of the isotope labeled paired peptides *in vivo*.

The incorporation efficiencies of isotopically labeled peptides in Table 3 demonstrates that amyloid P component was 10% higher than albumin; suggesting a faster turnover rate during up regulation. Serum albumin and liver Akt1/PKB*α* appear to have similar enrichments ~55%. Classically, individual protein fractional synthesis rate (FRS) is calculated by the relative isotope enrichment ratio of the labeled protein vs. precursor acyl-tRNA over the labeling time period

http://dx.doi.org/10.5772/54849

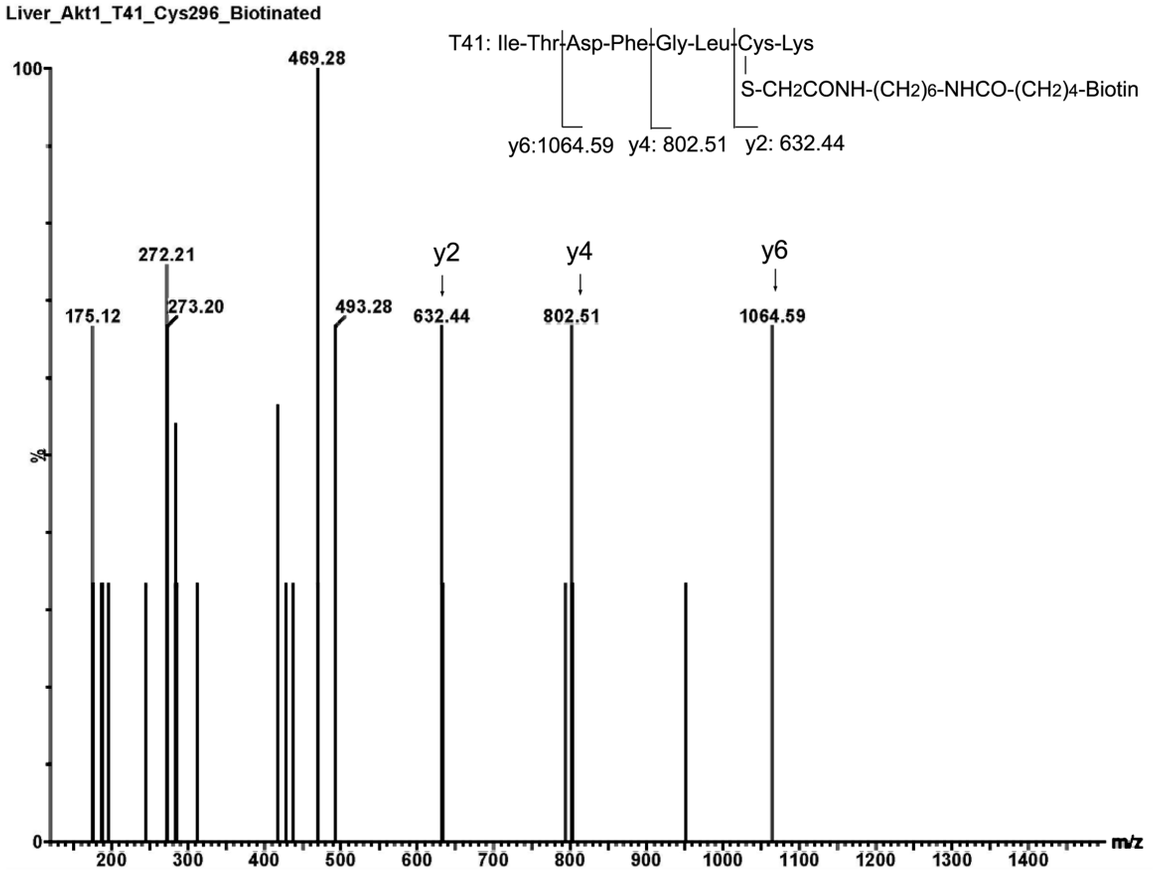

Figure 19. Identification of the kinase loop peptide derivatized with the iodoacetyl-LC-Biotin Cysteine residue monoisotopic mass C_3H_5NOS = 103.01 Da was replaced with the iodoacetyl-LC-Biotin derivatized adduct monoisotopic mass $C_{21}H_{35}N_5O_4S_2$ = 485.21 Da. Three biotinylated y2, y4 and y6 ions at m/z 632.44, 802.51 and 1064.59 unambiguously confirmed the loop peptide sequence with biotinylated mass shifts for kinase bioactivity measurements.

for a given isotope tracer [144,145]. FSR is a very important parameter for assessing effects of clinical interventions by comparisons between patients and healthy controls. In general, information about protein synthesis obtained with FRS and partially labeled SILAM are very similar and either can be used to optimize therapeutic strategies.

Our previous studies with thermally injured rats have demonstrated that there is no apparent alteration in binding of insulin to its receptors in liver, skeletal muscle or adipose tissue. Thus, acute and chronic insulin resistances induced by surgical trauma, burn injury, hemorrhage and sepsis are primarily post-receptor effects in the insulin-like growth factor-phosphatidylinositol-3 kinase-Akt pathway. Phosphorylations of specific Ser and Thr residues in the C-terminus of IRS-1 induce its degradation via the ubiquitin-proteosome pathway; which may early biological effect after receptor binding. Impaired Akt1/PKBα kinase activity after injury may be a later downstream event. Deficiency of Akt1/PKBα causes decreased somatic cell and body size [146], while knockout of Akt2/PKBα leads to insulin resistance [147]. Akt1/PKBα is involved in cellular survival pathways, by inhibiting apoptotic processes and stimulating protein synthesis pathways. It is also a key signaling protein in cellular pathways of skeletal

muscle differentiation [148,149]. Currently, assays of Akt1/PKBα | | activity in vitro and in vivo are performed with antibodies specific for the phosphorylated Ser^{473} and Thr^{308} residues which are critical for stabilizing the global and loop active conformations of the kinase. Difficulties with using anti-phospho-serine, but not anti-phospho-tyrosine antibodies, have been occurred in our phosphoproteomic research. NO production is elevated after burn injury and in patients with type 2 diabetic and it has been shown that the Cys^{297}-Cys^{311} disulfide bond in the kinase loop may be formed in association with dephosphorylation under oxidative stress in vitro. Reversible S-nitrosylation at Cys^{296} in the kinase loop is another PTM which complements reversible phosphorylation at Thr^{308}in the regulation of kinase activity. It has been shown that Akt1/PKBα undergoes transient phosphorylation/dephosphorylation which regulates the kinase active conformation cycle; kinase disulfide bond formation, Cys^{297}-Cys^{311}, and dephosphorylation at $pThr^{308}$ are induced simultaneously by H_2O_2 oxidative stress *in vitro* [46];and high levels of nitric oxide production occurs in both burn injured rats and diabetic patients. Freethiol group of Cys^{296} undergoes loop conformational changes by capture of nitric oxide, or chemical modifications with other reactive oxygen species produced under the burn injury; thus blocking substrate recognition. Intact loop peptide with a trace amount of free cysteine in the peptide population, ^{290}ITDFGLCK^{297}, after burn injury was developed as an unambiguous index for bioactivity. However, this peptide is not related to kinase protein expression in responses to the burn, since varying degrees of different thiol modifications in the loop may occur at the same time. In contrast, the control peptide, ^{252}FYGAEIVSALDYLHSEK^{268}, locatedjust outside of kinase loop, was a useful index of protein level. Kinase bioactivity measured with tandem mass spectrometry was comparable with previously reported data measured with immune complex kinase assay and anti-$pThr^{308}$ as well as anti-Ser^{437}mAbs, whereas protein levels were slightly increased in responses to injury. MS/MS sequence analysis and [isopropyl-$^2H_7$]-L-Leu incorporation in the paired peptides indicated that after thermal injury kinase activity is significantly reduced, despite increased protein expression. These findings indicate that neither complete labeling of nor measurement of acyl-tRNA enrichment are necessary or critical for quantitative proteomics with SILAM. Cys^{296}thiol state is considered as one of the important factors for the kinase activity. The limitations of partially labeled SILAM for clinical studies are: 1. Specific protein enrichment must be measured in tissues labeled with heavy isotopes under stress conditions; unfortunately, many proteins of clinical interest occur at low abundance and thus there is a high rate of false negative discovery. 2. Sequence confirmation of individual proteins requires that SDS-PAGE bands be visible by Coomassie brilliant blue R-250 staining (at least 0.1 μg). Despite these limitations our observations may provide new insights into the treatment of muscle wasting and other aspects of insulin resistance after critical injury.

As the central mediator of the IR/IRS/ PI3K/FOXO pathway, Akt1/PKBα kinase loop conformational changes are induced via a transition from the physiological salt bridge Lys^{297}-Ser^{308} and the pathphsiological disulfide bond Cys^{296}-Cys^{310}, which inhibits kinase substrate recognition. Impaired Akt1/PKBα kinase activity and enhancement of the activities of other stress kinases leads to FOXO3 translocation from the cytosolic compartment into the nuclear compartment, where FOXO3 transcriptional activity is further regulated by reversible acetylation.

http://dx.doi.org/10.5772/54849

4.3. Acetylation of transcription factor FOXO3 in muscle wasting post-burn injury

Skeletal muscle serves as the major protein reservoir from which amino acids can be mobilized for gluconeogenesis, new protein synthesis or as an energy source. With starvation and in many systemic disease states, including sepsis, cancer, burn injury, diabetes, cardiac and renal failure, there is generalized muscle wasting, which results primarily from increased breakdown of muscle proteins combined with reduced protein synthesis in most of these conditions [150,151]. In all these catabolic states, the loss of muscle mass involves a common pattern of transcriptional responses, including induction of genes for protein degradation and decreased expression of genes for growth-related and energy-yielding processes [152]. In atrophying muscles, two independent degradation pathways, lysosomal autophagy and proteasomal proteolysis are activated to catalyze the degradation of muscle proteins, including myofibrillar components and organelles [153,154,155,156,157,158]. Recent findings suggest that FOXO1 is a major regulator of energy metabolism in general (159) while FOXO3 may play significant roles in skeletal muscle wasting in responses to stresses [160,161,162,163,164].

FOXO3 activity is highly regulated by post-translational modifications, including phosphorylation, acetylation and ubiquitination in response to oxidative stress [165,166,167,168,169,170]. Under physiological conditions, insulin induces FOXO3 phosphorylation in muscle via IGF-1/insulin-IRS-PI3K-Akt, leading to the exclusion of FOXO3 from the nucleus and binding with 14-3-3γ protein. Consequently poly-ubiquitination and degradation occur in the cytoplasm (171,172,173,174,175). Therefore, the finely tuned equilibrium between FOXO3 transcription activities in the nuclear compartment and degradation in the cytosolic compartment is maintained. However, pathophysiologic changes not only impair Akt/PKB activity (reduced levels of $pSer^{308}$ and $pThr^{473}$ and enhanced Cys^{296}*S*-nitrosylation as discussed above), but also increase the activities of a number of stress kinases which phosphorylate FOXO3 at sites different from those acted upon by IGF-1/insulin-IRS-PI3K-Akt. This results in nuclear translocation and transactivation with modulation of FOXO3 activities by p300/CB-mediated acteylation and Sirt1- mediated deacetylation [176,177,178,179,180].

Within thenucleus, FOXO3 binds to the target gene promoter; p300/CBP is recruited to the DNA-FOXO3 complex and transcription of target proteins is stimulated; initially by acetylating nucleosomal histones. Subsequently, there is p300/CBP mediated acetylation of FOXO3 which leads to dissociation from the promotor.At the same time, Sirt1 may stimulate or maintain the binding of FOXO3 to DNA which stimulates deacetylation of acetylated FOXO3 under conditions of oxidative stress.FOXO3 may also be monoubiquitinated, which enhances its transcriptional activity. Recent data has shown that nuclear Sirt1 deacetylation may render the acetylated FOXO3 lysine residues (Lys^{242}, Lys^{259}, Lys^{290}, Lys^{569} and possible Lys^{270}, Lys^{271}) susceptible to polyubiquitination. Degradation of deacetylated FOXO3 appears to be mediated by Skp2, a subunit of E3 ubiquitin ligase, which also binds to the Ser^{256} residue that is phosphorylated by Akt/PKB. These regulatory pathways are illustrated in Figure 1. Therefore, the hypothesis is that, burn injury stimulates muscle FOXO3 activities by altering an intricate combination of phosphorylation, acetylation and ubiquitination,named “the FOXO3 code” [181]. These PTMs are likely to occur concurrently and to affect each other, leading to burn induced muscle wasting. Investigations of the complicated interlocking processes mediating post translational modulations of regulatory proteins with a focus on nuclear protein FOXO3,

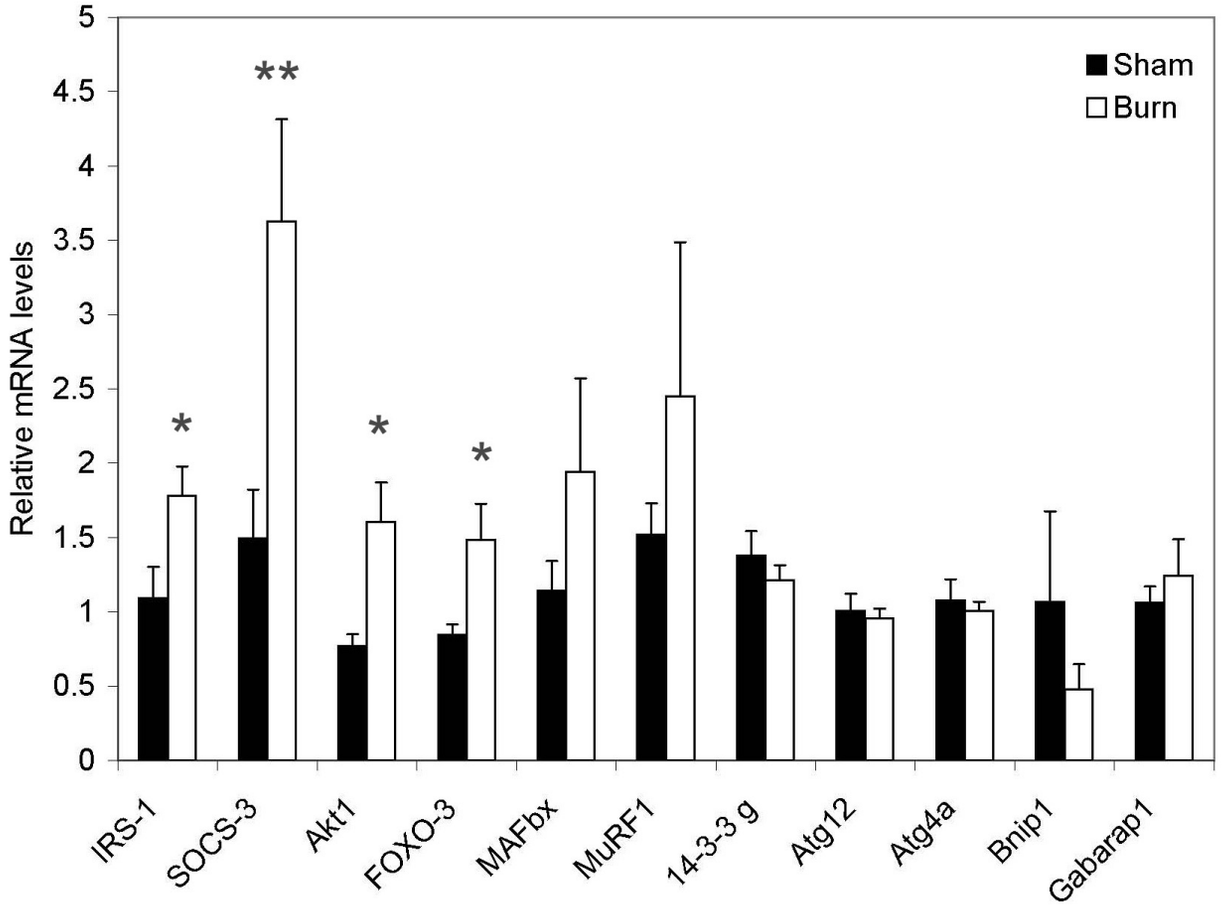

Figure 20. Burn-induced proteasomal and lysosomal proteolysis gene expression in mouse skeletal muscle. Gene profiles in sham treated (n=8) and burned mice; 3rd degree of 30% TBSA on day 7 after injury (n=15) indicate reduced cytosolic FOXO3 degradation and enhancement in the proteasomal proteolysis pathway.

in relation will lead to new knowledge about the mechanism(s) of muscle wasting after burn injury. The effects of FOXO3 PTMs on its function have been studied extensively, but discrepant results have been reported by many investigators under different conditions. Unfortunately, little information about FOXO3 PTM in muscle after burn injury is currently available.

Determination of acetylation state of lysine residues in FOXO3 protein is dependent on NanoLC-Q-TOF tandem mass spectrometry technology. Unlike labile phosphorylated or O-GlcNac modified Ser residues, acetylated lysine residues are stable during tissue extraction processes. The likelihood of false negative findings is minimal. Therefore, NanoLC-Q-TOF tandem mass spectrometry provides accurate site-specific identification of acetylation on lysine residue by detecting a mass shift (Δmass) of 42.01 Da [182]. In this project, we propose to explore the relationship between FOXO3 acetylation and muscle wasting after burn injury.

Initially, quantitative real-time RT-PCR was performed to evaluate factors related to muscle wasting at the mRNA level. IRS-1, SOCS3, Akt1, FOXO3, MAFbx, MuRF1, 14-3-3γ, Atg12, Atg4a, Bnip3, and Gabarapl1 mRNA levels were measured as shown in Figure 20. In contrast to the decrease in cellular IRS-1 protein levels, its mRNA expression was increased by 35%

http://dx.doi.org/10.5772/54849

($p<0.05$). SOCS-3 and Akt1 mRNA expressions were also increased by 140% ($p<0.005$) and 110% ($p<0.05$), respectively. Increased Akt1 mRNA expression was observed even though there were decreased phosphorylations of Akt1 Ser473 and Thr308, and increased S-nitrosylation of Cys296 in the kinase loop. These data suggest that impairment of the Akt mediated anabolic pathway show an early tendency for transcriptional recovery on day 7 after injury. In contrast, significant up-regulation of FOXO3 and no change in 14-3-3γ mRNA indicates that cytosolic FOXO3 degradation via the 14-3-3γ complex continues to be reduced in responses to the burn injury on day 7. Atg proteins, Binlp1, Gabarapl1 and many other proteins act together to generate double-membrane autophagosomes, which transfer their contents to lysosomers. However, all of these autophagy-related mRNAs were not significantly changed. In contrast, increased atrogin-1/MAFbx and MuRF-1 mRNAs, although not significant on Day 7, suggest that E3 ligase promoted proteasomal proteolysis is mainly responsible for muscle wasting after burn injury, challenging the lysosome hypothesis [183,184].

The activity of FOXO3 is dependent on sub-cellular location which is regulated by a broad range of PTMs: phosphorylation, acetylation and ubiquitination. Specifically, FOXO3 regulation mechanisms in association with nucleosomal histones are primarily controlled by reversible acetylations as illustrated in Figure 1. Nineteen phosphorylated residues are listed in the UniProtKB/Swiss-Prot and five acetylated sites in FOXO3 and seven sites in FOXO1 are observed [185]. However, these data are not consistent between laboratories. For the first time, two PTM isomers of muscle FOXO3 induced by burn injury were unambiguously confirmed at the amino acid sequence level with the NanoLC-Q-TOF approach. As illustrated in Figure 22 (left panel) Western blot analysis confirmed the SDS-PAGE FOXO3 band splitting in skeletal muscle of burned mice. The apparent SDS-PAGE MW of FOXO3 in skeletal muscle of sham treated mice was ~87 kDa (672 AA, calc MW: 71,064) from varying amounts of FOXO3 in lanes S30, S15 and S5. One extra band, located at apparent molwt of ~80 kDa as seen in lanes B30, B15 and B5, was detected in skeletal muscle from burned mice. These two FOXO3 isomers were clearly verified with recombinant human FOXO3 as shown in the right panel of Figure 21.

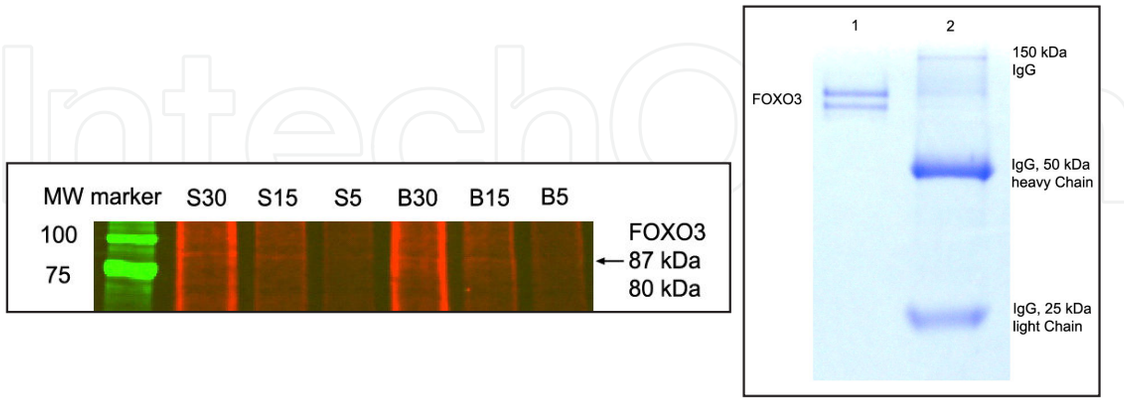

Figure 21. SDS-PAGE band splitting of FOXO3 Left panel:Immunoprecipitations of muscle lysates from burned and sham treated mice were performed using anti-C-terminal antibody (sc-34895, 2 µg). The membrane was scanned over near-infrared range. Right panel:Recombinant human FOXO3 was loaded onto the 12% Ready Gels with intact and reduced goat IgG. Two FOXO3 bands were also found with molecular weights of above 87 and 80 kDa as compared with intact IgG (150 kDa) and reduced IgG heavy chains (50 kDa).

NanoLC-Q-TOF tandem mass spectrometry data revealed that burn-induced skeletal muscle FOXO3 undergoing multiple phosphorylations and acetylations. These PTMs increase overall FOXO3 negative charge which changes electrophoretic mobility during SDS-PAGE. Both FOXO3 SDS-PAGE bands, obtained *in vitro* and *in vivo*, were unambiguously confirmed with MS/MS sequencing. Criteria for positive skeletal muscle FOXO3 PTM identification were defined as follows: 1. Tryptic peptides in digests must be unambiguously confirmed with MS/MS sequencing with reference to protein data banks; 2. Both SDS-PAGE bands are verified as FOXO3 isomers with at least two peptide sequence matches; 3. Mass accuracy of phosphorylated and acetylated MS/MS ion shifts are: 79.97 ± 0.10 and 42.01 ± 0.10 Da; 4. S/N of phosphorylated and acetylated MS/MS ions are >2. FOXO3 acetylated at the 241-Lys residue (~80 kDa) in mouse muscle after burn injury was sequenced as shown in Figure 22.

Our MS/MS data confirmed phosphorylation and acetylation in two domains of FOXO3, the FOXO3 DNA binding domain and the FOXO3 transactivation/chromatin remodeling domain as shown below:

FOXO3 DNA binding domain

Human FOXO3 tryptic peptide T4, triply charged

VLAPGGQDPGSGPATAAGGLSGGTQALLQPQQPLPPPQPGAAGGpS144GQPR

Burned mouse skeletal muscle FOXO3 tryptic peptide T18, doubly charged

SSWWIINPDGG**ACK241**

FOXO3 transactivation/Chromatin remodeling domain

Human FOXO3 tryptic peptide T30-31, doubly charged

ACK271AALQTAPEpS280ADDpS284PSQLSACK290

In summary. Under physiological conditions, insulin induces FOXO3 phosphorylation in muscle via IGF-1/insulin-IRS-PI3K-Akt, leading to the exclusion of FOXO3 from the nucleus and binding to 14-3-3γ protein with subsequent poly-ubiquitination and degradation in the cytoplasm. Similarly, acetylation of FOXO3 results in neutralization of the positive charges on lysine residues and facilitates entry into the nuclear compartment. In the nucleus FOXO3 up-regulates genes mediating skeletal muscle protein degradation and down-regulates genes mediating skeletal muscle protein synthesis. The net result of the processes is muscle wasting. In primitive man (i.e. "cave-man") this was a highly adaptive process. For example when a cave-man suffered from major trauma such as being "mauled by a saber tooth tiger" and survived the insult to return to his cave, skeletal muscle wasting was critical for survival. Since primitive man probably did not have significant amounts of adipose tissue and glycogen stores provide limited substrates for energy production and anabolic function survival depended on mobilization of skeletal muscle (in addition to some nutritional supplementation by friends and relatives).

In modern society, after major trauma, the victim is usually confined to an intensive care unit and nutritional metabolic requirements after injury are met by carefully controlled enteral and

http://dx.doi.org/10.5772/54849

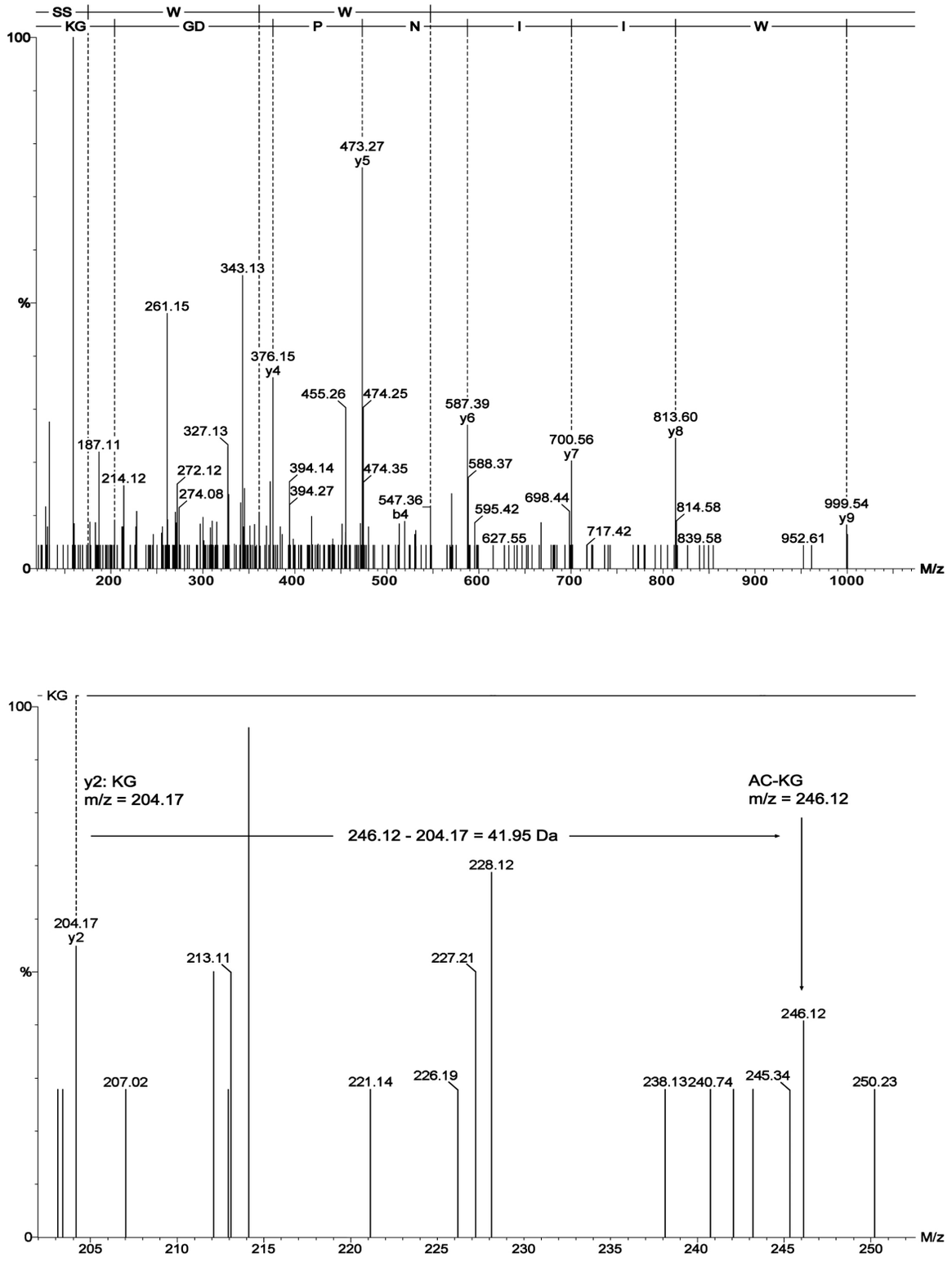

Figure 22. Site-specific pinpointing of acetylated Lys241 of FOXO3 in burned mouse muscle. Upper panel: Identification of mouse FOXO3 peptide T18 $[M+2H]^{+2}$ = m/z 680.34, found: m/z 680.52. Lower panel: Zoom of the T18 peptide y2 ion m/z 204.17 (241-Lys-Gly) and corresponding acetylated y2 ion m/z 246.12 (AC-241-Lys-Gly) indicates a mass shift of 41.95 Da.

parenteral nutrition. However the processes mediating FOXO3 entry in to the nucleus continue to be manifest and muscle wasting persists leading to weakness and in severe cases respiratory failure. Thus, a critical survival mechanism in primative man has transitioned to a major factor in morbidity and mortality for victims of severe trauma and burns in today's society.

5. Conclusion

PTM profiling of burn-induced IRS-1 C-terminal phosphorylation, S-nitrosylation of Akt1/PKBα|| Cys^{296} and acetylation of FOXO3 Lys^{241}, Lys^{271} and Lys^{290} expands our understanding of insulin resistance and muscle wasting after burn injury. These findings reveal that Cys^{296}-Cys^{310} disulfide bond formation together with dephosphorylation of Thr^{308} in the kinase Akt1/PKBα|| loop regulates FOXO3 sub-cellular distribution and transcriptional activity. The PTM profiling enables new recognition patterns for partner's molecules turn "on" and "off" of enzyme activity and control the lifetime and location of the mediators in insulin signal transduction [137,186]. IRS-1 integrity is reduced by 10% which is not a major factor in downstreamsignaling. However, impaired Akt1/PKBa activity by 70% due to enhanced S-nitrosylation of Cys^{296} and reduction of phosphor-Thr^{308} and Ser^{473} has major impact on FOXO3 sub-cellular distribution and activities. Muscle wasting but not insulin resistance is significant in burned vs sham treated groups between days 3 and 7 post-burn injury. Our studies provide a deep insight into the interrelationships between burn-induced oxidative and metabolic stresses and muscle wasting in human patients [187].

Author details

Xiao-Ming Lu[1,2], Ronald G. Tompkins[1,2] and Alan J. Fischman[1,2]

1 Surgical Service, Massachusetts General Hospital and Harvard Medical School, Boston, MA, USA

2 The Shriners Hospitals for Children, Boston, MA, USA

References

[1] Taniguchi CM, Emanuelli B, Ronald KC. Critical nodes in signaling pathways: insights into insulin action. Nature Reviews Molecular Cell Biology 2006; 7:85-96.

[2] Jeschke MG, Mlcak RP, Finnerty CC, Norbury WB, Gauglitz GG, Kulp GA, Herdon DN. Burn size determines the inflammatory and hypermetabolic response. Critical Care 2007; 11:R90.

[3] Gauglitz GG, Halder S, Boehning DF, Kulp GA, Herdon DN, Barral JM, Jeschke MG. Post-burn hepatic insulin resistance is associated with endoplasmic reticulum (ER) stress. Shock 2010; 33(3):299-305.

[4] Evers LH, Bhavsar G, Mailander P. The biology of burn injury. Experimental Dermatology 2010; 19:777-783.

[5] Przkora R, Herdon DN, Finnerty CC, Jeschke MG. Insulin attenuates the cytokine response in a burn wound infection model. Shock 2007; 27(2):205-208.

[6] Jeschke MG, Boehning DF, Finnerty CC, Herndon DN. Effect of insulin on the inflammatory and acute phase response after burn injury. Critical Care Medicine 2007; 35(9 Suppl): S519-S523.

[7] Barrow RE, Dasu MRK, Ferrando AA, Spies M, Thomas ST, Perez-Polo JP, Herndon DN. Gene expression patterns in skeletal muscle of thermally injured children treated with oxandrolone. Annual Surgery 2003; 237(3):422-428.

[8] Dasu MR, Barrow RE, Herndon DN. Gene profiling in muscle of severely burned children: Age-and Sex-dependent changes. The Journal of Surgical Research 2005; 123:144-152.

[9] Pidcoke HF, Wade CF, Wolf SE. Insulin and burned patient. Critical Care Medicine 2007; 35(9): suppl. S524-S530.

[10] Gauglitz GG, Herndon DN, Kulp GA, Meyer III WJ, Jeschke MG. Abnormal insulin sensitivity persists up to three years in pediatric patient post-burn. The Journal of Clinical Endocrinology & Metabolism. 2009; 94(5):1656-1664.

[11] Gauglitz GG, Herndon DN, Jeschke MG. Insulin resistance postburn: Underlying mechanisms and current therapeutic strategies. Journal of Burn Care & Research 2008; 29:683-694.

[12] Khoury W, Klausner JM, Benabraham R, Szold O. Glucose control by insulin for critically ill surgical patients. The Journal of Trauma 2004; 57(5):1132-1138.

[13] Carter EA, Burks D, Fischman AJ, White MF, Tompkins RG. Insulin resistance in thermally-injured rats is associated with post-receptor alterations in skeletal muscle, liver and adipose tissue. International Journal of Molecular Medicine 2004; 14:653-658.

[14] Johan Groeneveld AB, Beishuizen A, Visser FC. Insulin: a wonder drug in the critically ill? Critical Care 2002; 6(2):102-105.

[15] Ikezu T, Okamato T, Yonezawa K, Tompkins RG, Martyn JAJ. Analysis of thermal injury-induced insulin resistance in rodents. Journal of Biological Chemistry 1997; 272 (40):25289-25295.

[16] White MF. Insulin signaling in health and disease. Science 2003; 302:1710-1711.

[17] Zhang Q, Cater EA, Ma B-Y, White MF, Fischman AJ, Tompkins RG. Molecular mechanism(s) of burn-induced insulin resistance in murine skeletal muscle: role of IRS phosphorylation. Life Science 2005; 77:3068-3077.

[18] Carey LC, Lowery BD, Cloutier CT. Blood sugar and insulin response of humans in shock. Annual Surgery 1970; 172:342-350.

[19] Allison SP, Hinton P, Chamberlain MJ. Intravenous glucose-tolerance, insulin, and free-fatty-acid levels in burned patients. Lancet 1968; 2:1113-1116.

[20] Taylor FHL, Levenson SM, Adams MA. Abnormal carbohydrate metabolism in human thermal burns. The New England Journal of Medicine 1944; 231:437-445.

[21] Rayfield EJ, Curnow RT, George DT, Beisel WR. Impaired carbohydrate metabolism during a mild viral illness. The New England Journal of Medicine 1973; 289:618-621.

[22] Williams JL, Dick GF. Decreased dextrose tolerance in acute infectious disease. Archives of Internal Medicine 1932; 50:801-818.

[23] Wilmore DW, Mason AD Jr, Pruitt BA Jr. Insulin response to glucose in hypermetabolic burn patients. Annual Surgery 1976; 183:314-320.

[24] Mizock BA. Alterations in carbohydrate metabolism during stress: a review of the literature. The American Journal of Medicine 1995; 98:75-84.

[25] Grecos GP, Abbott WC, Schiller WR, Long CL, Birkhahn RH, Blakemore WS. The effect of major thermal injury and carbohydrate-free intake on serum triglycerides, insulin and 3-methylhistidine excretion. Annual Surgery 1984; 200:632-637.

[26] Thomas R, Aikawa N, Burke JF. Insulin resistance in peripheral tissues after a burn injury. Surgery 1979; 86:742-747.

[27] Turinsky J, Patterson SA. Proximity of a burn wound as a new factor in considerations of postburn insulin resistance. The Journal of Surgical Research 1979; 26:171-174.

[28] Woolfson AMJ, Heatley RV, Allison SP. Insulin to inhibit protein catabolism after injury. The New England Journal of Medicine 1979; 300:14-17.

[29] Wolfe RR, Drukot MJ, Wolfe MH. Effect of thermal injury on energy metabolism, substrate kinetics and hormonal concentrations. Circulatory Shock 1982; 9:383-394.

[30] Wolfe RR, Durkot MJ, Allsop JR, Burke JF. Glucose metabolism in severely burned patients. Metabolism 1979; 28(10):1031-1039.

[31] Jahoor F, Herndon DN, Wolfe RR. Role of insulin and glucagon in the response of glucose and alanine kinetics in burn-injured patients. The Journal of Clinical Investigation 1986; 78:807-814.

[32] Jahoor F, Shangraw RE, Miyoshi H, Wallfish H, Herndon DN, Wolfe RR. Role of insulin and glucose oxidation in mediation the protein catabolism of burns and sepsis. American Journal of Physiology 1989; 257:E323-E331.

[33] Black PR, Brooks DC, Bessey PQ, Wolfe RR, Wilmore DW. Mechanism of insulin resistance following injury. Annual Surgery196:420-435.

[34] Frayn KN. Effects of burn injury on insulin secretion and sensitivity to insulin in the rat in vivo. European Journal of Clinical Investigation 1975; 5(4):331-337.

[35] Allsop JR, Wolfe RR, Burke JF. Glucose kinetics and responsiveness to insulin in the rat injured by burn. Surgery Gynecology and Obstetrics. 1978; 147:565-573.

[36] Frayn KN, Le Marchand-Brustel Y, Freychet P. Studies on the mechanism of insulin resistance after injury in the mouse. Diabetologia 1978; 14:337-341.

[37] Turinsky J, Saba TM, Scovil WA, Chesnut T. Dynamics of insulin secretion and resistance after burns. The Journal of Trauma 1977; 17:344-350.

[38] Turinsky J. Glucose metabolism in the region recovering from burn injury: effect of insulin on 2-deoxyglucose uptake in vivo. Endocrinology 1983; 113:1370-1376.

[39] Wogensen L, Jensen M, Svensson P, Worsaae H, Welinder B, Nerup J. Pancreatic beta-cell function and interleukin-1 beta in plasma during the acute phase response in patients with major burn injuries. European Journal of Clinical Investigation 1993; 23:311-319.

[40] Lang CH, Dobrescu C, Burke JF. Tumor necrosis factor impairs insulin action on peripheral glucose disposal and hepatic glucose output. Endocrinology 1992; 130:43-52.

[41] Ling PR, Bristrian BR, Mendez B, Igtfan NW. Effects of systemic infusion of endotoxin, tumor necrosis factor, and interleukin-1 on glucose metabolism in the rat: relationship to endogenous glucose production and peripheral tissue glucose uptake. Metabolism 1994; 43:279-284.

[42] Portoles MT, Pagan R, Ainaga MJ, Diaz-Laviada I, Municio AM. Lipopolysaccharide-induced insulin resistance in monolayers of cultured hepatocytes. British Journal of Experimental Pathology 1989; 70:199-205.

[43] Christ B, Nath A, Heinrich PC, Jungermann K. Inhibition by recombinant human interleukin-6 of the glucagon-dependent induction of phosphopyruvate carboxykinase gene expression in cultured rat hepatocytes: regulation of gene transcription and messenger RNA degradation. Hepatology 1994; 20(6):1577-1583.

[44] Cryer PE. Hypoglycemia: the limiting factor in the management of IDDM. Diabetes 1994; 43:1378-1389.

[45] de Bandt JP, Chollet-Martin S, Hernvann A, Lioret N, du Roure LD, Lim SK, Vaubaudole M, Guiechot J, Saizy R, Giboudeau J. Cytokine response to burn injury: relationship with protein metabolism. The Journal of Trauma 1994; 36(5):624-628.

[46] Burke JF, Wolfe RR, Mullanye CJ, Matthews DE, Bier DM. Glucose requirements following burn injury. Parameters of optimal glucose infusion and possible hepatic and respiratory abnormalities following excessive glucose intake. Annual Surgery 1979; 190(3):274-283.

[47] Feinstein R, Kanetyh H, Papa MZ, Lunenfield B, Karazik A. Tumor necrosis factor alpha suppresses insulin-induced tyrosine phosphorylation of insulin receptor and its substrates. Journal of Biological Chemistry 1993; 268:26055-26058.

[48] Hotamisligil GS, ?rray DL, Choy ?, Spiegelman BM. Tumor necrosis factor inhibits signaling from the insulin receptor. Proceeding of the National Academy of Sciences of United States of America 1994; 91:4854-4858.

[49] Hotamisligil GS. Reduced tyrosine kinase activity of the insulin receptor in obesity-diabetes: central role of tumor necrosis factor. The Journal of Clinical Investigation 1994; 94:1543-1549.

[50] Wilmore DW, Aulick HL, Goodwin CW. Glucose metabolism following severe injury. Acta Chirurgica Scandinavica Supplementum 1980; 498:43-47.

[51] Ikezu T, Okamoto T, Yonezawa K, Tompkins RG, Martyn JA. Analysis of thermal injury-induced insulin resistance in rodents. Implication of postreceptor mechanisms. Journal Biological Chemistry 1997; 272:25289-95.

[52] Sun XJ, Crimmins DL, Myers MG Jr., Miralpeix M, and White MF. Pleiotropic insulin signals are engaged by multisite phosphorylation of IRS-1. Molecular and Cellular Biology 1993; 13(12):7418-7428.

[53] Liberman Z, and Eldar-Finkelman H. Serine 332 phosphorylation of insulin receptor substrate-1 by glycogen synthase kinase-3 attenuates insulin signaling. Journal of Biological Chemistry 2005; 280(6):4422-4428.

[54] De Fea K, Roth RA. Protein kinase C modulation of insulin receptor substrate-1 tyrosine phosphorylation requires serine 612. Biochemistry. 1997; 36(42):12939-12947.

[55] Goodyear LJ, Giorgino F, Sherman LA, Carey J, Smith RJ, and Dohm GL. Insulin receptor phosphorylation, insulin receptor substrate-1 phosphorylation, and phosphatidylinositol 3-kinase activity are decreased in intact skeletal muscle strips from obese subjects. The Journal of Clinical Investigation 1995; 95:2195-2204.

[56] Tanasijevic MJ, Myers MG Jr, Thoma RS, Crimmins DL, White MF, and Sacks DB. Phosphorylation of the insulin receptor substrate IRS-1 by casein kinase II. Journal of Biological Chemistry 1993; 268(24):18157-18166.

[57] Giraud J, Hass M, Feener EP, Copps KD, Dong X, Dunn SL, and White MF. Phosphorylation of IRS1 at Ser-522 inhibits insulin signaling. Molecular Endocrinology 2007; 21(9):2294-2302.

[58] Luo M, Langlais P, Yi Z, Lefort N, Filippis EAD, Hwang H. Christ-Roberts CY, and Mandarino LJ. Phosphorylation of human insulin receptor substrate-1 at serine 629 plays a positive role in insulin signaling. Endocrinology 2007; 148(10): 4895-4905.

[59] Scioscia M, Gumaa K, Kunjara S, Paine MA, Selvaggi LE, Rodeck CH, and Rademacher TW. Insulin resistance in human preeclamptic placenta is mediated by serine phosphorylation of insulin receptor substrate-1 and -2. Journal of Clinical Endocrinology 2006; 91(2):709-717.

[60] Nawaratne R, Gray A, Jogensen CH, Downes CP, Siddle K, and Sethi JK. Regulation of insulin receptor substrate 1 pleckstrin homology domain by protein kinase C: role of serine 24 phosphorylation. Molecular Endocrinology 2006; 20(8):1838-1852.

[61] Danielsson A, Ost A, Nystrom FH, and Strafors P. Attenuation of insulin-stimulated insulin receptor substrate-1 serine 307 phosphorylation in insulin resistance of type 2 diabetes. Journal of Biological Chemistry 2005; 280(41):34389-34392.

[62] Li Y, Soos TJ, Li X, Wu J, DeGennaro M, Sun X, Littman DR, Birnbaum MJ, and Polajiewicz RD. Protein kinase C theta inhibits insulin signaling by phosphorylation IRS1 at Ser1101. Journal of Biological Chemistry 2004; 279(44):45304-45307.

[63] Gao Z, Zuberi A, Quon MJ, Dong Z, and Ye J. Aspirin inhibits serine phosphorylation of insulin receptor substrate 1 in tumor necrosis factor-treated cell through targeting multiple serine kinases. Journal of Biological Chemistry 2003; 278(27): 24944-24950.

[64] Hers I, Bell CJ, Poole AW, Jiang D, Denton RM, Schaefer E, and Tavare JM. Reciprocal feedback regulation of insulin receptor and insulin receptor substrate tyrosine phosphorylation by phosphoinositide 3-kinase in primary adipocytes. Biochemistry Journal 2002; 368(pt 3):875-884.

[65] Yu C, Chen Y, Cline GW, Zhang D, Zong H, Wang Y, Bergeron R, Kim JK, Cushman SW, Cooney GJ, Atcheson B, White MF, Kraegen EW, and Shulman G I. Mechanism by white fatty acids inhibit insulin activation of insulin receptor substrate-1 (IRS-1)-associated phosphatidylinositol 3-kinase activity in muscle. Journal of Biological Chemistry 2002; 277(52):50230-50236.

[66] Amoui M, Craddock BP, and Miller WT. Differential phosphorylation of IRS-1 by insulin and insulin-like growth factor 1 receptors in Chinese hamster ovary cells. Journal of Endocrinology 2001; 171:153-162.

[67] Gual P, Gremeaux T, Gonzalez T, Marchand-Brustel YL, and Tanti J.-F. MAP kinase and mTOR mediate insulin-induced phosphorylation of insulin receptor substrate-1 on serine residues 307, 612 and 632. Diabetologia 2003; 46:1532-1542.

[68] Werner ED, Lee J, Hansen L, Yuan M, and Shoelson SE. Insulin resistance due to phosphorylation of insulin receptor substrate-1 at serine 302. Journal of Biological Chemistry 2004; 279(34):35298-35305.

[69] Sommerfeld MR, Metzger S, Stosik M, Tennagels N, and Eckel J. In vitro phosphorylation of insulin receptor substrate 1 by protein kinase C- zeta: Function analysis and identification of novel phosphorylation sites. Biochemistry 2004; 43:5888-5901.

[70] Lehr S, Kotzka J, Herkner A, Sikmann A, Meyer HE, Krone W, and Muller-Wieland D. Identification of major tyrosine phosphorylation sites in the human insulin receptor substrate Gab-1 by insulin kinase receptor kinase in vitro. Biochemistry 2000; 39:10898-10907.

[71] Luo M, Reyna S, Wang L, Yi Z, Carroll C, Dong LQ, Langlais P, Weintraub ST, and Mandarino LJ. Identification of insulin receptor substrate 1 serine/threonine phosphorylation sites using mass spectrometry analysis: Regulatory role of serine 1223. Endocrinology 2005; 146(10):4410-4416.

[72] Yi Z, Luo M, Carroll CA, Weintraub ST, and Mandarino LJ. Identification of phosphorylation sites in insulin receptor substrate-1 by hypothesis-driven high-performance liquid chromatography-electrospray ionization tandem mass spectrometry. Analytical Chemistry 2005; 77:5693-5699.

[73] Yi Z, Luo M, Mandarino LJ, Reyna SM, Carroll CA, and Weintraub ST. Quantification of phosphorylation of insulin receptor substrate-1 by HPLC-ESI-MS/MS. Journal of the American Society for Mass Spectrometry 2006; 17:562-567.

[74] Beck A, Moeschel K, Deeg M, Haring H-U, Voelter W, Schleicher ED, and Lehmann R. Identification of an in vitro insulin receptor substrate-1 phosphorylation site by negative-ion ▪ LC/ES-API-CID-MS hybrid scan technique. Journal of the American Society for Mass Spectrometry 2003; 14 (4):401-405.

[75] Gual P, Marchand-Brustel YL, and Tanti J-F. Positive and negative regulation of insulin signaling through IRS-1 phosphorylation. Biochimie. 2005; 87(1):99-109.

[76] Zick Y. Ser/Thr phosphorylation of IRS proteins: A molecular basis for insulin resistance. 2005; Science STKE 2005(268):pe4.

[77] Liu Y-F, Herschkovitz A, Boura-Halfon S, Ronen D, Paz K, LeRoith D, and Zick Y. Serine phosphorylation proximal to its phosphotyrosine binding domain inhibits insulin receptor substrate 1 function and promotes insulin resistance. Molecular and Cellular Biology 2004; 24(21):9668-9681.

[78] Zick Y. Insulin resistance: a phosphorylation-based uncoupling of insulin signaling. Trends in Cell Biology 2001; 11(11):437-441.

[79] Bouzakri K, Karlsson HKR, Vestergaard H, Madsbad S, Christiansen E, and Zierath JR. IRS-1 serine phosphorylation and insulin resistance in skeletal muscle from pancreas transplant recipients. Diabetes 2006; 55:785-791.

[80] Sugita H, Fujimoto M, Yasukawa T, Shimizu N, Sugita M, Yasuhara S, Martyn, JM, and Kaneki M. Inducible nitric-oxide synthase and NO donor induce insulin receptor

substrate-1 degradation in skeletal muscle cells. Journal of Biological Chemistry 2005; 280(14):14203-14211.

[81] Usui I, Imamura T, Huang J, Satoh H, Shenoy SK, Lefkowitz RJ, Hupfeld CJ, and Olefsky JM. -Arrestin-1 competitively inhibits insulin-induced ubiquitination and degradation of insulin receptor substrate 1. Molecular and Cellular Biology 2004; 24(20):8929-8937.

[82] Pederson T, Kramer DL, and Rondinone CM. Serine/Threonine phosphorylation of IRS1 triggers its degradation, possible regulation by tyrosine phosphorylation. Diabetes 2001; 50:24-31.

[83] Potashnik R, Bloch-Damti A, Bashan N, and Rudich A. IRS1 degradation and increased serine phosphorylation cannot predict the degree of metabolic insulin resistance induced by oxidative stress. Diabetologia 2003; 46:639-648.

[84] Lee AV, Gooch JL, Oesterreich S, Guler RL, and Yee D. Insulin-like growth factor I-induced degradation of insulin receptor substrate1 is mediated by the 26S proteasome and blocked by phosphatidylinositol 3′-kinase inhibition. Molecular and Cellular Biology 2000; 20(5):1489-1496.

[85] Sun XJ, Goldberg JL, Qiao L-Y, and Mitchell JJ. Insulin-induced insulin receptor substrate-1 degradation is mediated by the proteasome degradation pathway. Diabetes 1999; 48:1359-1364.

[86] Zhande R, Michell JJ, Wu J, and Sun XJ. Molecular mechanism of insulin-induced degradation of insulin receptor substrate 1. Molecular and Cellular Biology 2002; 22(4):1016-1026.

[87] White MF. IRS proteins and the common path to diabetes. American Journal of Physiology, Endocrinology and Metabolism 2002; 283:E413-E422.

[88] Thirone ACP, Huang C, and Klip A. Tissue-specific roles of IRS proteins in insulin signaling and glucose transport. Trends in Endocrinology and Metabolism 2006; 17(2):72-78.

[89] Youngren JF. Regulation of insulin receptor function. Cellular and Molecular Life Sciences 2007; 64(7-8):873-91.

[90] Lu XM, Lu M, Tompkins RG, and Fischman AJ. Site-specific detection of S-nitrosylated PKB/Akt1 from rat solues muscle using CapLC-Q-TOF^{micro} mass spectrometry. Journal of Mass Spectrometry 2005; 40 (9):1140-1148.

[91] Lu XM, Lu M, Fischman AJ, and Tompkins RG. A new approach for sequencing human IRS1 phosphotyrsine-containing peptides using CapLC-Q-TOFmicro. Journal of Mass Spectrometry 2005; 40 (5):599-607.

[92] Dong X, Park S, Lin X, Copps K, Yi X, White MF. Irs1 and Irs1 signaling is essential for hepatic glucose homeostasis and systemic growth. The Journal of Clinical Investigation 2006; 116 (1):101-114.

[93] Danielsson A, Nystrom FH, Stralfors P. Phosphorylation of IRS1 at serine 307 and serine 312 in response to insulin in human adipocytes. Biochemical and Biophysical Research Communications 2006; 342(4):1183-1187.

[94] Lowell BB, Shulman GI. Mitochondrial dysfunction and type 2 diabetes, Science 2005; 307:384-387.

[95] Manning G, Whyte DB, Martinez R, Hunter T, Sudarsanam S. The protein kinase complement of the human genome. Science 2002; 298:1912-1934.

[96] Sykiotis GP, Papavassiliou AG, Serine phosphorylation of insulin receptor substrate-1: A novel target for the reversal of insulin resistance. Molecular Endocrinology 2001; 15 (11):1864-1869.

[97] Le Marchand-Brustel Y, Gual P, Gremeaux T, Gonzalez T, Barres R, Tanti J-F. Fatty acid-induced insulin resistance: role of insulin receptor substrate 1 serine phosphorylation in the retroregulation of insulin signaling. Biochemical Society Transactions 2003; 31(pt 6):1152-1156.

[98] Sciocia M, Gumaa K, Kunjara S, Paine MA, Selvaggi LE, Rodeck CH, Rademacher TW. Insulin resistance in human preeclamptic placenta is mediated by serine phosphorylation of insulin receptor substrate-1 and -2. The Journal of Clinical Endocrinology and Metabolism 2006; 91(2):709-717.

[99] Yang J, Cron P, Thompson V, Good VM, Hess D, Hemmings BA, Barford D. Molecular mechanism for the regulation of protein kinase B/Akt by hydrophobic motif phosphorylation. Molecular Cell 2002; 9:1227-1240.

[100] Yang J, Cron P, Good VM, Thompson V, Hemmings BA, Barford D. Crystal structure of an activated Akt/protein kinase B ternary complex with GSK3-peptide and AMP-PNP. Nature Structural Biology 2002; 9(12):940-944.

[101] Huang X, Begley M, Morgenstern KA, Gu Y, Rose P, Zhao H, Zhu X. Crystal structure of an inactive Akt2 kinase domain. Structure 2003; 11:21-30.

[102] Kumar CC, Madison V. Akt crystal structure and Akt-specific inhibitors. Oncogene 2005; 24:7493-7501.

[103] Fayard E, Tintignac LA, Baudry A , Hemmings BA. Protein kinase B/Akt at a glance. Journal of Cell Science 2005; 118(pt 24):5675-5678.

[104] Brazil DP, Yang ZZ, Hemmings BA. Advances in protein kinase B signaling: AKTion on multiple fronts. Trends in Biochemical Sciences 2004; 29(5):233-242.

[105] Brazil DP, Park J, Hemmings BA. PKB binding proteins: getting in on the Akt. Cell 2002; 111:293-303.

[106] Huang BX, Kim HY. Interdomain conformational changes in Akt activation revealed by chemical cross-linking and tandem mass spectrometry. Molecular& Cellular Proteomics 2006; 5:1045-1053.

[107] Sugita H, Kaneki M, Sugita M, Yasukawa T, Yasuhara S, Martyn JA. Burn injury impairs insulin-stimulated Akt/PKB activation in skeletal muscle. American Journal of Physiology, Endocrinology and Metabolism 2005; 288:E585-E591.

[108] Carvalho-Filho MA, Ueno M, Hirabara SM, Seabra AB, Carvalheira JB, de Oliveira MG, Velloso LA, Curi R, Saad MJ. S-nitrosation of the insulin receptor, insulin receptor substrate 1, and protein kinase B/Akt: A novel mechanism of insulin resistance. Diabetes 2005; 54(4):959-967.

[109] Yasukawa T, Tokunaga E, Ota H, Sugita H, Martyn JA, Kaneki M. S-Nitrosylation-dependent inactivation of Akt/protein kinase B in insulin resistance. Journal of Biological Chemistry 2005; 280(9):7511-7518.

[110] Carter EA, Derojas-Walker T, Tamir S, Tannenbaum SR, Yu YM, Tompkins RG. Nitric oxide production is intensely and persistently increased in tissue by thermal injury. Biochemistry Journal 1994; 304(pt 1):201-204.

[111] Auguin D, Barthe P, Auge-Senegas MT, Stern MH, Noguchi M, Roumestand C. Solution structure and backbone dynamics of the Pleckstrin homology domain of the human protein kinase B (PKB/Akt). Interaction with inositol phosphates. Journal of Bimolecular NMR 2004; 28(2):137-155.

[112] Murata H, Ihara Y, Nakamura H, Yodoi J, Sumikawa K, Kondo T. Glotaredoxin exerts an antiapoptotic effect by regulating the redox state of Akt. Journal of Biological Chemistry 2003; 278(50):50226-50233.

[113] Jaffrey SR, Erdjument-Bromage H, Ferris CD, Tempst P, Snyder SH. Protein S-nitrosylation: a physiological signal for neuronal nitric oxide. Nature Cell Biology 2001; 3:193-197.

[114] Jaffrey SR, Snyder SH. The biotin switch method for detection of S-nitrosylated proteins. Science's STKE 2001; 2001(86): pl1,1-9.

[115] Greco TM, Hodara R, Parastatidis I, Heijnen HFG, Dennehy MK, Liebler DC, Ischiropoulos H. Identification of S-nitrosylation motifs by site-specific mapping of the S-nitrosocysteine proteome in human vascular smooth muscle cells. Proceedings of the National Academy of Sciences of the Unites States of America 2006; 103(19): 7420-7425.

[116] Hao G, Derakhshan B, Shi L, Campagne F, Gross SS. SNOSID, a proteomic method for identification of cysteine S-nitrosylation sites in complex protein mixtures. Proceedings of the National Academy of Sciences of the United States of America 2006; 103 (4):1012-1017.

[117] Kuncewicz T, Sheta EA, Goldknopf IL, Kone BC. Proteomic analysis of S-nitrosylated proteins in mesangial cell. Molecular & Cellular Proteomics 2003; 2:156-163.

[118] Martinez-Ruiz A, Lamas S. Detection and proteomic identification of S-nitrosylated proteins in endothelial cells. Archives of Biochemistry and Biophysics 2004; 423:192-199.

[119] Lu XM, Tompkins RG, Fishman AJ. SILAM for quantitative proteomics of liver Akt1/PKB ▪ after burn injury. International Journal of Molecular Medicine 2012; 29:461-471.

[120] Beynon RJ, Pratt JM. Metabolic labeling of proteins for proteomics. Molecular & Cellular Proteomics 2005; 4:857-872.

[121] Harsha HC, Molina H, Pandey A. Quantitative proteomics using stable isotope labeling with amino acids in cell culture. Nature Protocols 2008; 3(3):505-516.

[122] Beynon RJ. The dynamics of the proteome: strategies for measuring protein turnover on a proteome-wide scale. Brief Functional Genomics Proteomics 2005; 3(4):382-390.

[123] Moresco JJ, Dong MQ, Yates JR. Quantitative mass spectrometry as a tool for nutritional proteomics. The American Journal of Clinical Nutrition 2008; 88:597-604.

[124] Nair KS, Jaleel A, Asmann YW, Short KR, Raghavakaimal S. Proteomic research: potential opportunities for clinical and physiological investigators. American Journal of Physiology, Endocrinology and Metabolism 2004; 286:E863-E874.

[125] Krijgsveld J, Ketting RF, Mahmoudi T, Johansen J, Artal-Sanz M, Verrijzer CP, Plasterk RH, Heck AJ. Metabolic labeling of C. elegans and D. melanogaster for quantitative proteomics. Nature Biotechnology 2003; 21(8):927-931.

[126] Doherty MK, Whitehead C, McCormack H, Gaskell SJ, Beynon RJ. Proteome dynamics in complex organisms: using stable isotopes to monitor individual protein turnover rates. Proteomics 2005; 5:522-533.

[127] Hayter JR, Doherty MK, Whitehead C, McCormack H, Gaskell SJ, Beynon RJ. The subunit structure and dynamics of the 20S proteasome in chicken skeletal muscle. Molecular & Cellular Proteomics 2005; 4:1370-1381.

[128] Wu CC, Maccoss MJ, Howell KE, Matthews DE, Yates JR. Metabolic labeling of mammalian organisms with stable isotopes for quantitative proteomic analysis. Analytical Chemistry 2004; 76:4951-4959.

[129] Kruger M, Moser M, Ussar S, Thievessen I, Luber CA, Former F, Schmidt S, Zanivan S, Fassler R, Mann M. SILAC mouse for quantitative proteomics uncovers kindling-3 as an essential factor for red blood cell function. Cell 2008; 134:353-364.

[130] Gouw JW, Tops BB, Mortensen P, Heck AJ, Krijgsveld J. Optimizing identification and quantitation of ^{15}N-labeled proteins in comparative proteomics. Analytical Chemistry 2008; 80:7796-7803.

[131] Huttlin EL, Hegeman AD, Harms AC, Sussman MR. Comparison of full versus partial metabolic labeling for quantitative proteomics analysis in arabidopsis thaliana. Molecular & Cellular Proteomics 2007; 6:860-881.

[132] Mcclatchy DB, Dong MQ, Wu CC, Venable JD, Yates JR 3rd. ^{15}N Metabolic labeling of mammalian tissue with slow protein turnover. Journal of Proteome Research 2007; 6(5):2005-2010.

[133] Liao L, McClatchy DB, Park SK, Xu T, Lu B, Yates JR. Quantitative analysis of brain nuclear phosphoproteins identifies developmentally regulated phosphorylation events. Journal of Proteome Research 2008; 7:4743-4755.

[134] Bachi A, Bonaldi T. Quantitative proteomics as a new piece of the systems biology puzzle. Journal of Proteomics 2008; 71:357-367.

[135] Gan HT, Chen JDZ. Roles of nitric oxide and prostaglandins in pathogenesis of delayed colonic transit after burn injury in rats. American Journal of Physiology-Regulatory Integrative and Comparative Physiology 2005; 288:R1316-R1324.

[136] Torres SH, De Sanctis JB, de L Briceno M, Hernandez N, Finol HJ. Inflammation and nitric oxide production in skeletal muscle of type 2 diabetic patients. Journal of Endocrinology 2004; 181:419-427.

[137] Walsh CT. Modification of cysteine and methionine by oxidation-reduction. In: Post-translational modification of proteins: expanding nature's inventory. Roberts and company publishers, Colorado, USA; 2006. p95-119.

[138] Benhar M, Forrester MT, Stamler JS. Nitrosative stress in the ER: A new role for S-nitrosylation in neurodegenerative diseases. ACS Chemical Biology 2006; 1(6): 355-358.

[139] Tannenbaum SR, White FM. Regulation and specificity of S-nitrosylation and denitrosylation. ACS Chemical Biology 2006; 1(10):615-618.

[140] Hogg N. The biochemistry and physiology of S-nitrosothiols. Annual Review of Pharmacology and Toxicology 2002; 42(1):585-600.

[141] Arnelle DR, Stamler JS. NO+, NO., and NO- donation by S-nitrosothiols: implications for regulation of physiological functions by S-nitrosylation and acceleration of disulfide formation. Archives of Biochemistry and Biophysics 1995; 318: 279-285.

[142] Wu W-I, Voegtli WC, Sturgis HL, Dizon FP, Viger GPA, Brandhuber BJ. Crystal structure of human AKT1 with an allosteric inhibitor reveals a new mode of kinase inhibition 2010; PLos ONE 5(9): e12913.

[143] Carvalho-Filho MA, Ueno M, Carvalheira JB, Velloso LA, M.J. Saad. Targeted disruption of iNOS prevents LPS-induced S-nitrosation of IR/IRS-1 and Akt and insulin resistance in muscle of mice. American Journal of Physiology, Endocrinology and Metabolism 2006; 291:E476-E482.

[144] Vogt JA, Hunzinger C, Schroer K, Holzer K, Bauer A, Schrattenholz A, Cahill MA, Schillo S, Schwall G, Stegmann W, Albuszies G. Determination of fractional synthesis rates of mouse hepatic proteins via metabolic ^{13}C-labeling, MALDI-TOF MS and analysis of relative isotopologue abundances using average masses. Analytical Chemistry 2005; 77:2034-2042.

[145] Zhao Y, Lee WN, Lim S, Go VL, Xiao J, Cao R, Zhang H, Recker RR, Xiao GG. Quantitative proteomics: measuring protein synthesis using ^{15}N amino acid labeling in pancreatic cancer cells. Analytical Chemistry 2009; 81:764-771.

[146] Cho H, Thorvaldsen JL, Chu Q, Feng F, Brinbaum MJ. Akt1/PKBalpha is required for normal growth but dispensable for maintenance of glucose homeostasis in mice. Journal of Biological Chemistry 2001; 276:38349-38352.

[147] Chi H, Mu J, Kim JK, Thorvaldsen JL, Chu Q, Crenshaw EB, Kaestner KH, Bartolomer MS, Shulman GI, Birnbaum MJ. Insulin resistance and a diabetes mellitus-like syndrome in mice lacking the protein kinase Akt2 (PKB beta). Science 2001; 292:1728-1731.

[148] Wilson EM, Rotwein P. Selective control of skeletal muscle differentiation by Akt1. Journal of Biological Chemistry 2007; 282(8):5106-5110

[149] Rotwein P, Wilson EM. Distinct actions of Akt1 and Akt2 in skeletal muscle differentiation. Journal of Cellular Physiology 2009; 219(2):503-511.

[150] Braun T, Cautel M. Transcriptional mechanisms regulating skeletal muscle differentiation, growth and homeostasis. Nature Review Molecular Cell Biology 2011; 12(6): 349-361.

[151] Jespersen JG, Nedergaard A, Reitelseder S, Mikkelsen UR, Dideriksen KJ, Agergaard A, Kreiner F, Pott FC, Schjerling P, Kjaer M. Activated protein synthesis and suppressed proten breakdown signaling in skeletal muscle of critically ill patients. PLoS ONE 2011; 6(3):e18090.

[152] Xiao W, Mindrinos, Seok J, Cuschieri J, Cuenca AG Gao H, Hayden DL, Hennessy l, Moore EE, Minei JP, Bankey PE, Johnson JL, Sperry J, Nathens AB, Billiar TR, West MA, Brownstein BH, Mason PH, Baker HV, Finnerty CC, Jeschke MG, Lopez MC, Klein MB, Gamelli RL, Gibran NS, Arnoldo B, Xu W, Zhang Y, Calvno SE, McDonald-Smith GP, Schoenfeld DA,Storey JD, Cobb JP, Warren HS, Moldawer LL, Herndon DN, Lowry SF, Maier RV, Davis RW, Tompkins RG. A genomic storm in critically injured humans. Journal of Experimental Medicine 2011; 208(13):2581-90.

[153] Frost RA, Lang CH. Protein kinase B/Akt: a nexus of growth factor and cytokine signaling in determining muscle mass. Journal of Applied Physiology 2007; 103:378-87.

[154] Zhang P, Chen X, Fan M. Signaling mechanisms involved in disuse muscle atrophy. Medical Hypotheses 2007; 69:310-321.

[155] Sartorell V, Fulco M. Molecular and cellular determinants of skeletal muscle atrophy and hypertrophy. 2004; www.stke.org/cgi/content/full/sigtrans: /244/re11.

[156] Nader GA. Molecular determinants of skeletal muscle mass: getting the "AKT" together. The International Journal of Biochemistry & Cell Biology 2005; 37:1985-1996.

[157] Glass DJ. Signaling pathways perturbing muscle mass. Current Opinion in Clinical Nutrition & Metabolic Care 2010; 13:225-229.

[158] Mckinnell IW, Rudnicki MA. Molecular mechanisms of muscle atrophy. Cell 2004; 119:907-910.

[159] Kousteni S. FoxO1, the transcriptional chief of energy metabolism. Bone 2012; 50(2): 437-43.

[160] Attaix D, Bechet D. FoxO3 controls dangerous proteolytic liaisons. Cell Metabolism 2007; 6:425-427.

[161] Clavel S, Siffroi-Fernandez S, Coldefy AS, Boulukos K, Pisani DF, Derijard B. Regulation of the intracellular localization of Foxo3a by stress-activated protein kinase signaling pathways in skeletal muscle cells. Molecular and Cellular Biology 2010; 30(2): 470-480.

[162] Mammucari C, Milan G, Romanello V, Masiero E, Rudolf R, Piccolo PD, Burden SJ, Lisi RD, Sandri C, Zhao J, Goldberg AL, Schiaffino S, Sandri Marco. FoxO3 controls autophagy in skeletal muscle in vivo. Cell Metabolism 2007; 6:458-471.

[163] Senf SM, Dodd SL, Judge AR. FOXO signaling is required for disuse muscle atrophy and is directly regulated by Hsp70. American Journal of Physiology-Cell Physiology 2010; 298(1):C38-C45.

[164] Zheng B, Ohkaw S, Li H, Roberts-Wilson TK, Price SR. FOXO3a mediates signaling crosstalk that coordinates ubiquitin and atrogin-1/MaFbx expression during glucocorticoid-induced skeletal muscle atrophy. FASEB Journal 2010; 24:2660-2669.

[165] Brunet A, Sweeney LB, Sturgill JF, Chua KF, Greer PL, Lin Y, Tran H, Ross SE, Mostoslavsky R, Cohen HY, Hu LS, Cheng H-L, Jedrycowski MP, Gygi SP, Sinlair DA, Alt FW, Greenberg ME. Stress-dependent FOXO transcription factors by Sirt1 deacetylase. Science 2004; 303:2011-2015.

[166] Daitoku H, Sakamaki J-I, Fukamizu A. Regulation of FoxO transcription factors by acetylation and protein-protein interactions. Biochimica et Biophysica Acta. 2011; 1813(11):1954-60.

[167] Barhel A, Schmoll D, Unterman TG. FoxO proteins in insulin action and metabolism. Trends in Endocrinology & Metabolism 2005; 16(4):183-189.

[168] Greer EL, Oskoui P, Banko MR, Maniar JM, Gygi MP, Gygi SP. The energy sensor AMP-activated protein kinase directly regulates the mammalian FOXO transcription factor. Journal of Biological Chemistry 2007; 282(41):30107-30119.

[169] Hay N. Interplay between FOXO, TOR, and Akt. Biochimica et Biophysics Acta 2011; 1813:1965-1970.

[170] Bertaggia E, Coletto L, Sandri M. Posttranslational modifications control FoxO3 activity during denervation. American Journal Physiology-Cell Physiology 2012; 302:C587-C596.

[171] Dobson M, Ramakrishnan G, Ma S, Kaplun L, Balan V, Fridman R, Tzivion G. Bimodal regulation of FoxO3 by Akt and 14-3-3. Biochimica et Biophysica Acta. 2011; 1813:1453-1464.

[172] Aitken A. 14-3-3 proteins: A historic overview. Seminars in Cancer Biology 2006; 16:162-172.

[173] Morrison DK. The 14-3-3 proteins: integrators of diverse signaling cues that impact cell fate and cancer development. Trends in Cell Biology 2008; 19(1):16-23.

[174] Obsilova V, Silhan J, Boura E, Teisinger J, Obsil T. 14-3-3 proteins: A family of versatile molecular regulators. Physiology Research 2008; 57(Suppl 3):S11-S21.

[175] He M, Zhang J, Shao L, Huang Q, Cen J, Chen H, Chen X, Liu D, Luo Z. Upregulation of 14-3-3 isoforms in acute rat myocardial injury induced by burn and lipopolysaccharide. Clinical and Experimental Pharmacology and Physiology 2006; 33:374-380.

[176] Senf SM, Sandesara PB, Reed SA, Judge AR. p300 Acetyltransferase activity differentially regulates the localization and activity of the FOXO homologues in skeletal muscle. American Journal of Physiology-Cell Physiology 2011; 300(6):C1490-C1501.

[177] Wang F, Chan C-H, Chen K, Guan X, Lin H-K, Tong Q. Deacetylation of FOXO3 by Sirt1 or Sir2 leads to Skp2-mediated FOXO3 ubiquitination and degradation. Oncogene 2012; 31(12):1546-1557.

[178] Bell EL, Guarente L. The Sirt3 divining rod points to oxidative stress. Molecular Cell 2011; 42:561-568.

[179] Rahman S, Islam R. Mammalian Sirt1: insights on its biological functions. Cell Communication and Signaling 2011; 9:11.

[180] Guarente L. Sirtuins, aging, and medicine. The New England Journal of Medicine 2011; 364:2235-2244.

[181] Galnan DR, Brunet A. The FoxO code. Oncogene 2008; 27:2276-2288.

[182] udhary C, Mann M. (2010) Decoding signaling networks by mass spectrometry-base proteomics. Nature Reviews Molecular Cell Biololy 11(6):427-439.

[183] Murton AJ, Constantin D, Greenhaff PL. The involvement of the ubiquitin proteasome system in human skeletal muscle remodeling and atrophy. Biochimica et Biophysica Acta 2008; 1782(12):730-743.

[184] Ciechanover A. Intracellular protein degradation: from a vague idea thru the lysosome and ubiquitin-proteasome system and onto human diseases and drug targeting. Neuro-degenerative Diseases 2012; 10(1-4):7-22.

[185] Qiang L, Banks AS, Accili D. Uncoupling of acetylation from phosphorylation regulates FoxO1 funaction independent of its subcellular localization. Journal of Biological Chemistry 2010; 285(35):27396-27401.

[186] Walsh CT, Garneau-Tsodikova S, Gatto GJ Jr. Protein posttranslational modifications: the chemistry of proteome diversifications. Angewandte Chemie International Edition 2005; 44(45):7342-72.

[187] Kraft R, Herndon DH, Al-Mousawi AM, Williams FN, Finnerty CC, Jeschke MG. Burn size and survival probability in paediatric patients in modern burn care: a prospective observational cohort study. Lancet 2012; 379(9820):1013-1021.

IntechOpen